6-7-2018 9:30 AM

Microclimate Variability of Select Toronto Neighbourhoods Under Hot Summertime Conditions

Timothy Wiechers
The University of Western Ontario

Supervisor
Voogt, James A.
The University of Western Ontario

Graduate Program in Geography
A thesis submitted in partial fulfillment of the requirements for the degree in Master of Science

Abstract

Micrometeorological variability within cities has important implications for urban air and water quality, building energy consumption, and human health and thermal comfort. However, the monitoring of microscale climate is not routinely conducted. In most instances, primary meteorological observations are made under reproducible standard conditions (typically at an airport); but these open field observations tend to be unrepresentative of the intra-urban meteorological conditions.

This thesis used an alternative approach of conducting mobile traverse measurements using vehicle-mounted sensors to characterize the microclimates of Toronto, ON under hot, summertime weather conditions. Sampling occurred along two routes and incorporated sampling 8 intra-urban neighbourhoods with contrasting surface properties. In addition, a rural reference and two areas identified by Toronto Public Health (TPH) as 'high-risk' in relation to human health were sampled – the Thorncliffe Park and Moss Park neighbourhoods. These observations were used to address the following:

1) What is the intra-urban meteorological variability observed by vehicle traverses under daytime and nighttime conditions?
2) Compared to the other neighbourhoods, do the Thorncliffe Park and Moss Park neighbourhoods exhibit microclimates associated with higher human thermal discomfort?
3) How does an urban-scale numerical model perform in predicting neighbourhood-scale microclimates?

The results presented in this thesis demonstrate significant microscale intra-urban variability from 9 daytime and 3 nighttime traverses. Numerical model outputs show relatively good agreement with vehicle traverse observations, where $\Delta T_{air\ (mod\text{-}obs)} < -1.1\ ^{o}C$ and $\Delta T_{dew\ (mod\text{-}obs)} < -1.7\ ^{o}C$ in 8 of 11 evaluated vehicle traverses. The application of these results can provide insight to where in Toronto public health is at highest risk and where heat mitigation strategies are most needed.

Keywords

Urban climate, micrometeorology, urban heat island, mobile traverses, urban numerical modeling, Toronto.

Acknowledgements

I would firstly like to thank my supervisor Dr. James Voogt for his guidance and input throughout this project. It's been a memorable few years and I've learned a tremendous amount working together. Thanks for the opportunity.

Thank you to my examination committee Dr. Yolanda Morbey, Dr. Gordon McBean, and Dr. Katrina Moser for taking the time to evaluate my thesis and provide prompt, constructive, comments. I would also like to thank Dr. Chris Smart who provided valuable insight and knowledge throughout several stages of this project.

Thank you to Dr. David Sills, Dr. Paul Joe, and several others at ECCC for helping coordinate our traverses and provide parking during the study period. Thank you to Dr. Sylvie Leroyer for providing access to the modeled data.

Thank you to my labmates Dimuth, Michael, Rainer, and Samantha. Thank you to Lara, Julia, Craig, Nolan, Maria, and all fellow geograds for the great friendships we've developed and many GC experiences. I'd also like to thank D.J. Brian for his assistance in the field, Liz for the GIS help, and all faculty and staff in the Department of Geography. A big thank you is also extended to Marcela for the immense support over the duration of this project.

I would also like to thank my family for the ongoing support that they have provided me.

Table of Contents

List of Tables

List of Figures

List of Symbols and Abbreviations

T_{air}	Air Temperature (°C)
aUHI	Air Temperature Urban Heat Island Magnitude (°C)
YTZ	Billy Bishop Toronto City Airport
CBD	Central Business District
R^2	Coefficient of Determinization
CF	Correction Factor
T_{dew}	Dewpoint Temperature (°C)
ΔT_d	Dewpoint Temperature Urban-Rural Magnitude (°C)
DT	Downtown Neighbourhood
GEM-LAM	Global Environmental Multiscale model in Limited-Area Mode
GPS	Global Positioning Device
GTA	Greater Toronto Area
ISBA	Interactions Between the Surface, Biosphere, and Atmosphere
LST	Land Surface Temperatures (°C)
LCZ	Local Climate Zone
MAE	Mean Absolute Error
MP	Moss Park Neighbourhood
OHR	Open-High Rise Neighbourhood

d_r	Refined Index of Agreement
R1	Residential #1 Neighbourhood
R2	Residential #2 Neighbourhood
R3	Residential #3 Neighbourhood
T_{road}	Road Temperature (°C)
RMSE	Root-Mean-Square-Error
rUHI	Road Temperature Urban Heat Island Magnitude
SC	Shopping Center Neighbourhood
SVF	Sky View Factor
$RMSE_s$	Systematic Root-Mean-Square-Error
TP	Thorncliffe Park Neighbourhood
YYZ	Toronto International Pearson Airport
TPH	Toronto Public Health
TEB	Town Energy Balance
$RMSE_u$	Unsystematic Root-Mean-Square-Error
UCL	Urban Canopy Layer
UCM	Urban Climate Models
UHI	Urban Heat Island

Chapter 1

1 Introduction

1.1 Urban Climates

Urban development leads to significant changes in the Earth's surface properties. Land cover, structure, and materials are all modified from their pre-urbanized state and anthropogenic emissions of heat, water vapour, and pollutants alter the composition of the atmosphere. Together, these serve to form distinctly urban climates relative to their surrounding rural area. Local impacts on temperature, humidity, precipitation, and wind have been well documented in cities. One of the most studied impacts is the general warming associated with urban areas, a phenomenon termed the Urban Heat Island (UHI). First observed by Luke Howard (1833), this urban effect is typically expressed by elevated air and surface temperatures and is generally found in all urban areas across the world (Oke, 1995). This leads to several practical implications within cities, including impacts on urban building energy consumption (e.g. Fung et al., 2006; Kolokotroni et al., 2007; Skelhorn et al., 2016), urban air and water quality (e.g. James, 2002; Huizenga et al., 2006; Lai & Cheng, 2009), and human health and thermal comfort (e.g. Harlan et al., 2006; Johansson & Emmanuel, 2006; Ng & Cheng, 2012). As development expands and the number of people living in an urban environment increases (United Nations, 2014), understanding our effect on the climate and the implications of the UHI remains evermore critical.

1.2 Defining the Urban Climate

The vertical structure and the different scales of an urban-modified atmosphere can be seen in Figure 1-1. The meso, local, and micro-scales all represent different conceptual divisions within the urban boundary layer –the upper most layer of an urban-modified atmosphere. Each scale has unique dominant drivers of climate. For example, mesoscale climate is more heavily governed by vertical mixing within the urban boundary layer whereas local building and canyon geometry more heavily governs microscale climate. Nevertheless, it is essential to note that all urban climates are under the control of current

synoptic weather conditions and, on long time-scales, the background climate of a location (Lowry, 1977). Understanding how climate is modified at different scales is important since each climate parameter is a part of a continuum in which they interact with each other across multiple scales (Oke et al., 2017).

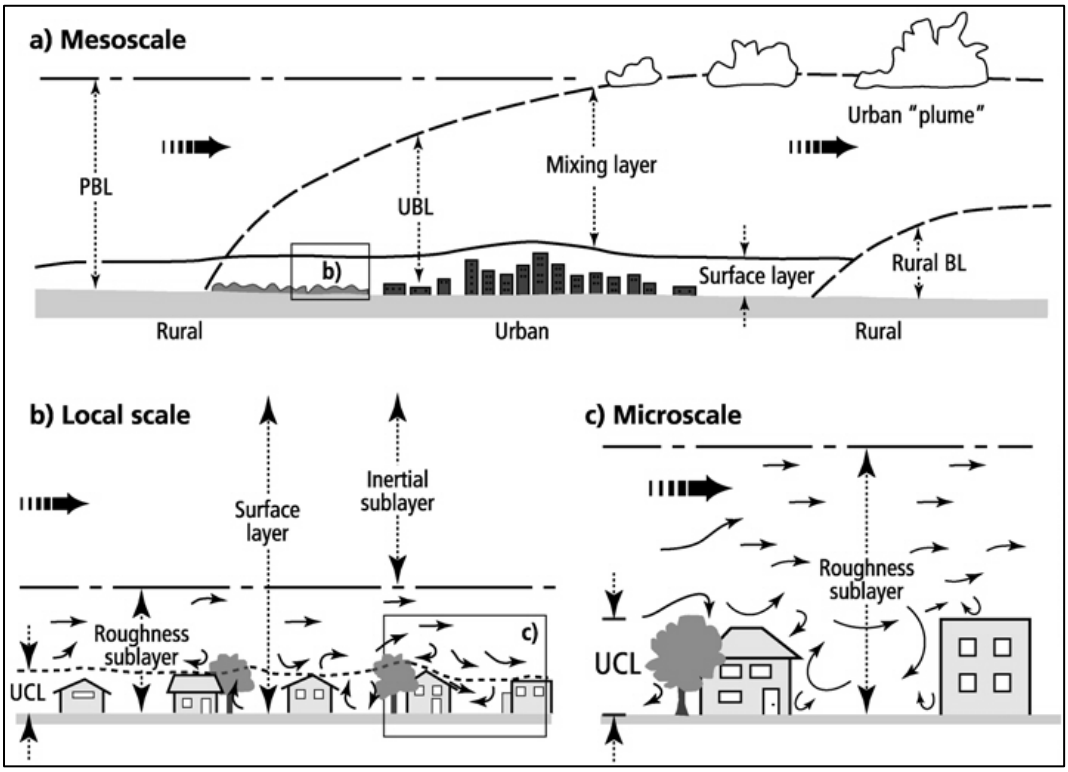

Figure 1-1. A schematic of the urban boundary layer, including the different vertical layers and three scales of observation. Abbreviations defined as: PBL = Planetary boundary layer; UBL = Urban boundary layer; UCL = Urban canopy layer (Piringer et al., 2002, after Oke, 1995).

Shown in Figure 1-1, the scale of this thesis focuses within the urban canopy layer (UCL). The UCL represents the lowest layer of an urban-modified atmosphere, i.e. the layer beneath the mean height of buildings and trees *(z_H)*. UCL climate conditions are of great concern to researchers as this is the layer in which the majority of urban development and daily human activity occurs.

1.3 Urban Canopy Layer Climate

UCL climate is dominated by complex and unique combinations of physical properties at the microscale. In other words, the climate at any location within the UCL will be affected

by both the intrinsic (i.e. radiative, thermal, moisture, and aerodynamic) properties of the area studied, as well as properties of the surrounding environment (e.g. building heights and density). As per Oke (1982), the interactions of these intrinsic surface properties with the surrounding environment produces an almost limitless array of microclimate conditions. Table 1-1 shows the effects of varying surface properties, and how these influence local climate processes within the UCL, ultimately contributing to elevated urban temperatures.

Table 1-1. UCL surface properties and their effects on climate processes (Modified from Oke, 1982).

Surface Property	Effect	Climate Process
Canyon geometry (i.e. Building height, spacing, and orientation)	• Increased surface area and multiple reflections • Reduction of sky view factor	• Increased absorption of shortwave radiation • Decreased longwave radiation loss • Decreased local turbulent heat transport • Reduction of wind speed
Construction and surface cover materials	• Increased impermeable surface cover	• Decreased evapotranspiration

Canopy layer heat islands (UHI_{ucl}) are traditionally measured by screen-level (~1.5 m above ground level) observations between 'urban' and 'rural' locations, e.g. for air temperature, $\Delta T_{urban\text{-}rural}$. This urban-rural difference is also described as the "heat island magnitude". The heat island magnitude is strongest at night, due to the relatively fast cooling rate of a rural area relative to a city, and is maximized approximately 3 to 4 hours following sunset and under clear skies and calm wind conditions. These 'ideal' conditions, help maximize urban-rural cooling rates by limiting turbulent and advective exchanges between the city and rural area and maximizing upwelling longwave radiation (Oke, 1987). In mid-latitude cities during the summertime, nocturnal heat island magnitudes can exceed 10 °C, while in daytime conditions a negative "cool" island can occasionally be observed (Oke, 1982; Runnalls & Oke, 2013). Additionally, heat island magnitudes have been linked to a city's population size, in which higher magnitudes are observed in more populous cities (Oke, 1973).

Despite the vast UHI literature dating back two centuries, Stewart (2011) has argued that the heat island magnitude is arguably the most misrepresented climate expression. At the root of Stewart's argument is that conventional nomenclature, $\Delta T_{urban\text{-}rural}$ is far too simplistic, as the words 'urban' and 'rural' provide no means of describing the field site or local surroundings. In an effort to enhance the communication of field site data and provide a basis for inter-site comparisons, the Local Climate Zone (LCZ) classification system was developed (Stewart & Oke, 2012).

1.4 Local Climate Zones

LCZs classify areas of uniform surface properties and human activity that span hundreds of metres to several kilometers in horizontal scale (Stewart & Oke, 2012). Each LCZ has a unique microclimate resulting from distinctive surface properties that make it distinguishable, including: mean building height, terrain roughness, building, impervious, and pervious surface fractions, surface admittance, albedo, and anthropogenic heat flux (Stewart & Oke, 2012). There are 17 standard built and land cover LCZs in total. In addition, 2 or more standard LCZs can be combined to form a subclass. For example, a large low-rise LCZ (LCZ 8) can be combined with scatter trees (LCZ B) to form LCZ 8_B, large low-rise with scattered trees. Common LCZ examples found within cities can be seen in Figure 1-2. Using LCZs can enhance UHI communication by defining heat island magnitudes according to their LCZ, and not simply 'urban' and 'rural', e.g. $\Delta T_{LCZ\ x\text{-}y}$.

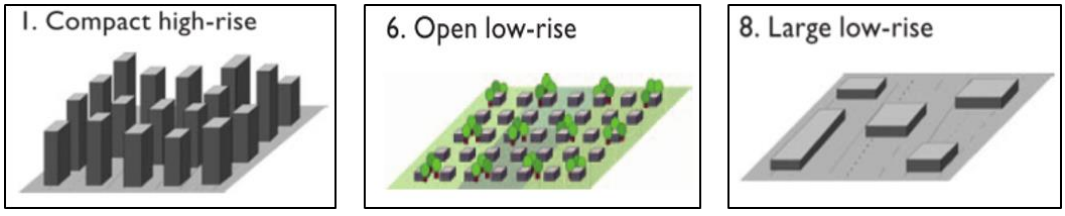

Figure 1-2. Three examples of LCZs commonly found within cities (Stewart & Oke, 2012).

1.5 Assessing UCL Climate

The use of fixed weather stations is the most commonly used approach to assess UCL climate and the resulting microclimate conditions. According to the World Meteorological Organization (2008), to conduct representative UCL observations, an instrument's source

area, defined as the surface area 'seen' by a sensor, must be based within a single LCZ. Figure 1-3 provides a hypothetical source area for an air temperature sensor placed within the UCL (Stewart & Oke, 2012). The location of a source area is always upwind from the sensor, and the size and orientation varies depending on the wind speed and direction. By "rule of thumb" a source area under relatively calm wind conditions extends no more than a few hundred meters (Mizuno et al., 1991; Runnalls & Oke, 2006).

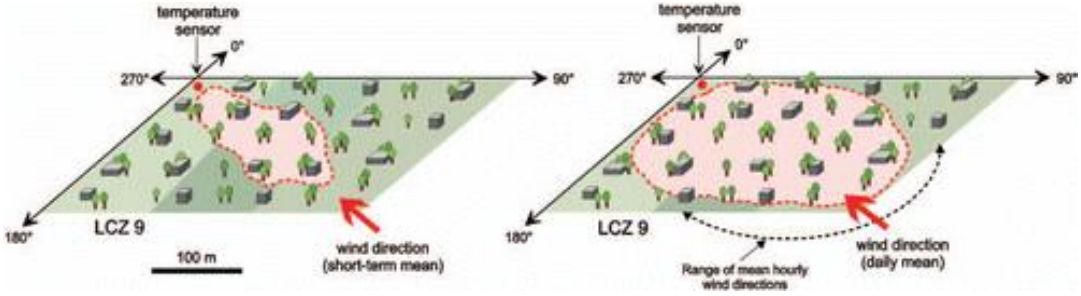

Figure 1-3. Hypothetical source area for an air temperature sensor in the UCL. (Left) represents short-term source, (right) represents mean daily source area (Stewart & Oke, 2012).

This ultimately makes conducting representative UCL observations a very challenging task, and in the majority of cities, the monitoring of microscale urban climate is not regularly undertaken.

1.5.1 Approaches to Conducting UCL Observations

One approach used in cities to characterize UCL climates is to use a network of observing stations (e.g. Micro-scale UScan in Tokyo, Japan (Ono et al., 2008); Oklahoma City Micronet (OKCNET) (Basara & Rowell, 2012). A network can vary in the number of stations and scale it represents, yet to ensure representability, the location of each station should follow the same protocol outlined in Assessing UCL Climate. A network can provide long-term meteorological observations (typically of air temperature and humidity) over a variety of LCZs yet challenges in implementing a network include finding secure and representative station sites, and adequate funding and maintenance.

Another approach is through mobile observations. Mobile observations, known as traverses, use a measurement platform that carries instruments and makes meteorological observations while in motion. Within the UCL, traversing can be conducted on foot (e.g.

Nakayoshi et al., 2015; Tsin et al., 2016), by bicycle (e.g. Heusinkveld et al., 2010; Vanos et al., 2012) or from a vehicle (e.g. Conrads & Van Der Hage, 1971; Voogt & Oke, 1998; Sofer & Potchter, 2006; Leconte et al., 2015). Traverses can provide detailed spatial observations along a route, covering a variety of LCZs; however, they are often limited in their ability to represent temporal variation. This is because a fixed number of traverses can typically be conducted within a day and are often limited to a select number of days. In addition, the representativeness of traverse observations can be difficult to determine while driving within a city due to consistently varying source areas. Lastly, this approach requires that the data collected be refined, namely, by correcting for temperature changes (i.e. heating or cooling) during a traverse as well as filtering out data while stationary as extraneous heat sources, such as vehicle exhaust, may contaminate the signal.

A third approach is to use thermal remote sensing techniques. These techniques observe radiative surface temperatures, or more specifically upwelling thermal radiance, and are often used to assess the surface urban heat island, perform land cover classifications, and provide input for models. Remote sensing techniques can provide large, repetitive, area coverage that leads to important observations of the surface conditions. However, the thermal remote sensing of urban climates includes a variety of spatial and temporal biases. Spatially, remote sensing techniques under sample complex urban 3-dimensional surfaces as what the sensor "sees" depends on the sensor viewing angle and thus a significant portion of the complete urban surface may not be viewed (Voogt & Oke, 2003). Temporally, satellite overpass times are discontinuous and require clear skies to view the surface, thus limiting the applicability of remote sensing techniques.

1.5.2 Urban-Scale Numerical Models

The use of urban-scale numerical models is another approach to characterizing UCL climate. Urban climate models (UCMs) are used to simulate UCL meteorological conditions using mathematical relationships that represent the surface-atmosphere processes. There is a large variety of UCMs, that differ based on the scale they represent (micro-macro), surface description (1D-3D), and overall complexity (the number of urban-atmosphere processes included). Currently, a common approach is to 'couple' models, meaning that a mesoscale model is run to provide the upper boundary layer conditions for

a microscale model, that in turn provides the lower boundary conditions for the mesoscale model. Adding to the complexity of these models, a microscale model may also consist of multiple parts – referred to as a 'tiled' scheme. For example, a tiled-microscale model may incorporate two different models to represent the vegetated and urban parts of a grid cell. For these models, the final output is weighted and then combined according to the vegetated and urban fraction of a grid cell. UCMs allow users to simulate urban effects by simplifying the real world and many of the inherently complex processes that occurs between a city and the atmosphere. A major benefit of this approach is the ability to predict future climate scenarios, which can only be achieved through computer simulations.

1.6 Thesis Context and Background

The majority of cities do not have proper monitoring platforms to make daily assessments of UCL climate. In most instances, primary meteorological observations are made under reproducible standard conditions (typically at an airport); but these open field observations tend to only represent one LCZ and thus are predominately unrepresentative of the variety of LCZs and conditions within an urban area. While urban-scale numerical modeling provides an alternative approach and has undergone significant improvements (synchronous with increasing computing power), the evaluation of these models to represent the microscale is an on-going process (Leroyer et al., 2011).

1.6.1 Pan and Parapan American Games

In the summer of 2015, Toronto, ON, Canada was host to the Pan and Parapan American Games, the world's third largest sporting event. During this time, a large scientific field campaign was initiated to provide enhanced weather, air quality, and health monitoring within the Greater Toronto Area (GTA). This included a variety of observation and modeling systems and provided urban meteorological observations and simulations not routinely made. See Joe et al. (2017) for a full description of the scientific field campaign.

1.7 The GEM-LAM Model

Of interest to this thesis is the operation of the Global Environmental Multiscale model (GEM; Zadra et al., 2008) run in Limited-Area Mode (GEM-LAM) during the field

campaign. The GEM-LAM model simulates UCL conditions using a 'tiled-scheme' to represent different surface categories; the Town Energy Balance scheme (TEB: Masson, 2000) is used to represent urban areas and the Interactions between the Surface, Biosphere, and Atmosphere scheme (ISBA; Noilhan & Planton, 1989) is used to represent land surfaces and vegetation . Throughout the games, the spatial domain of the modeling system was set-up over Southwestern Ontario to include the 2015 Pan-American Games venues and the GTA. The model was operated at 1 km and 250 m resolutions; this thesis assesses the 250 m outputs.

The evaluation of the GEM numerical model for simulating UCL conditions has only been assessed in a few case-specific studies. Lemonsu et al. (2009) tested the modeling system over Oklahoma City (OKC). One of their main goals was to test the ability of the system to simulate street-level air temperature on two separate dates in July (clear sky conditions). Their evaluation included two intensive observational periods, on July 16th and another on July 26th. The evaluation was conducted using a variety of fixed stations, set up as three different networks, in and surrounding the central business district (CBD) of the city. Instrumentation heights ranged from 3 m to 8 m above the ground. Their analysis compared observed and simulated air temperature within the CBD, a commercial and industrial area within the city, and a rural location. Model results showed good agreement with the observations to represent the nocturnal heat island, but did not succeed in representing the 'cool' island observed throughout the day. The authors state this is likely due to limitations in radiative calculations in the TEB scheme. Ultimately, their results indicated satisfactory agreement between modeled and observed air temperature (with differences less than 1.5 °C). Another evaluation of the model was conducted in Montréal (Leroyer et al., 2011). This study evaluated air temperature and humidity using the EPiCC measurement network, that included two tower sites (one defined as "urban", the other "sub-urban") with mounted instrumentation (25 m) and a rural weather station (2 m). Findings at the rural location indicated a warm modeled air temperature bias (about 3 °C) during nighttime conditions and a diurnal modeled underestimation of specific humidity. At the urban site, air temperature was slightly underestimated by the model during both daytime and nighttime conditions. While specific humidity also showed an underestimation, near-surface relative humidity showed relatively good agreement. At the

suburban site, air temperature was better modeled during the nighttime than at the urban site, yet daytime air temperature was still slightly underestimated. Specific humidity and relative humidity showed similar trends to that at the urban site. The authors conclude with stating that modifications to TEB are currently being made to improve the representation of urban vegetation inside street canyons. A third evaluation was conducted in Vancouver (Leroyer et al., 2014). This evaluation also used the EPiCC measurement network, that consisted of two instrumented towers located in an urban residential neighbourhood south of downtown Vancouver. Both locations represent the "open midrise" LCZ 6 (Stewart & Oke, 2012). At both sites, diurnal air temperature was relatively well modeled, except for a 1 °C underestimation of the maximum value. Diurnal relative humidity also showed similar trends at both sites and in general the model underestimated relative humidity. These findings show similar trends to that presented in Lemonsu et al. (2009) and Leroyer et al. (2011). Past evaluations have used fixed station sites and have evaluated a limited number of LCZs, this thesis attempts to expand on these evaluations by including a larger number of LCZs and evaluating the modeled outputs with in-situ urban canyon observations.

1.8 Toronto's Urban Climate

The first intra-urban spatial observations of Toronto's climate were made by Middleton and Millar (1936). Using a vehicle traverse approach, their findings showed "surprising" spatial air and dewpoint temperature variability along Yonge St under a range of conditions and seasons. During summer daytime conditions, the lowest air temperatures were observed near the lakefront, with air temperature increasing until approximately 8 km north of the lake. Dewpoint temperature had the opposite trend and decreased the further away from the lakefront. These insights provided the first evidence of intra-urban microclimatic variability within the city and the strong influence Lake Ontario has on the city's climate. Munn et al. (1969) used a "volunteer-observer-network" of fixed weather stations to examine the UHI under two seasons – a warm and cold season. During the warm season they found the highest air temperatures north of Bloor Street and the central business district. The UHI was identified as more intense during the nighttime and under light winds. The authors also state that changes in local topography (e.g. valleys and interfluves)

within the city may also contribute to observed air temperature variability. More recently, Gough and Rozanov (2002) assessed Toronto's UHI using historical climate data observed from three fixed stations (2 rural, 1 downtown Toronto). Their findings suggest a 3-4 °C heat island increase from 1930-1980. They also note a strong lake breeze effect during the summer and estimate this contributes a cooling effect of 0.8 °C. Furthermore, Mohsin and Gough (2010) stated that ongoing urban development within the GTA has contributed to at least 30% of the total increasing trend in annual average air temperature. This study was followed up in 2012, when the authors examined the spatiotemporal trend of Toronto's UHI and highlighted the importance of site selection when defining an UHI. In general, these studies suggest an increasing trend in Toronto's intra-urban air temperature dating back to post World War I with a strong connection to increasing urban development. This thesis provides an updated insight on the intra-urban meteorological conditions observed within the city.

A select number of studies have used thermal remote sensing to obtain land surface temperatures (LST) in the GTA. Rinner and Hussain (2011) used a Landsat Thematic Mapper thermal image (60 m resolution) and identified statistically significant differences in LST between commercial/industrial land covers (29.1 °C) and parks/recreational land covers (23.1 °C). Ye et al. (2017) used Landsat and ASTER thermal images with 120 m resolution to analyze surface temperature heat island intensity from 1984-2014 in the GTA. Using the normalized difference vegetation index to assess land cover change their findings suggest an increasing LST trend with increasing urban development. To date, Toronto's intra-urban surface temperatures have only been observed through thermal remote sensing techniques with relatively large (< 60 m resolution) pixel resolution; this thesis will provide the first insights into surface temperature variations at the microscale, within the UCL. However, as using a vehicle traverse methodology only allows a portion of the surface (i.e. road) to be sampled, we make the distinction between surface temperature, that may include roof and vegetated temperatures, and strictly road temperature. Road temperature variability during hot summertime periods within cities is important to study as it contributes to the thermal loading on nearby pedestrians, specifically in busy districts such as downtown Toronto.

1.9 UCL Climate and Toronto's Public Health

Toronto experiences the highest number of extreme heat events or heat waves in Canada, defined as lasting two days or longer (Smoyer-Tomic et al., 2003). With projected large scale anthropogenic climate change, the frequency of these events is expected to increase substantially (Meehl & Tebaldi, 2004). UCL surface properties can further increase temperatures that impact inhabitants (Li & Bou-Zeid, 2013). Prolonged exposure to heat can result in a wide variety of physiological effects, ranging from heat exhaustion and cramps to mortality. In the city of Toronto, there is a clear link between temperature and death rates – on average, there are 120 heat-related deaths per year (Pengelly et al., 2007).

Since 2000, Toronto Public Health (TPH) has developed a Hot Weather Response Plan as well as a Heat Warning alert in order to prepare for and spread awareness of the dangers of unusually hot weather (TPH, 2017). Since then, the city has continued to implement policies and initiatives intended to counter heat-related risks to the public. These initiatives range from improving urban green space (e.g. The Green Development Standard) to enhancing energy efficiency in existing buildings and new construction projects (e.g. The Better Buildings Partnership) (Penney, 2008). More recently, TPH has identified two neighbourhoods in the city as being "high-risk" in relation human health – Moss Park and Thorncliffe Park (S. Dutfield, personal communication, July 16, 2015). These two neighbourhoods contain large and mid-rise multi-residential towers and are characterized by low income housing with known human health concerns arising in these neighbourhoods. Yet, to date, no monitoring of the local urban microclimates has been conducted.

1.10 Research Rationale and Questions

With urban development and the number of people living in the GTA expected to increase (United Nations, 2016; Ontario Ministry of Finance, 2017), along with the known heat-related health implications in the city of Toronto, this thesis endeavors to investigate microscale intra-urban variability captured by vehicle traverse observations and evaluate the ability of the GEM-LAM model to represent microscale variability during hot summertime periods. From past evaluations of the model, this thesis expands on the

number of LCZs used in the evaluation and the number of days, as typically only a select number (1 or 2) days are evaluated. Furthermore, at the time of writing, the GEM-LAM model has never been evaluated by mobile vehicle traverse observations. These observations typically provide better representation of UCL climate compared to fixed weather stations and also provides the ability to see the variability within LCZs to assess any neighbourhood variability not resolved by the model.

Using Stewart and Oke's (2012) scheme, select Toronto neighbourhoods were classified as LCZs and meteorological differences of air, road, and dewpoint temperature associated with the physical characteristics between neighbourhoods are identified. The use of representative LCZs to classify neighbourhoods in the city allows for both vehicle traverse observations and urban scale numerical modeling to be evaluated. Each of these methods have tradeoffs in coverage, resolution, and error, but the use of LCZs provides a means of reconciling the two data sources (i.e. traverse and modeled data) to more accurately account for intra-urban variability. Ultimately, these findings can help provide insight to where in Toronto public health is at greatest risk and where heat mitigation strategies are most needed.

The research questions of this thesis are categorized as 'observational' or 'modeling' and meteorological variability is defined by air (T_{air}), road (T_{road}), and dewpoint (T_{dew}), temperature. The research questions are as follows:

*Observational based**:***

1. What is the meteorological variability observed by vehicle traverses under daytime and nighttime conditions in the city of Toronto?

2. How do microclimates of select urban neighbourhoods differ under the same synoptic conditions?

3. Identified as 'high-risk' neighbourhoods by TPH, do the Thorncliffe Park and Moss Park neighbourhoods exhibit microclimates associated higher heat related health risks compared to other urban neighbourhoods?

*Modeling based**:***

4. How does an urban-scale numerical model perform in predicting neighbourhood-scale microclimates?

a. Does the model show the same ranking of neighbourhood temperatures compared to the observations?

1.11 Thesis Outline

Chapter 2 details the study site, period, and the logistics of the mobile vehicle traverses; including a description of the vehicle-traverse platform, the routes, and the neighbourhoods that were sampled. It describes the post-collection data filtering and time-correction schemes that have been applied to the traverse observations. Furthermore, it describes the GEM-LAM modeling system and the data processing associated with the model outputs and provides an overview of the statistical tests used this thesis.

Chapter 3 presents results and discussion from the vehicle traverses and addresses research questions 1 – 3. The chapter concludes with a summary that highlights the key findings.

Chapter 4 presents results and discussion from the GEM-LAM model evaluation and addresses research question 4. Similar to the previous chapter, the chapter concludes with a summary that highlights the key findings.

Chapter 5 summarizes the primary findings shown in Chapter 3 and Chapter 4. It provides insight on future work and concludes with final remarks.

Chapter 2

2 Methods

2.1 Study Site and Period

Toronto, Ontario, Canada, is currently Canada's most populous city with a population of over 2.7 million people (Statistics Canada, 2018). The city is located within a larger, highly urbanized region on the north shore of Lake Ontario that extends to the western end of the lake – the GTA (Figure 2-1). The climate is represented by the Dfa Köppen-Geiger climate classification code (Kottek et al., 2006): characterized by hot, humid summers and cold winters. The climate is greatly influenced by its proximity to Lake Ontario. During the summertime, strong local "lake-effect" winds often blow inland, producing a strong moderating effect on the climate.

Figure 2-1. A map of Toronto, Ontario, Canada (43°42′ N, 79°24′ W) and the surrounding GTA region (ESRI, 2012). The Claremont fixed weather station is indicated by the red star (see Section 2.6).

A climograph depicting Toronto's seasonal variability in T_{air} and precipitation can be seen in Figure 2-2. Aimed to target hot, humid, summertime conditions, the field work took place from July 7 – July 29, 2015; coinciding with Toronto's warmest month on average

of the year and with the GEM-LAM model simulations as part of the Pan and Parapan American Games science campaign.

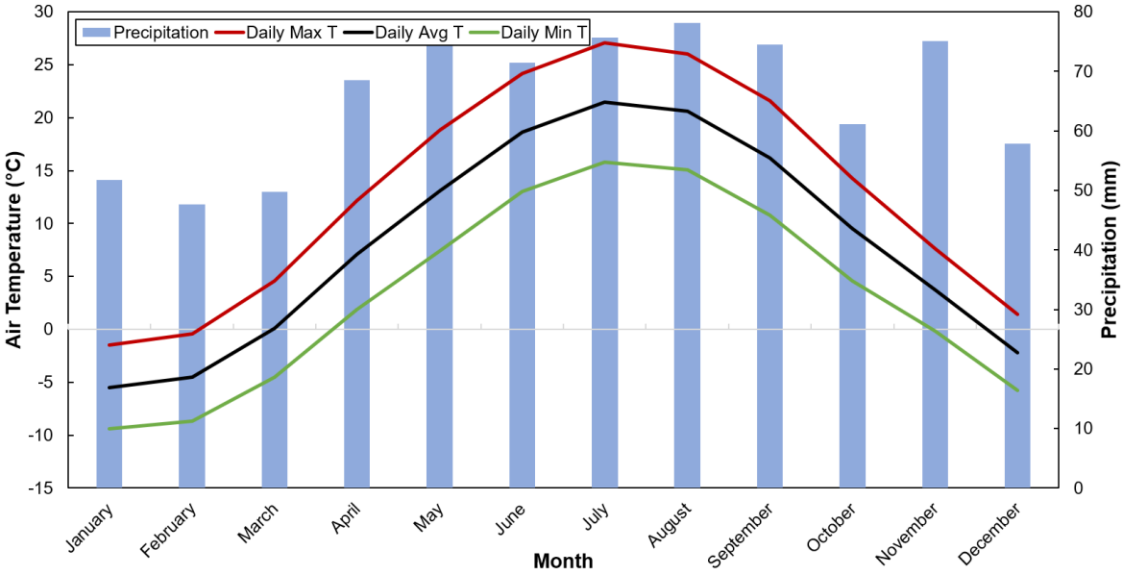

Figure 2-2. A climograph depicting the seasonal variability in air temperature and precipitation of Toronto, ON. Data represent the Climate Normals from 1981 – 2010 recorded from Toronto Pearson International Airport.

2.2 Vehicle Traverse Platform

An instrumented pickup truck was used to conduct vehicle traverses (Figure 2-3). The measured meteorological variables include: T_{air}, relative humidity, T_{road}, incoming shortwave and longwave radiation, and left and right canyon wall temperatures. These variables were included to characterize the conditions within the UCL and external radiative environment that humans are exposed to. A global positioning system (GPS) was also included in the instrumentation which provided the truck's latitude, longitude, and elevation during a traverse. All instrumentation was wired into a datalogger in the backseat and observations were recorded at 1 second intervals; this was chosen to minimize the spatial resolution and capture the best representative data of a specific location while driving at speeds up to 60 km h^{-1}. Multiple T_{air} sensors included in the instrumentation showed very similar trends to each other. Results presented in Chapter 4 are based on the HC2S3 thermistor and this thesis does not include observations of incoming radiation or wall temperatures. See Appendix E for the datalogger program written in CRBasic.

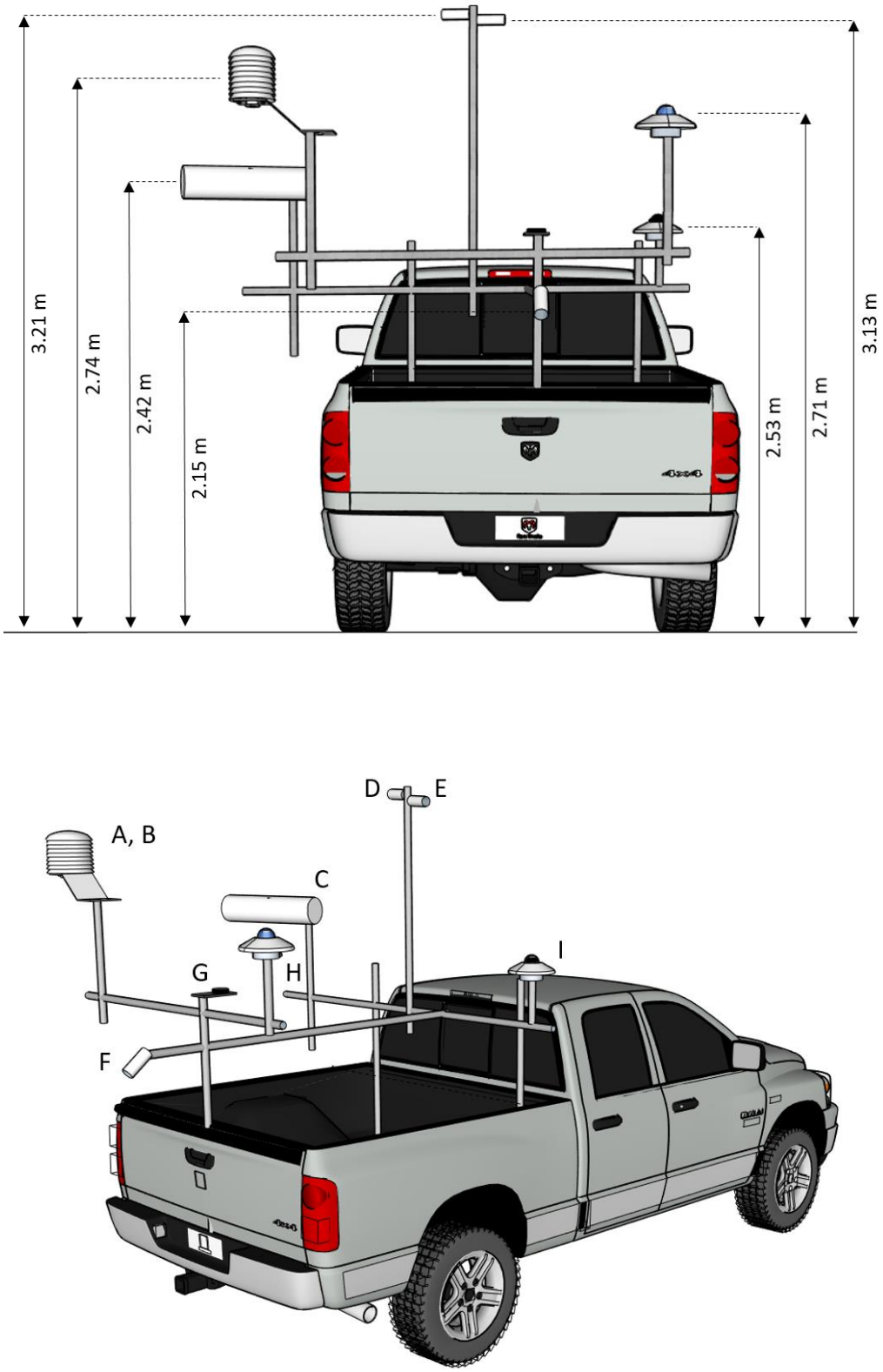

Figure 2-3. (Above) Instrument configuration and mounted heights. (Below) Labeled instrumentation. See Table 2-1 for instrument descriptions.

Table 2-1. Instrumentation list and measurements. Note: the viewing angle for the road facing infrared radiometer was 40° (relative to nadir view = 0°), representing a field of view of 5.97 m^2 and all air temperature sensors were placed inside aspirated radiation shields.

Instrument & Model	Measurement	Company	Label
Pyrgeometer, PIR	Incoming longwave radiation	The Eppley Laboratory Inc	I
Infrared radiometer (right facing), SI-131	Radiative surface "canyon wall" temperature	Apogee Instruments Inc	E
Infrared radiometer (left facing), SI-131	Radiative surface "canyon wall" temperature	Apogee Instruments Inc	D
Fine wire thermistor, ST-200	Air temperature	Apogee Instruments Inc	C
Pyranometer, TSP-400	Incoming shortwave radiation	Yankee Environmental Systems Inc	H
GPS, 16X-HVS	X, Y, Z coordinates	Garmin International Inc	G
Thermistor and hygrometer, HC2S3	Air temperature and relative humidity	Campbell Scientific Inc	A
Thermocouple, Type T (24 AWG)	Air temperature	Omega Engineering Inc	B
Infrared radiometer (road facing), SI-1H1	Radiative surface "road" temperature	Apogee Instruments Inc	F
Data logger, CR3000	Data acquisitioning system	Campbell Scientific Inc	-

2.3 Vehicle Traverse Routes

Vehicle traverses were conducted along two routes (A and B) primarily along Yonge St (Figure 2-4). Yonge St is a major north-south street within Toronto that extends northward from the shoreline of Lake Ontario to Newmarket, ON. Each route incorporated sampling urban neighbourhoods with contrasting surface properties, classified using the LCZ scheme. The use of two different routes allowed for three additional neighbourhoods to be sampled, including the two areas identified by TPH as being "high-risk" – the Thorncliffe Park and Moss Park neighbourhoods. Route A (solid line) included sampling: Residential 1, Residential 2, Open-High Rise, Shopping Centre, and Downtown and route B (dashed line) included: Residential 1, Open-High Rise, Thorncliffe Park, Residential 3, Moss Park, and Downtown.

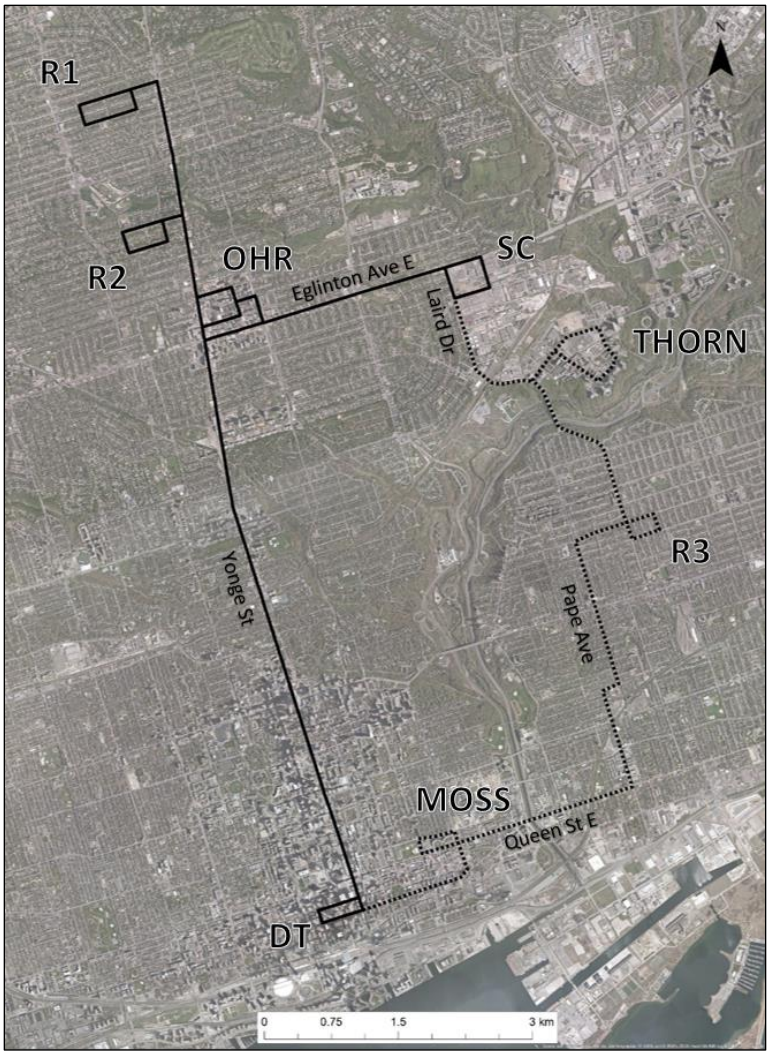

Figure 2-4. A map of the combined traverse routes (A and B) and sampled urban neighbourhoods overlaid on a satellite image. Neighbourhood codes include: R1,2,3: Residential 1,2,3, OHR: Open-high Rise, SC: Shopping Centre, THORN: Thorncliffe Park, MOSS: Moss Park, DT: Downtown

2.3.1 Nighttime Extended Route

Two nighttime traverses extended route A northbound to King Rd (Figure 2-5). These traverses were conducted under 'ideal' conditions and timed to maximize the UHI magnitude between urban and rural locations. This entailed beginning traverses approximately 3 hours after sunset (i.e. 1:00 EST) and under low wind and relatively clear sky weather conditions.

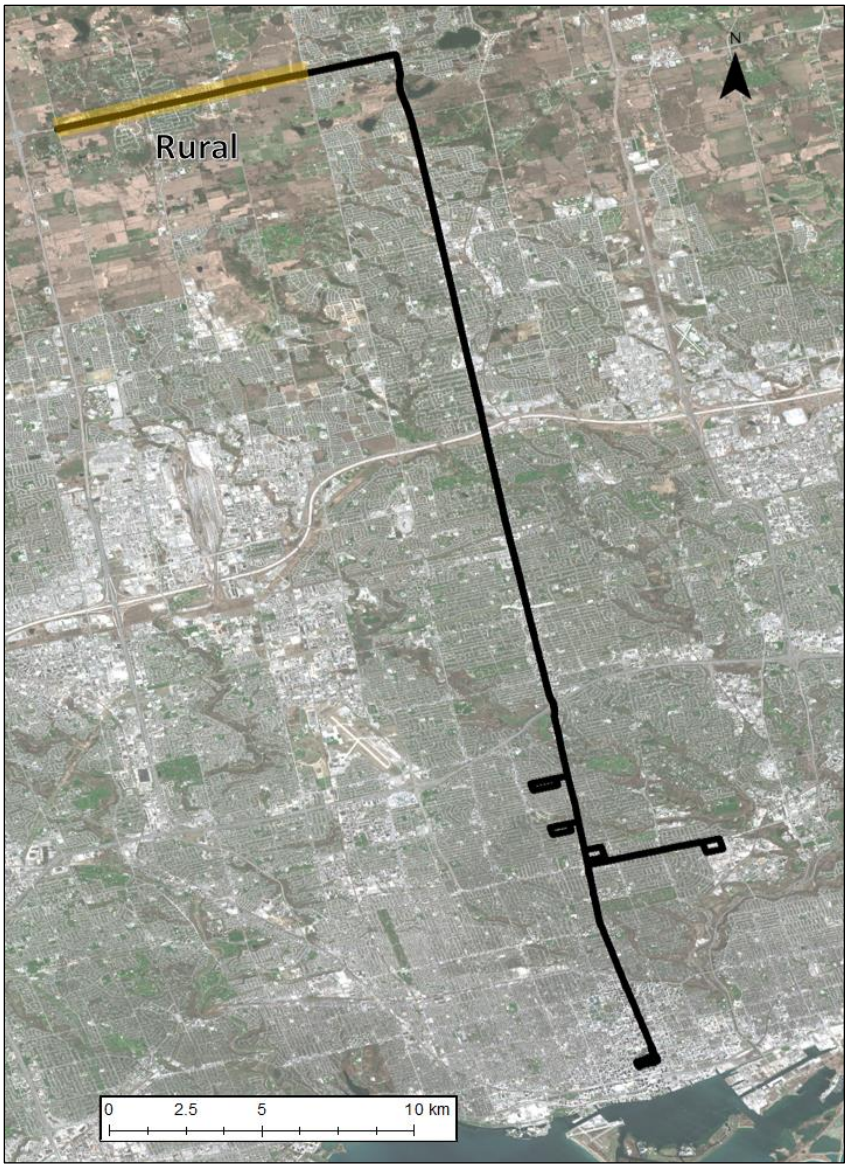

Figure 2-5. A map of the nighttime extended route. Highlighted in yellow is the defined "rural" transect.

2.4 Defining Sampled Neighbourhoods

Using a Sentinel-2 satellite image (10 m resolution) and open source lidar 3D massing data provided by the city of Toronto, a supervised land cover classification was conducted to calculate the building, impervious and pervious surface fraction for each sampled neighbourhood. The 3D massing data was also used to provide mean building heights. To account for T_{air} and humidity source area variations when driving through neighbourhoods,

a 200 m surrounding buffer for each neighbourhood was applied during the land cover classification. All analysis was conducted using ArcGIS.

The sky view factor (SVF), defined as the ratio of the amount of sky visible from ground level to that of an unstructured hemisphere, was calculated to represent the urban geometry and vegetation within each neighbourhood. This was conducted by taking hemispherical photographs using a Nikon CoolPix880 digital camera with a FC-E8 fisheye lens. Using the photographs, SVF was calculated using the open source SkyViewFactorCalculator model (Lindberg & Holmer, 2012). Sample hemispherical photographs for route A neighbourhoods can be seen in Figure 2-6.

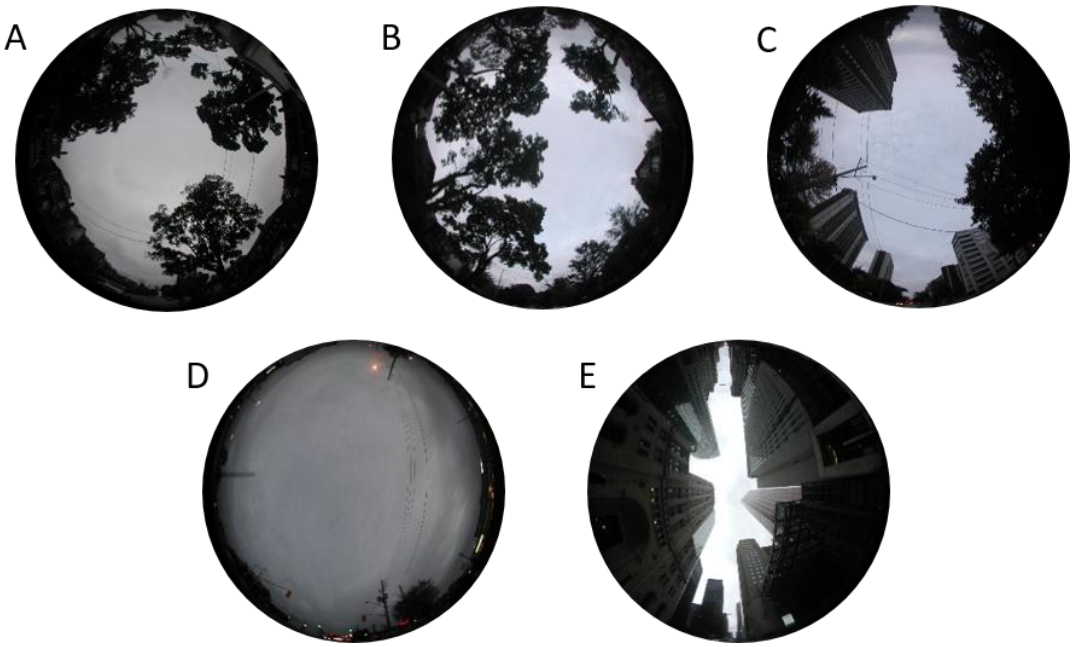

Figure 2-6. Sample hemispherical photos. A, B: residential neighbourhoods, C: open high-rise, D: shopping centre, E: downtown.

2.4.1 Classifying LCZs

Using the calculated values of surface land cover properties, neighbourhoods were classified according to the LCZ scheme (Table 2-2). Thermal, radiative, and metabolic values for each neighbourhood were not directly measured and are estimated according to Stewart and Oke (2012) (Table 2-3).

Table 2-2. Neighbourhood surface cover and geometric properties.

Neighbourhood (coordinates)	Building fraction (%)[1]	Impervious fraction (%)[2]	Pervious fraction (%)[3]	z_H (m)[4]	SVF[5]	LCZ[6]	Built and land cover types[6]
Residential 1 (43.7321 -79.4079)	25	44	31	7.0	0.65	6	Open low-rise
Residential 2 (43.7190, -79.4039)	22	42	36	7.7	0.54	6	Open low-rise
Residential 3 (43.6876, -79.3404)	26	59	15	5.7	0.71	6	Open low-rise
Open High Rise (43.7111, -79.3992)	60	25	15	28.0	0.70	4_E	Open paved high-rise
Shopping Centre (43.7135, -79.3648)	30	59	11	6.9	0.96	8	Large low-rise
Thorncliffe Park (43.7050, -79.3498)	26	52	22	16.2	0.81	5_3	Open midrise with compact low-rise
Moss Park (43.6546, -79.3695)	34	51	15	13.1	0.78	5	Open midrise
Downtown (43.6504, -79.3784)	62	33	5	62.9	0.24	1	Compact high-rise
Rural Transect (43.9390, -79.4815)	-	36	64	-	> 0.80	$6_{B,F}$	Open low-rise with scattered trees and agriculture

[1] Ratio of building plan area to total plan area.

[2] Ratio of impervious plan area to total plan area.

[3] Ratio of pervious plan area to total plan area.

[4] Geometric average of neighbourhood building heights (does not include vegetation).

[5] Value represents an average from five hemispherical photos within a neighbourhood. The 'Rural Transect' SVF was estimated using Stewart and Oke (2012).

[6] Classified LCZ based on neighbourhood surface cover and geometric properties (Stewart & Oke, 2012).

Table 2-3. Estimated values of thermal, radiative, and metabolic properties. Provided by Stewart and Oke (2012).

LCZ	Surface Admittance ($J\ m^{-2}\ s^{-1/2}\ K^{-1}$)[7]	Surface albedo	Anthropogenic heat output ($W\ m^{-2}$)[8]
1	1500-1800	0.10-0.20	50-300
4	1400-1800	0.12-0.25	<50
5	1400-2000	0.12-0.25	<25
6	1200-1800	0.12-0.25	<25
8	1200-1800	0.15-0.25	<50

2.5 Vehicle Traverse Criteria

Targeting hot summertime days when human thermal comfort is at greatest risk, a total of 23 vehicle traverses were conducted during the study period. The criteria for a traverse to be included in the analysis included: 1) cloud coverage ≤ 7 oktas, and 2) the lake breeze front was located north or south of the traverse route. Meteorological Terminal Aviation Routine Weather Report (METAR) data provided at its lowest recorded level was used to assess cloud coverage and radar data provided by Dave Sills (Environment Canada) was used to identify the location of a lake-breeze front (Figure 2-7). Sampling dates with relatively clear-sky conditions increases incident solar radiation and thus promotes high contrasts in surface temperatures and maximum differentiation between sampled neighbourhoods. Furthermore, ensuring all neighbourhoods are on the same side of the lake-breeze front is critical in assessing meteorological differences between neighbourhoods. Recently in Toronto, Mariani et al. (2017) found an average 2.1 ± 0.2 °C decrease in T_{air} and 2.3 ± 0.3 °C increase in T_{dew} when a lake-breeze front passes by. Thus, if a neighbourhood is within the lake-breeze frontal zone while others are not, observed neighbourhood differences will be influenced by the lake-breeze, rather than distinguished by surface properties of a neighbourhood. A summary table of all the eligible traverses including the start and end times, and meteorological conditions observed during the traverses is provided in Chapter 3.

---

[7] Ability of a surface to accept or release heat.

[8] Mean annual heat flux density from fuel combustion and human activity (e.g. transportation, space cooling/heating, industrial processing, human metabolism).

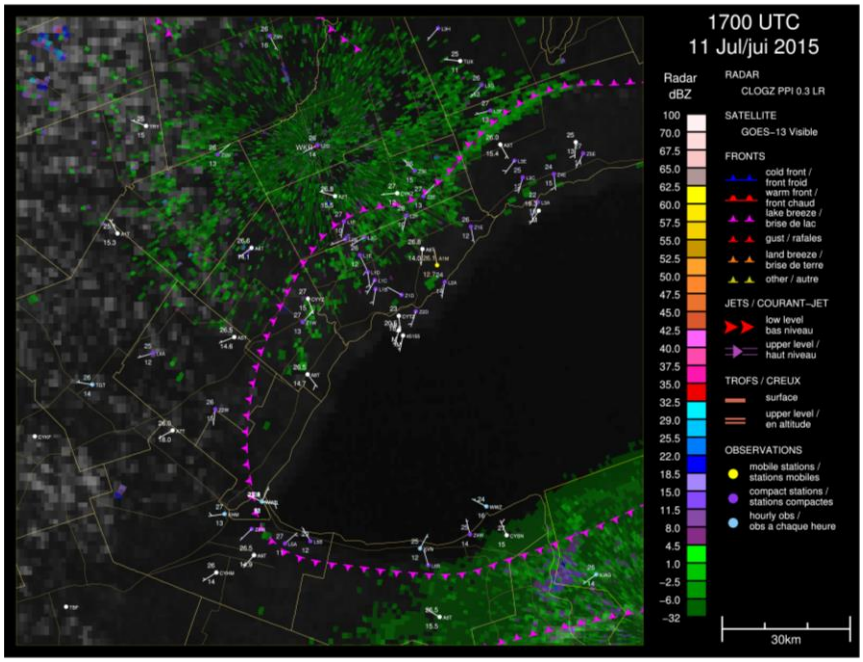

Figure 2-7. Example radar and satellite observations identifying the location of the lake-breeze front on July 11th (pink triangular dashed line).

2.6 Defining Urban-Rural Differences

Chapter 1 describes the importance of adequately defining 'urban' and 'rural' when assessing UHI magnitudes. To acknowledge this, the UHI magnitudes presented in this thesis are defined according to the differences within a select urban neighbourhood and a rural fixed weather station located in Claremont, ON (43°56'09.800" N, 79°05'05.400" W) (Figure 2-1). This weather station was chosen as it is approximately the same distance from the shoreline of Lake Ontario compared to the neighbourhoods, ensuring neighbourhoods and the weather station are on the same side of the lake-breeze front. In addition, a consistent rural reference allows for daytime and nocturnal heat island magnitudes to be compared. Using a consistent rural reference also allows observed and modeled urban-rural differences to be assessed. For modeled urban-rural differences, the rural reference is defined as the pixel value at the Claremont location. For the two nocturnal traverses that used the 'nighttime extended route', differences in UHI magnitudes corresponding to different rural locations is discussed in Chapter 3. Furthermore, urban-rural results presented in Chapter 3 and Chapter 4, are denoted as aUHI (T_{air}), rUHI (T_{road}), and ΔT_d (T_{dew}).

2.7 Post-Collection Data Processing

2.7.1 Data Filtering

Observation sequences in which the vehicle was travelling less than 15 km h^{-1} were eliminated. This was to remove any T_{air} or humidity observations more likely to be contaminated from nearby heat sources (e.g. vehicle exhausts) and for road surface temperature, to remove any observations that may be contaminated by vehicles located closely behind the truck while stopped in traffic or moving slowly. Vehicle speed was calculated based on GPS output.

2.7.2 Time-Correction Schemes

To account for any changes in temperature or humidity during a vehicle traverse (~2 hours), a time-correction scheme is applied to all observations. This adjusts all observations along a traverse to a common time and thus permits for spatial comparisons along the traverse route. For T_{air} and relative humidity, this thesis applies a linear-time correction. This methodology has been implemented in previous studies such as Richards (2005) and Leconte et al. (2015). For T_{road}, this thesis builds off work reported by Voogt and Oke (1998).

Air Temperature and Humidity Scheme

A linear trend assumes the temporal temperature or humidity changes occur at a constant rate. This requires a common start and end location; for the majority of traverses conducted, this was residential #1. As an example, using T_{air}, the correction factor (CF) is defined and applied as:

$$CF = \frac{-\Delta\overline{T_{air}}}{t} \tag{1.1}$$

$$T_{air}{}' = T_{air} + t \cdot CF \tag{1.2}$$

where $\Delta\overline{T_a}$ is the temperature difference between the average T_{air} at the start and end times at the common location, time (t) is the duration of the traverse in seconds, and $T_{air}{}'$ is time-

corrected T_{air}. As an example, a comparison between uncorrected and corrected T_{air} is shown in Figure 2-8.

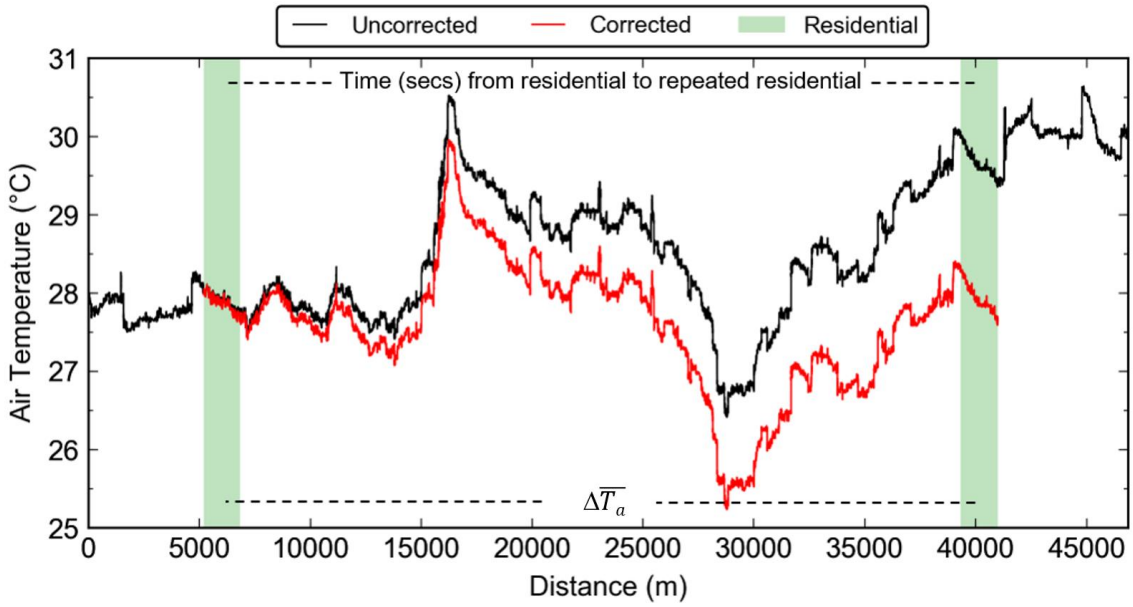

Figure 2-8. A comparison of uncorrected (black) versus corrected (red) air temperature observations for an early afternoon traverse (July 13). Note that on this traverse, the correction corresponds to a warming of approximately 1.2°C that occurred over the traverse duration.

Road Temperature Scheme

Correcting T_{road} for temporal changes is inherently more complex than correcting T_{air} and humidity. For T_{air} and humidity, under stable atmosphere conditions, one can assume a temporally "smooth" and continuous diurnal change. However, for surface temperature, the rate of changes are much larger and variable. At the microscale, the rate of heating or cooling of the surface depends on the temperature of the surface (i.e. shaded surfaces heat up faster than previously sunlit surfaces). The T_{road} scheme described in this section is for daytime conditions; for nighttime conditions, T_{road} is corrected using a linear scheme previously outlined for T_{air} and humidity. The daytime scheme follows a similar protocol as a linear correction, however it differs by calculating two CFs – one for sunlit observations and another for shaded observations. To classify the observations, histograms were created using commercially available software (PeakFit v4.12). The histograms were used to assess the temporal change in T_{road} distributions between the common start and end

neighbourhoods. Using Figure 2-9 as an example, the two CFs are based on the temperature differential between paired peaks at the start and end times; where the yellow-dashed peaks represent fully sunlit peaks and the blue-dashed peaks represent fully shaded peaks. The CF that is applied is based on the median of the starting neighbourhood's T_{road} distribution, for example if an observation is less than the median it is classified as "shaded" and the shaded CF is applied. Numerically this is represented in Equations 1.3 and 1.4.

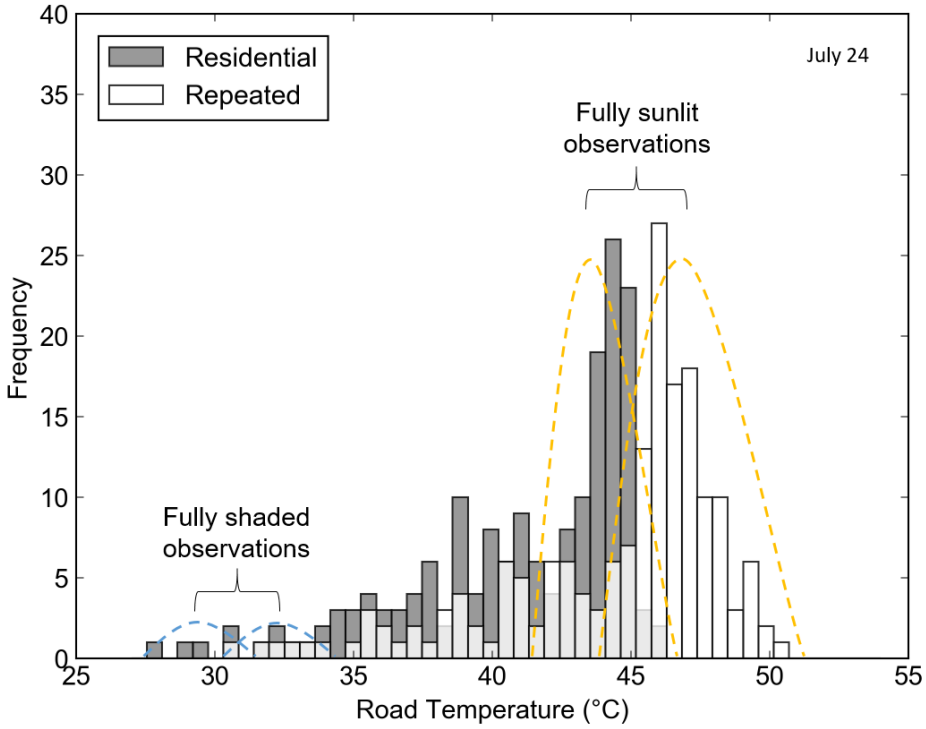

Figure 2-9. An example from July 24th of two overlaid road temperature histograms from Residential 1 used to represent how CFs are calculated based on the change in fully sunlit and fully shaded peaks.

$$CF_{shaded} = \frac{-\Delta \overline{T_{road,shaded}}}{t} \tag{1.3}$$

$$CF_{sunlit} = \frac{-\Delta \overline{T_{road,sunlit}}}{t} \tag{1.4}$$

2.8 GEM-LAM Modeling System

As introduced in 1.5.2, the GEM-LAM model is composed of two surface schemes: TEB (Masson, 2000) and ISBA (Noilhan & Planton, 1989) that are driven by Environment Canada's Regional Deterministic Prediction System (Fillion et al. 2010).

The TEB scheme follows a single-layer urban canopy approach to simulate energy exchanges between the UCL and overlying atmosphere. To simplify complex urban geometry, TEB calculates separate urban energy budgets for roofs, roads, and walls while assuming there is no vegetation present in the canyon. TEB inputs include geometric parameters: building fraction, building height, canyon aspect ratio, and the ratio between walls and horizontal built-up areas; radiative parameters: roof, road, and wall albedos and emissivities; and thermal parameters: thicknesses, thermal conductivities, and heat capacities of the roofs, roads, and walls (Masson, 2000). The effects of shadows and radiation trapping inside a street canyon are considered and turbulent exchanges inside a canyon, and between the canyon and atmosphere, are determined using an aerodynamic resistance network that consider wind speed and stability conditions (Lemonsu et al., 2009). Mean air temperature, mean specific humidity, and mean windspeed are calculated for the middle of the street at the mid-height of buildings (Lemonsu et al., 2009).

The ISBA scheme simulates energy exchanges over land, water, glaciers, and sea ice (Bélair, 2003). However, as the focus of this thesis was for vegetated land during the summertime, the schemes described here will only consider the processes over land. Thus, the required inputs are surface temperature, mean surface temperature, soil volumetric water content, rooting depth volumetric water content, leaf area index, and canopy intercepted liquid water (Noilhan & Planton, 1989). The turbulent fluxes are calculated by aerodynamic equations using a thermal drag coefficient from Delage and Girard (1992) and Delage (1997). The final output from the two surface schemes are calculated as a weighted average according to the fractions of pervious or impervious surface cover. Figure 2-10 provides a conceptual diagram of TEB and illustrates the energy exchanges that the surface scheme includes associated with canyon roofs, roads, and walls.

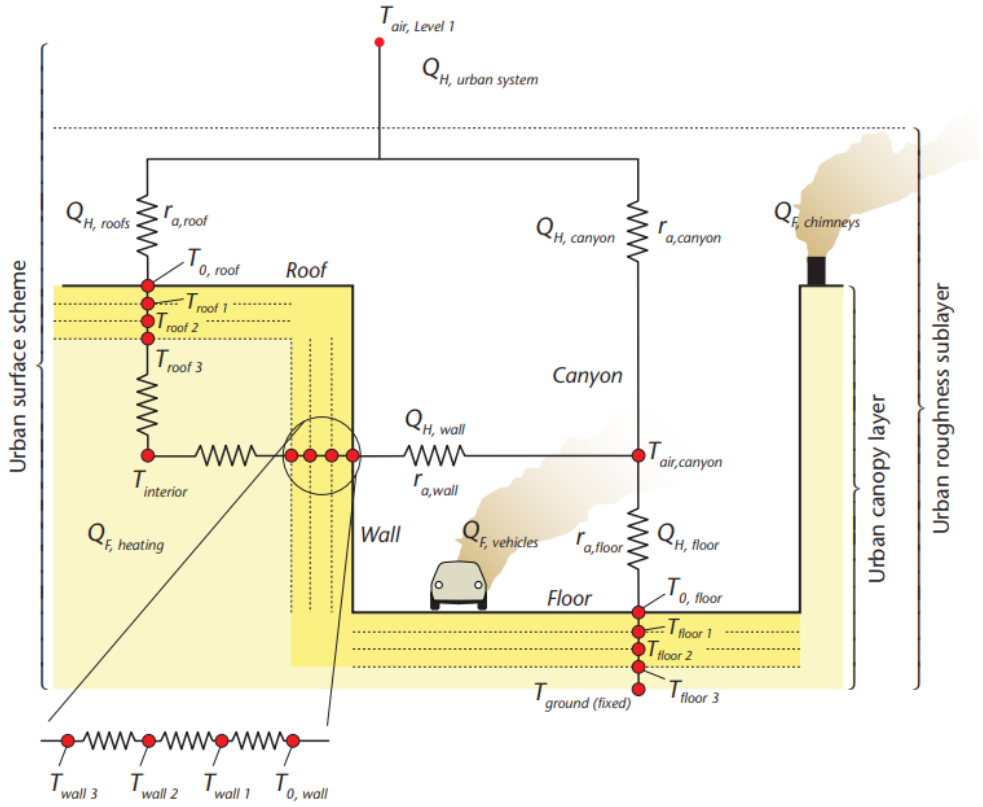

Figure 2-10. A conceptual diagram of the Town Energy Balance (TEB) surface scheme (Oke et al., 2017 modified after Masson et al., 2002).

2.8.1 Accessing and Analyzing GEM-LAM Outputs

GEM-LAM variables evaluated in this thesis are: "screen-level air temperature" and "dewpoint temperature". Outputs of the model were provided every 15 minutes, and therefore correspond to the closest matching observational start time. Modeled outputs were accessed from Environment Canada through a secure shell network. Using this network, modeled outputs were visualized and downloaded using a graphical user interface called SPI (version 7.7.3), developed by the Meteorological Service of Canada. The downloaded model output files are imported into ArcGIS as shapefile feature classes where individual pixel output values are obtained and map features are added. All outputs are geo-referenced in World Geodetic System 1984.

For an individual model pixel to be included in the evaluation (e.g. scatterplots), at least 5 *time-corrected and filtered* vehicle traverse observations were needed within the pixel (N=5 threshold). This value was chosen given that the source area of each observation

should extend at least 100 m and thus 5 observations covers a relatively large fraction of a 250 m model pixel. See Figure 2-11 for sample modeled output vehicle traverse observations overlaid.

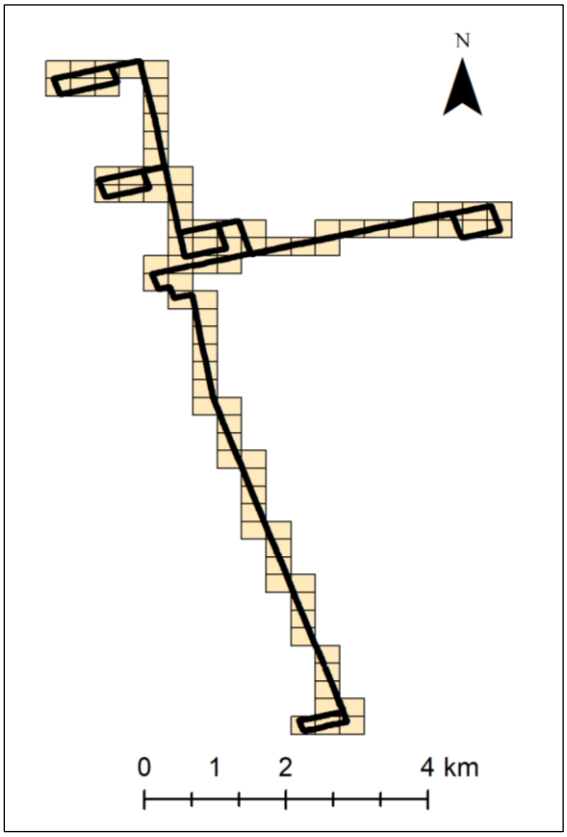

Figure 2-11. Sample modeled output pixels with at least 5 vehicle traverse observations overlaid.

2.9 Statistical Tests

All vehicle traverse data were found to be non-normally distributed upon using the Shapiro-Wilk (Shapiro & Wilk, 1965) test of normality (α=0.05). Therefore, the nonparametric Mann-Whitney U (Mann & Whitney, 1947) test (α=0.05) was used to determine significant differences between residential #1 and the other neighbourhoods. The test criteria includes: 1) neighbourhood observations are independent from each other; 2) Null hypothesis, the distributions of both neighbourhoods are equal; and 3) Alternative hypothesis, the distributions are not equal. Analysis of the U-value illustrates the degree of overlap

between neighbourhood distributions, where U = 0 indicates no overlap. The maximum value of U is the product of the two sample sizes.

Chapter 5 presents a variety of model evaluation statistics. These include regression coefficients: slope, y-intercept, and coefficient of determinization (R^2). The mean absolute error (MAE), root-mean-square-error (RMSE), systematic root-mean-square-error ($RMSE_s$), unsystematic root-mean-square-error ($RMSE_u$) and refined index of agreement (d_r) are also calculated (Willmott et al., 1985; Willmott et al., 2012). The equations for each model evaluation statistic are defined as:

$$MAE = \sqrt{\frac{\sum_1^n |p - o|}{n}} \tag{1.5}$$

$$RMSE = \sqrt{\frac{\sum_1^n (p - o)^2}{n}} \tag{1.6}$$

$$RMSE_s = \sqrt{\frac{\sum_1^n (\hat{p} - o)^2}{n}} \tag{1.7}$$

$$RMSE_u = \sqrt{\frac{\sum_1^n (p - \hat{p})^2}{n}} \tag{1.8}$$

$$d_r = 1 - \sqrt{\frac{\sum_1^n |p - o|}{\sum_1^n |p - \bar{o}| + |o - \bar{o}|}} \tag{1.9}$$

where, p is the modeled variable, o is the observed variable, $\bar{o}$ is the average observed variable, and $\hat{p}$ is the predicted variable based on the least square regression.

Chapter 3

3 Vehicle Traverse Results and Discussion

During the study period, 12 traverses – 9 daytime and 3 nighttime, met the required criteria to be included in the analysis and evaluation of the GEM-LAM model. Table 3-1 provides a summary of the eligible vehicle traverses, including each traverse start and end time, sampling route, cloud coverage conditions, wind speed, and observed median T_{air}, and T_{dew}, and T_{road}. The table also includes T_{air} and T_{dew} reported from the fixed rural station in Claremont, ON and indicates whether a lake-breeze front was present during the start time of a traverse.

Results presented in this chapter will address research questions 1 - 3. All observations are time-corrected and filtered as outlined in Section 2.7. To conclude, a summary of the chapter and key results are presented.

3.1 Daytime Traverse-Scale Observations

Two traverses (July 11th and July 24th) are used as examples to show the intra-urban variability of T_{air}, T_{road}, and T_{dew} observed along a vehicle traverse. These two traverses cover both routes and provide representative daytime conditions when a lake-breeze front is present (i.e. north of all sampled neighbourhoods). Figure 3-1 and Figure 3-2 show traverse-scale observed T_{air} variability. The warmest T_{air} is observed along Eglinton Rd. with a relatively consistent spike in T_{air} among all traverse dates. T_{air} decreases southbound along Yonge St. towards Lake Ontario, with the coolest T_{air} observed in Toronto's downtown core. From all daytime traverses, the largest observed range in intra-urban T_{air} was 4.8 °C (July 13th) and the smallest was 2.1°C (July 11th). These findings support previous results from Middleton and Millar (1936). In addition, similar spatial trends of T_{air} and T_{road} are observed between replicate traverses along the same route and expands from work conducted by Tsin et al. (2016) in which the authors suggest future studies focus on route-replication to increase the representativeness of traverse observations and to minimize day-to-day variability (Figure 3-7).

Table 3-1. A summary table of the 12-eligible daytime and nighttime (shaded) traverses.

Date (2015)	Start Time[1]	End Time	Route	Cloud Coverage[2]	Med T_{air} [3] (°C)	Med T_{road} (°C)	Med T_{dew} (°C)	Rural T_{air} [4] (°C)	Rural T_{dew} (°C)	Wind Speed[5] (km/h)	Lake-Breeze Front
July 10	15:20	17:16	A	Broken	26.4	43.9	11.5	26.7	11.7	14	Y
July 11	13:26	15:15	A	Few	27.7	44.9	12.7	26.8	16.3	16	Y
July 12	1:13	3:56	Extended	Clear	21.4	24.4	15.4	14.5	14.4	11	N
July 13	13:17	15:19	A	Clear	27.7	46.1	17.7	26.6	19.6	18	N
July 16	13:42	15:56	A	Few	22.7	40.9	8.7	22.0	11.2	14	N
July 19	1:12	2:29	A	Broken	25.1	28.1	20.8	19.5	19.5	14	N
July 19	13:09	14:47	A	Few	31.0	48.5	21.3	30.6	21.8	15	Y
July 20	14:00	15:45	B	Broken	28.6	42.2	16.3	28.2	15.6	27	Y
July 22	14:00	15:55	B	Few	25.5	43.5	8.9	24.4	11.6	23	N
July 24	14:01	15:50	B	Broken	28.0	44.2	8.9	26.5	13.0	11	Y
July 29	1:18	4:17	Extended	Scattered	24.8	28.4	16.2	17.1	16.2	12	N
July 29	13:51	15:49	B	Few	32.3	45.8	16.3	31.7	17.4	19	Y

[1] Traverse start and end times begin at the common location. Time is reported in Eastern Daylight Time (EDT).

[2] METAR data from YYZ where 'Few' = 1-2 oktas, 'Scattered' = 3-4 oktas, 'Broken' = 5-7 oktas.

[3] Traverse-scale medians of air temperature, road temperature, and dewpoint temperature. *'Med'* = median.

[4] Reported from the fixed weather station in Claremont, Ontario. Times correspond to closest 1-hr to traverse start time.

[5] Wind speed observations are from Toronto Pearson International Airport, reported by Environment Canada.

Figure 3-3 and Figure 3-4 show traverse-scale observed T_{road}. Relative to the other meteorological variables, T_{road} shows the largest degree of intra-urban variability as large temperature gradients are created between fully sunlit and fully shaded regions along a vehicle traverse. From all daytime traverses, the largest observed range in intra-urban T_{road} was 36.7 °C (July 11th) and the smallest range was 24.3 °C (July 20th). This is likely driven by differences in cloud cover and wind speed between the two dates, as for both a lake-breeze front is present and T_{air} and T_{dew} conditions are relatively similar. Like T_{air}, similar traverse-scale structural trends are observed.

Figure 3-5 and Figure 3-6 show traverse-scale observed T_{dew}. In general, T_{dew} shows more structural variability between dates and similar trends aren't definitively observed (Figure 3-7). An influence of the lake-breeze is present as traverse-scale T_{dew} is on average higher when a lake-breeze front is present. The maximum T_{dew} range observed along a traverse was 5.5 °C (July 29th) and the minimum range was 1.8°C (July 19th). For all traverse-scale plots of T_{air}, T_{road}, and T_{dew} from both routes, see Appendix A-1.

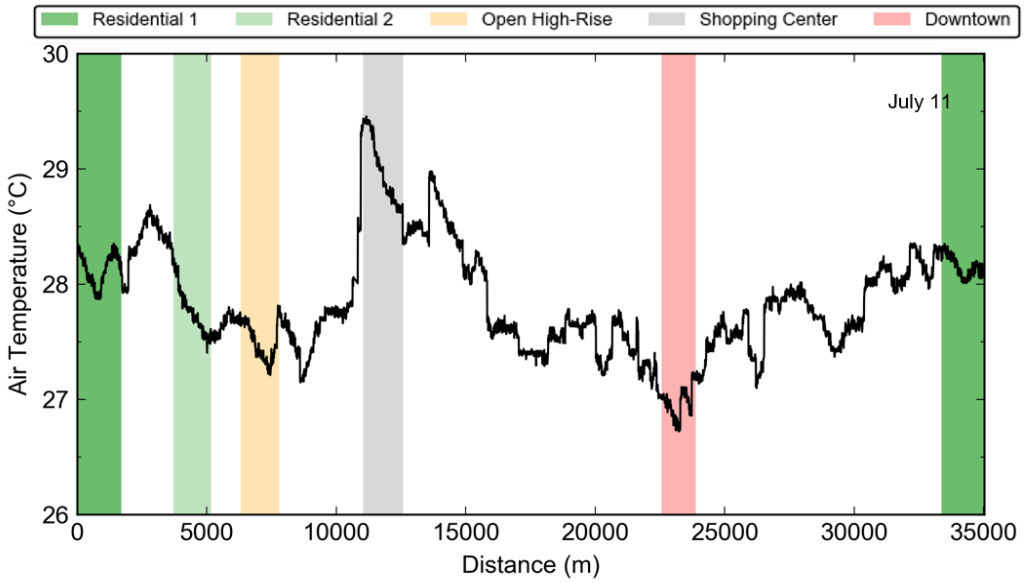

Figure 3-1. Daytime traverse-scale air temperature variability (route A). Med T_{air} = 27.7 °C. Note: shaded regions represent sampled intra-urban neighbourhoods.

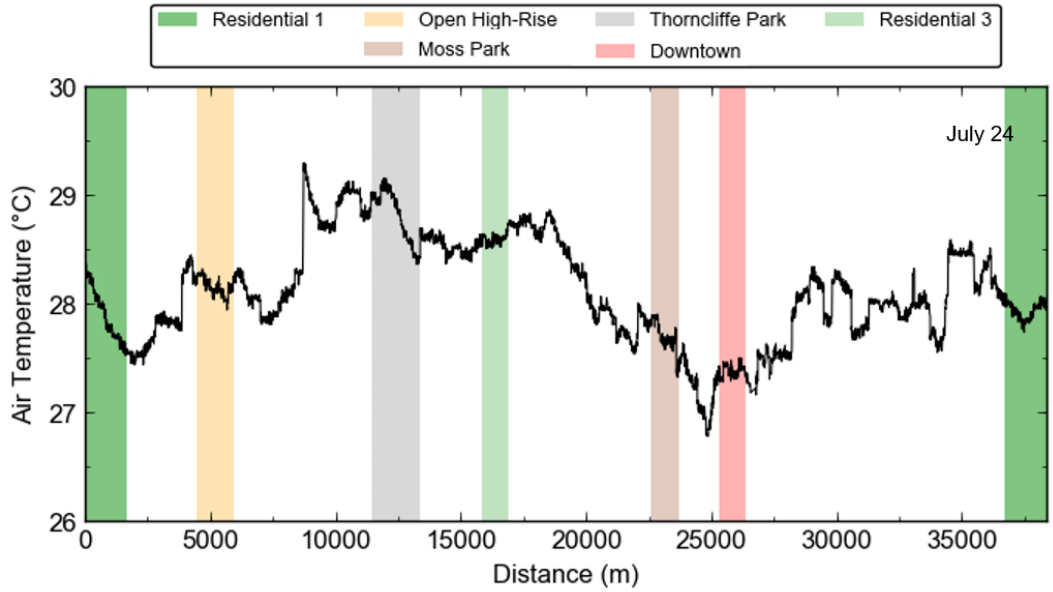

Figure 3-2. Daytime traverse-scale air temperature variability (route B). Med T_{air} = 28.0 °C.

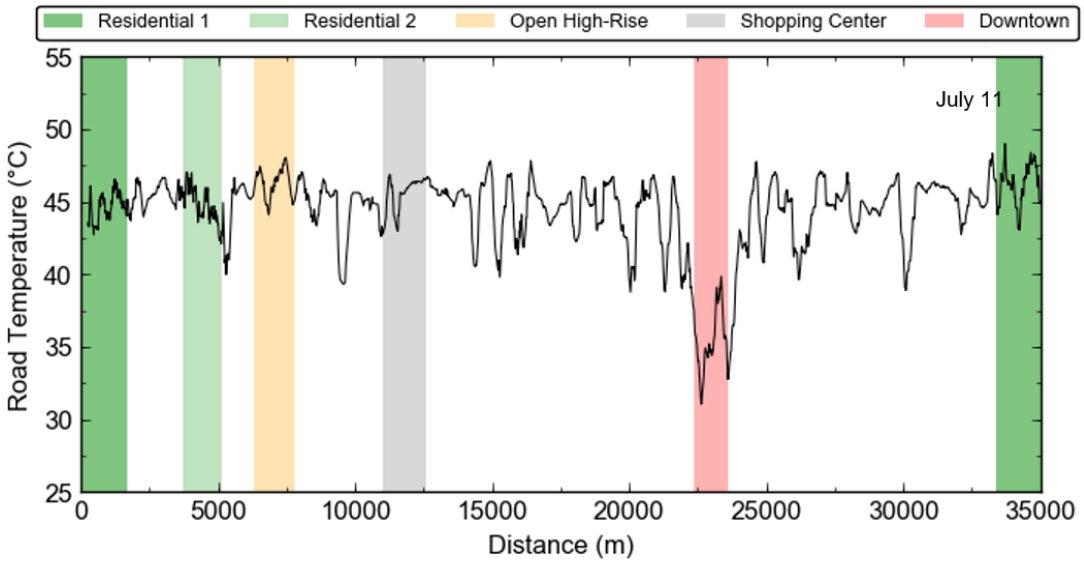

Figure 3-3. Daytime traverse-scale road temperature variability (Route A). Med T_{road}= 44.9 °C. Note: plot represents a 20-observational moving average.

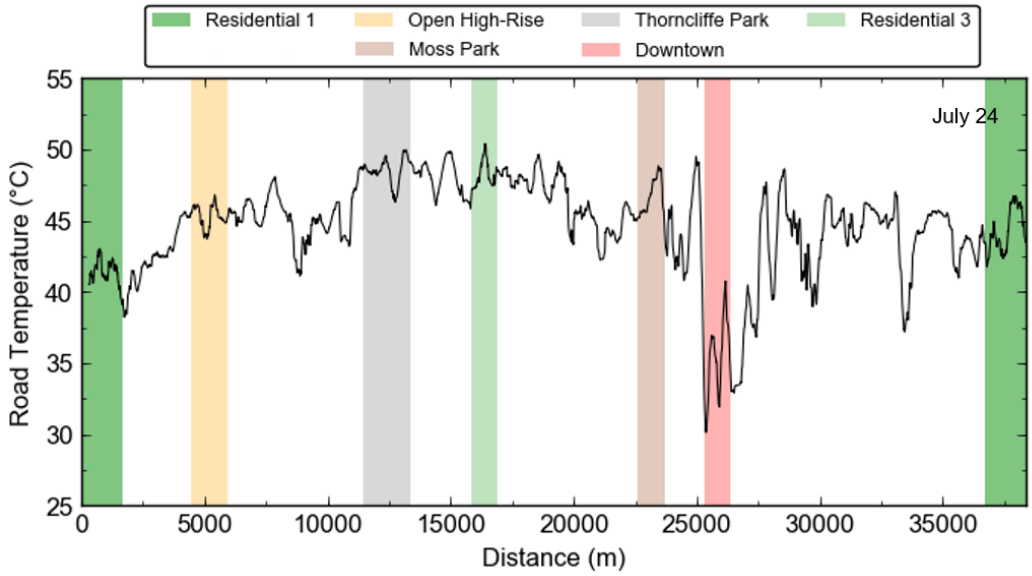

Figure 3-4. Daytime traverse-scale road temperature variability (Route B). Med T_{road}= 44.2 °C. Note: plot represents a 20-observational moving average.

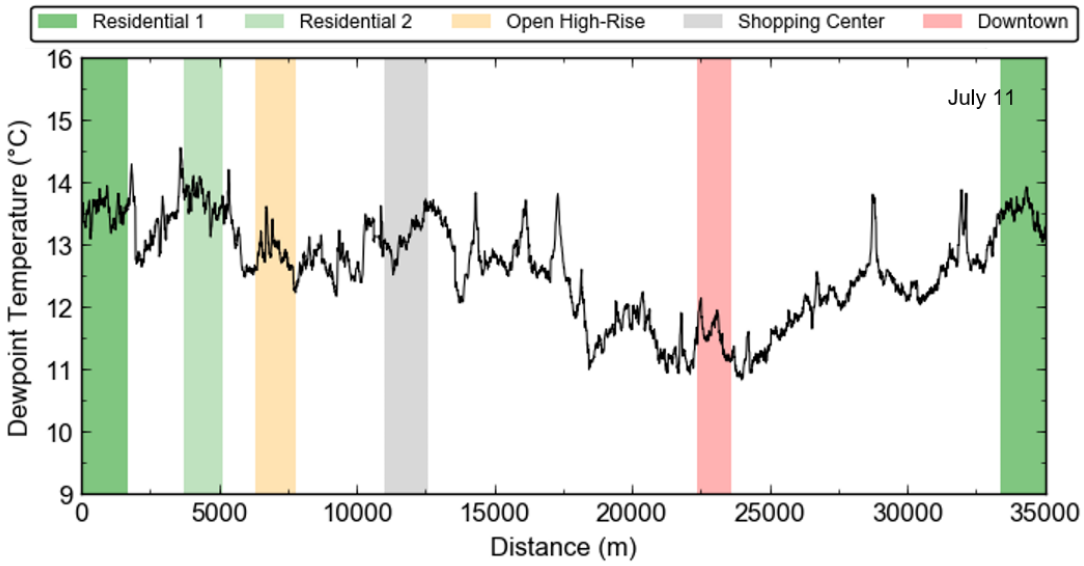

Figure 3-5. Daytime traverse-scale dewpoint temperature variability (Route A). Med T_{dew} = 12.7 °C.

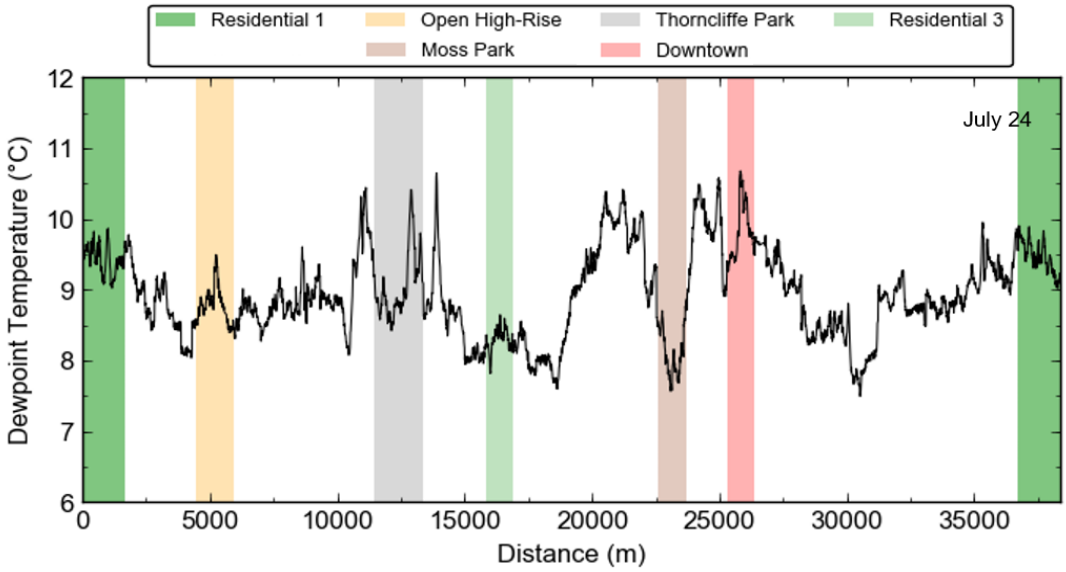

Figure 3-6. Daytime traverse-scale dewpoint temperature variability (Route B). Med T_{dew} = 8.9 °C**.**

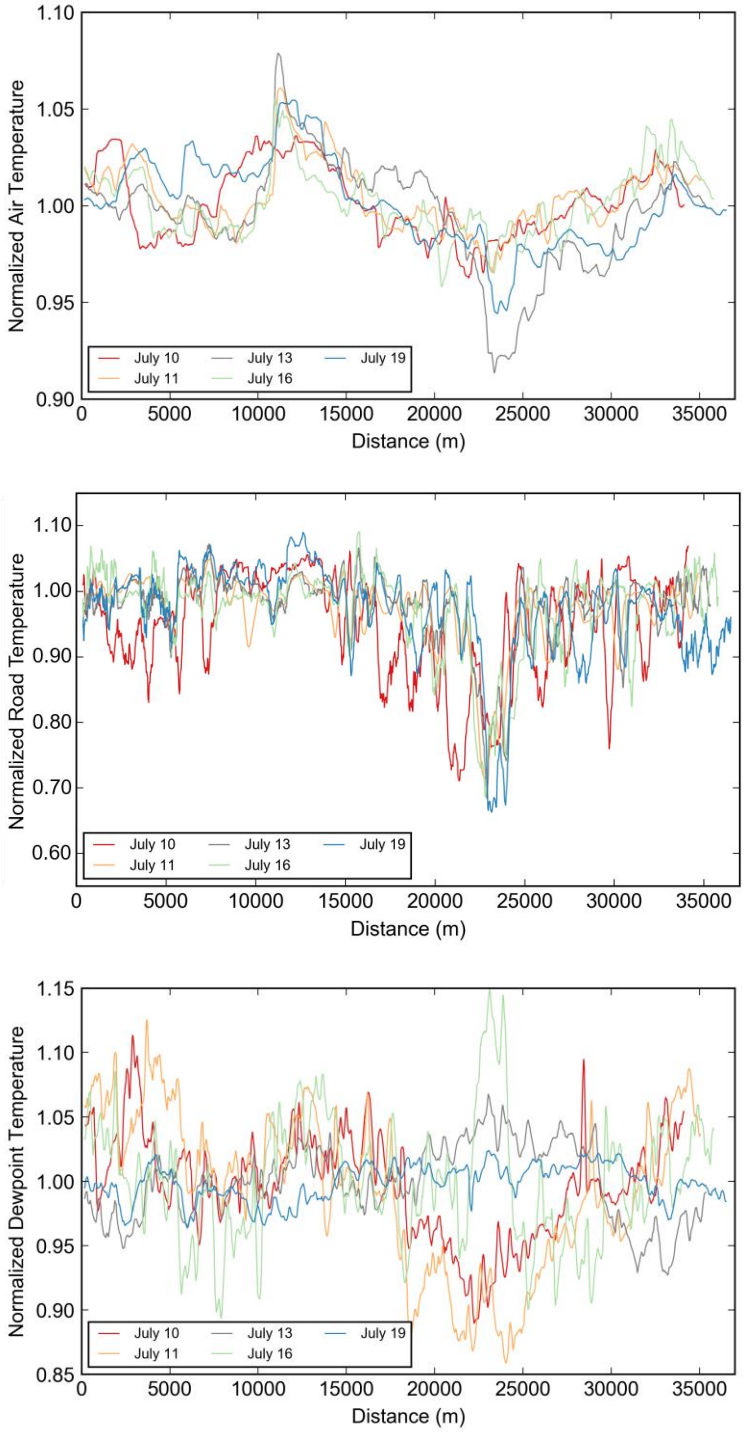

Figure 3-7. Normalized air, road, and dewpoint temperature from route A vehicle traverses. All observations are normalized by the traverse-scale median of the variable of interest.

3.2 Nocturnal Traverse-Scale Observations

Results from three nocturnal traverses are presented in this section. The traverse on July 12th is used as an example to show the intra-urban meteorological variability as it sampled the most intra-urban neighbourhoods and provided insight on the urban-rural contrast in meteorological conditions under ideal UHI conditions. Urban-rural conditions presented in this section are defined as differences between the Downtown neighbourhood and the traversed 'rural' transect along King Rd.

Figure 3-8 shows T_{air} variability observed along a nighttime vehicle traverse. As expected, large urban-rural contrasts in T_{air} exist, with maximum aUHI = 8.3 °C on July 12th. Like daytime T_{air} observations, similar spatial trends are observed between common traverse sections along the same route. The largest observed intra-urban T_{air} range was 5.6 °C (July 12) and the smallest observed intra-urban T_{air} range was 1.4 °C (July 19). As with daytime observations, nocturnal T_{road} shows the largest degree of variability relative to the other observed meteorological variables (Figure 3-9). Observed rUHI are smaller relative to aUHI, where rUHI = 5.1 °C. The largest observed intra-urban T_{road} range was 7.5 °C (July 12) and the smallest observed intra-urban T_{road} range was 3.3 °C (July 19). These dates also coincide with those of the largest and smallest nocturnal T_{air} ranges and is likely linked to cloud cover as according to METAR data, the night of July 19th was significantly cloudier than the night of July 12th, as humidity and wind speed conditions were relatively the same.

Observed urban-rural differences in T_{dew} (ΔT_d) are smaller relative to aUHI and rUHI, where ΔT_d = 0.18 °C on July 12th (Figure 3-10). Furthermore, the intra-urban ranges in nocturnal T_{dew} are similar to the ranges observed during the daytime, as the maximum T_{dew} range observed along a nocturnal traverse was 5.7 °C (July 29th) and the minimum range was 0.7 °C (July 19th). These dates also correspond to days with varying cloud cover.

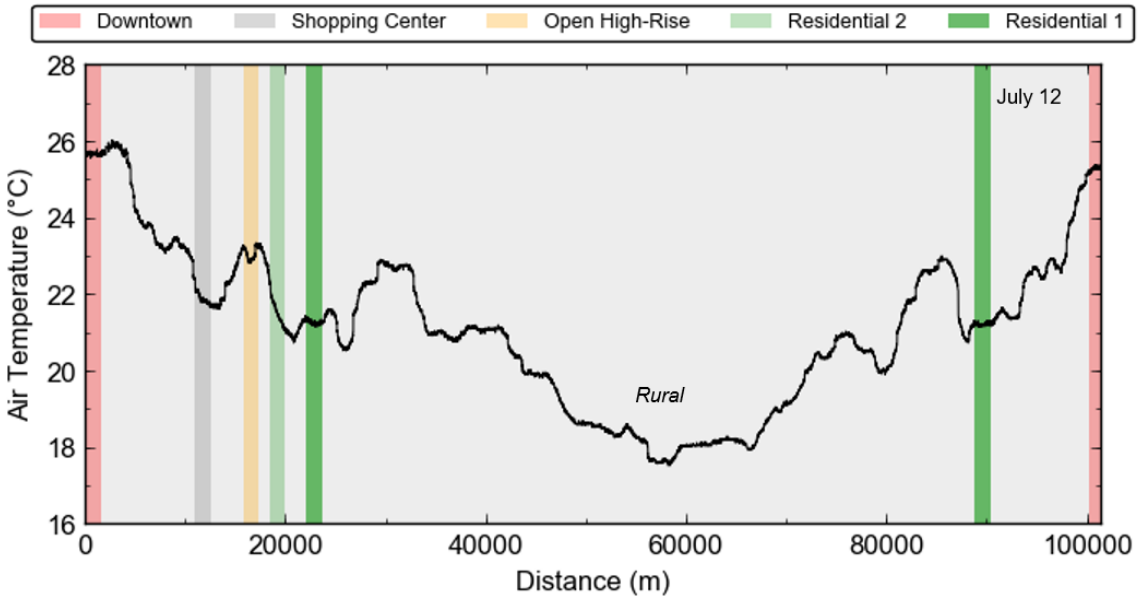

Figure 3-8. Nighttime traverse-scale air temperature variability (Route A - Extended). Med T_{air} = 21.4 °C.

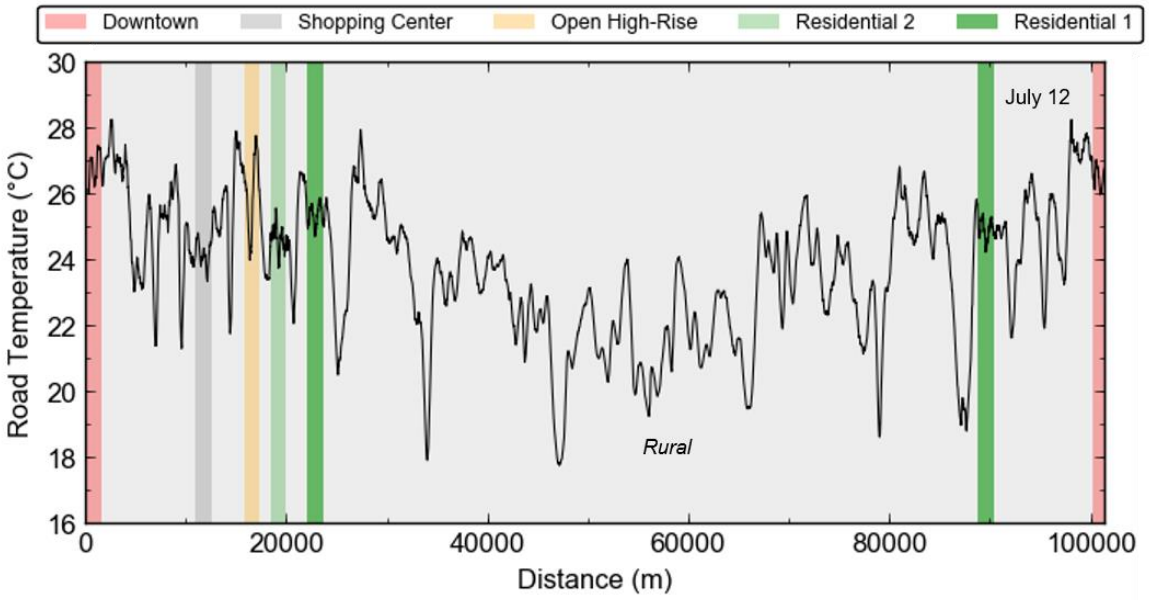

Figure 3-9. Nighttime traverse-scale road temperature variability (Route A - Extended). Med T_{road} = 24.4 °C.

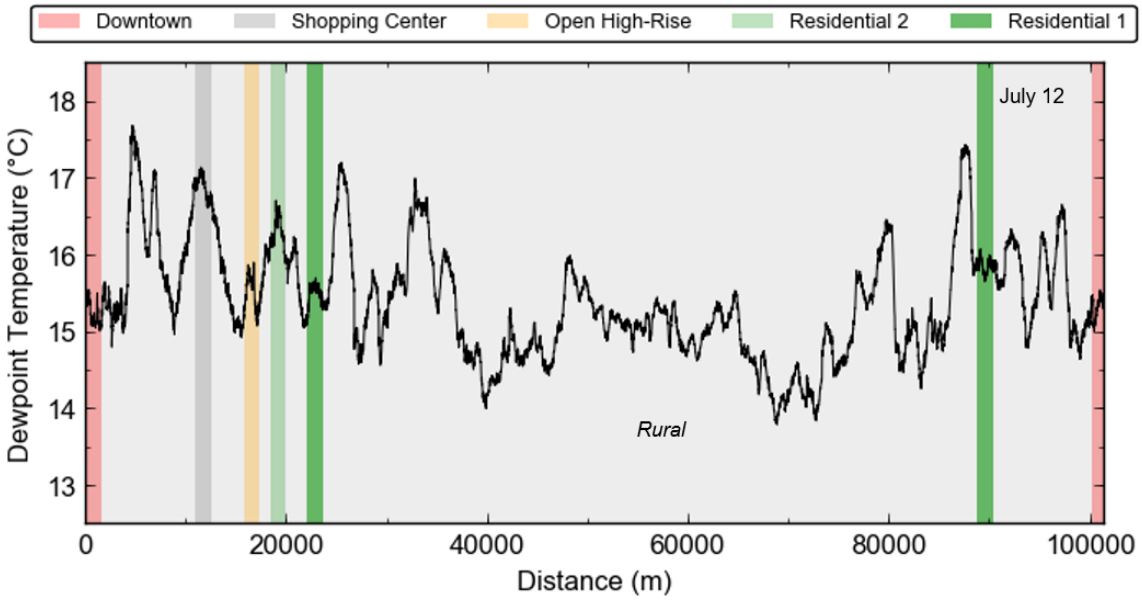

Figure 3-10. Nighttime traverse-scale dewpoint temperature variability (Route A - Extended). Med T_{dew} = 15.4 °C.

3.3 Neighbourhood-Scale Results

The results presented in this chapter show the T_{air}, T_{road}, and T_{dew} differences among the sampled intra-urban neighbourhoods. In total, 8 intra-urban neighborhoods were sampled. From the eligible traverses, route A neighbourhoods were sampled a total of 5 times and route B neighbourhoods were sampled 4 times. Normalized plots are constructed that use the traverse-scale median of each variable. This allows for vehicle traverse observations to be compared on a common scale, and permits observations on different dates, with varying synoptic meteorology, to be assessed. A summary of the neighbourhood-scale results is provided in Appendix B. This appendix contains daytime and nighttime medians of observed T_{air}, T_{road}, T_{dew} for all sampled neighbourhoods. The appendix also provides the T_{air} and T_{dew} conditions reported at Toronto International and Billy Bishop Toronto City Airports.

3.3.1 Daytime Neighbourhood-Scale Results

Boxplots of neighbourhood-scale T_{air}, T_{road}, and T_{dew} from the July 11th vehicle traverse are presented in Figure 3-11. These results reflect the differences commonly observed between neighbourhood distributions of route A. Generally, there is overlap in the observed distributions between the Residential 2 and Open High-Rise, neighbourhoods with Residential 1 for all meteorological variables, while very little overlap exists between Residential 1 and the Downtown and Shopping Center neighbourhoods. Of the three variables, T_{road} shows the most distribution overlap between sampled neighbourhoods. T_{road} distributions, with the exception of the Shopping Centre neighbourhood, also show the largest inter-neighbourhood range in temperature. This range reflects large temperature gradients between fully sunlit and fully shaded regions are observed, and supports previous results from Voogt and Oke (1998) in which T_{road} distributions are typically bi-modal. The anomaly within the Shopping Centre can be explained due to the neighbourhoods large SVF (0.96), in which there is seldom any afternoon shading provided by local buildings or vegetation and thus the distribution of T_{road} predominately represents fully sunlit regions within the neighbourhood.

Statistically, the degree of neighbourhood distribution overlap is reflected in the Mann-Whitney U values. Significant differences (α=0.05) of T_{air} and T_{dew} were found for all neighbourhoods. For $T_{road,}$ non-significant differences are observed between Residential 2, Open High-rise, and Shopping Center neighbourhoods. Complete Mann-Whitney U results are provided in Appendix C.

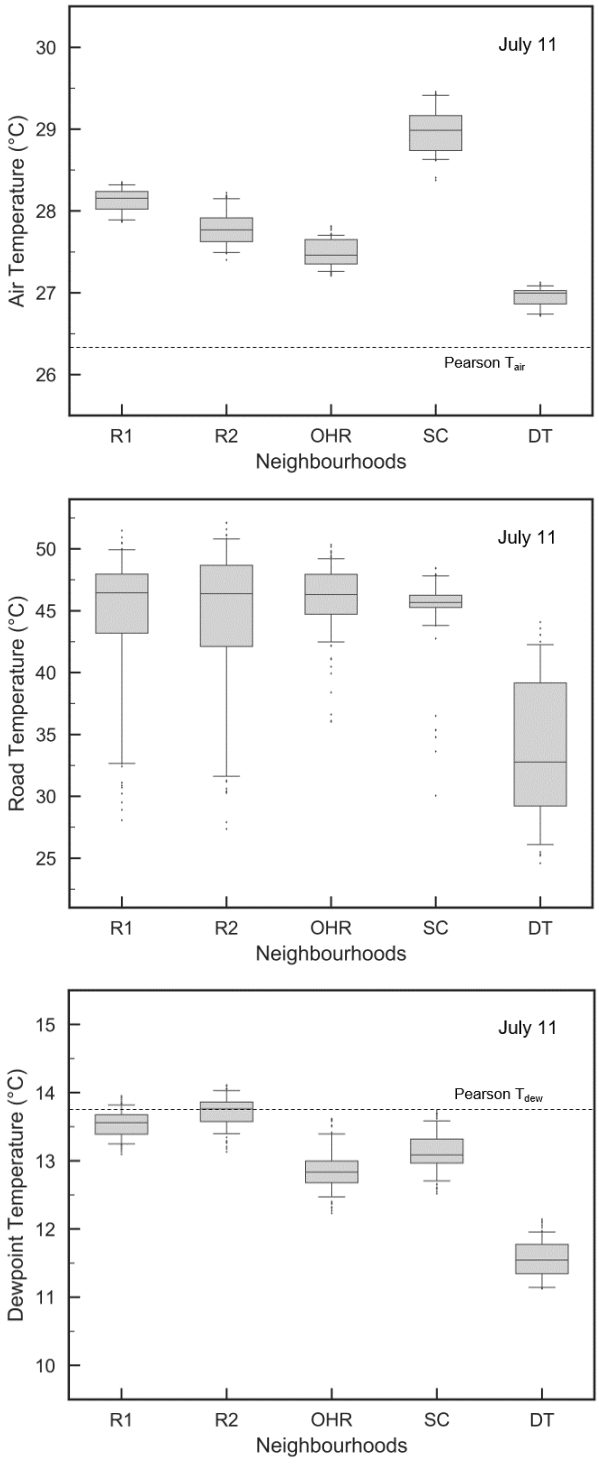

Figure 3-11. Daytime distributions of intra-neighbourhood air, road, and dewpoint temperature on July 11th (Route A). Traverse-scale med T_{air} = 27.7 °C; med T_{road} = 44.9 °C; med T_{dew} =12.7 °C. Neighbourhood medians are represented by the line and box whiskers represent 5th and 95th percentiles. X-axis abbreviations: R1 = Residential 1, R2 = Residential 2, OHR = Open High-Rise, SC = Shopping Centre, DT = Downtown. For reference, reported T_{air} and T_{dew} conditions at YYZ are superimposed (dashed line).

Figure 3-12 shows medians of normalized T_{air}, T_{road}, T_{dew} for all neighbourhoods from the 9 daytime traverses, sampling both routes. Most notable are daytime T_{air} differences between the Shopping Center and the Downtown neighbourhoods relative to the other sampled neighbourhoods, as for all daytime traverses the Downtown neighbourhood shows the lowest observed T_{air}, and for all daytime route A traverses, the Shopping Center experiences the highest T_{air}. As both neighbourhoods are highly urbanized, with building and impervious surface fraction accounting for greater than 90% of the surface cover within each neighbourhood, this difference is likely driven between SVF differences (SVF_{DT} = 0.24 and SVF_{SC} = 0.96) between the neighbourhoods. The relatively small SVF_{DT} reflects the tall urban geometry within the neighbourhood that provide significant shading within the UCL and limits the ability of incident radiation to reach the bottom of the street canyon. Local advection from Lake Ontario also contributes to the low daytime T_{air} within the Downtown neighbourhood. However, when comparing conditions between the Downtown and Moss Park neighbourhoods (i.e. roughly the same distance away from the shoreline), lower T_{air} conditions are observed in the Downtown neighbourhood, suggesting that SVF is the predominate driver.

The small SVF_{DT} also contributes to cool daytime T_{road}. Similar to T_{air}, significant shading within the Downtown neighbourhood contributes to the low observed T_{road} relative to the other neighbourhoods. Additional medians of T_{road} between neighbourhoods show less variability between each other, reflecting that the majority of T_{road} observed within the neighbourhoods represent sunlit locations, yet the long whiskers observed in Figure 3-11 support bi-modal distributions in the Residential neighbourhoods. Similar to traverse-scale results, neighbourhood differences in median T_{dew} shows relatively no consistently between dates. However, for 5 out of 9 traverses, the Downtown neighbourhood experiences the highest T_{dew}, likely due to its proximity to Lake Ontario. Based on vehicle traverse observations, the TPH "high-risk" neighbourhoods of Thorncliffe Park and Moss Park do not show anomalous T_{air}, T_{road}, T_{dew} conditions compared to other sampled intra-urban neighbourhoods. Both neighbourhoods contain a fraction of pervious surface cover (TP = 22%, MP = 15%) which helps alleviate daytime high temperatures via evaporative cooling and provides shade. The forested area surrounding the Thorncliffe Park helps

enhance this effect. Due to the Moss Park's proximity to Lake Ontario, local advection also contributes to moderate T_{air}.

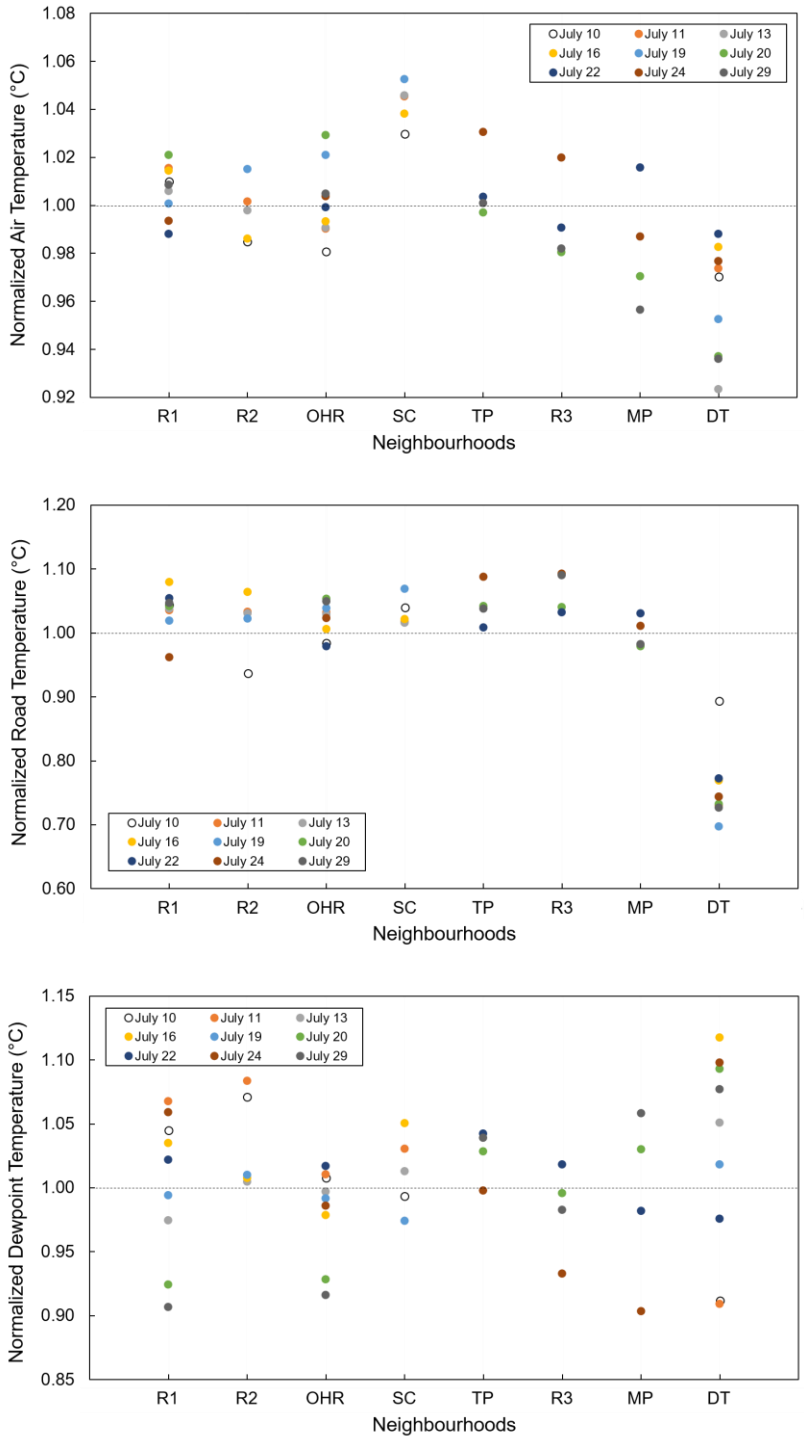

Figure 3-12. Normalized neighbourhood medians of air, road, and dewpoint temperature for all daytime traverses. The normalization uses the traverse-scale median variable of interest. X-axis abbreviations: R1 = Residential 1, R2 = Residential 2, OHR = Open High-Rise, SC = Shopping Centre, TP = Thorncliffe Park, R3 = Residential 3, MP = Moss Park, DT = Downtown.

3.3.2 Nocturnal Neighbourhood-Scale Results

Nocturnal neighbourhood boxplots of T_{air}, T_{road}, and T_{dew} from July 12th are presented in Figure 3-13. These results reflect the differences observed under ideal UHI conditions. For T_{air}, there is generally less overlap between neighbourhood distributions during the nighttime compared to those observed during daytime conditions and no overlap is observed with the Downtown neighbourhood. T_{road} also shows the most overlap between neighbourhood distributions and largest inter-neighbourhood range in temperature, however, the night time temperature range is greatly reduced relative to daytime as the differences between fully shaded and sunlit regions is significantly reduced. T_{dew} shows similar intra-neighbourhood distribution ranges relative to daytime conditions.

All T_{air} and T_{dew} neighbourhoods show significant differences with Residential 1 (reference neighbourhood). For T_{road} non-significant differences are observed between Residential 2, Open-High Rise, and Shopping Centre neighbourhoods. Complete results from the nocturnal Mann-Whitney U test are provided in Appendix C (shaded).

Figure 3-14 shows medians of normalized T_{air}, T_{road}, T_{dew} for all neighbourhoods from two nighttime traverses, sampling route A. Results indicate larger median differences between neighbourhoods during the night as compared to the daytime. Contrary to daytime conditions, T_{air} in the Downtown neighbourhood is the highest, relative to other sampled neighbourhoods. Additional neighbourhoods show less variability between each other with both residential neighbourhoods showing very similar nighttime conditions.

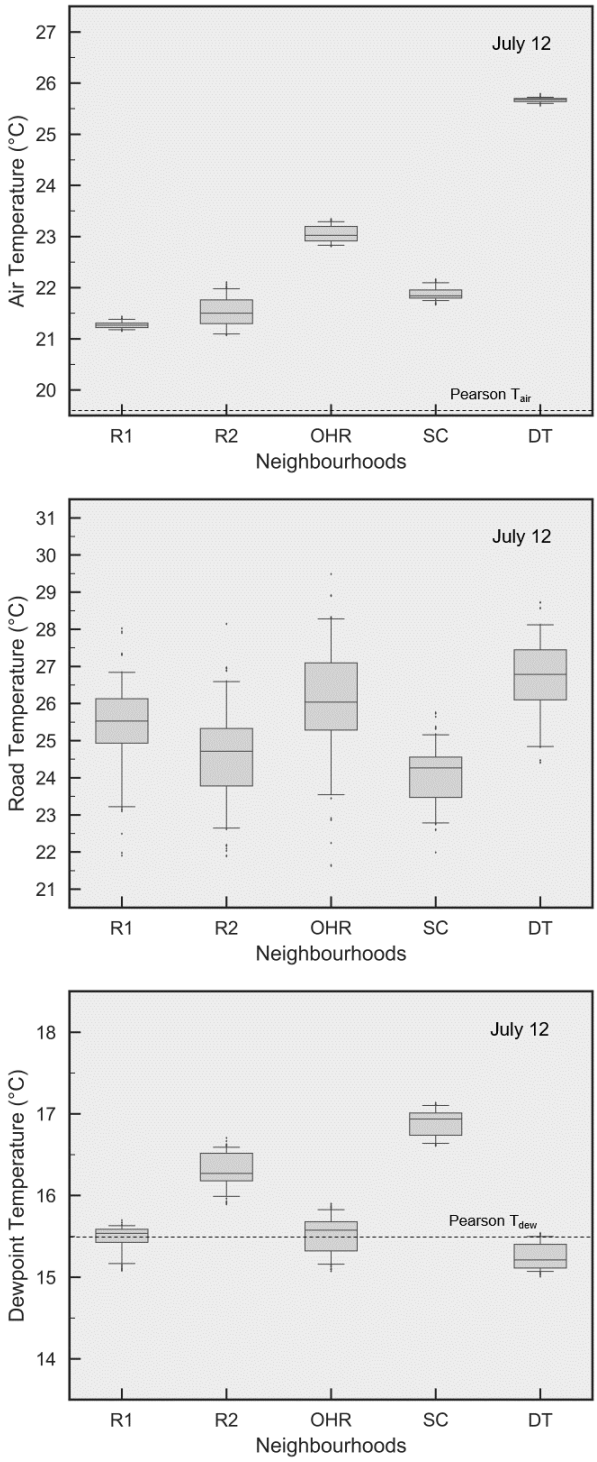

Figure 3-13. Air, road, and dewpoint temperature nocturnal intra-neighbourhood distributions on July 12th (Route A). Traverse-scale med T_{air} = 27.7 °C; med T_{road} = 24.4 °C; med T_{dew} =15.4 °C. See Figure 3-11 for x-axis neighbourhood abbreviation and for box and whisker interpretation.

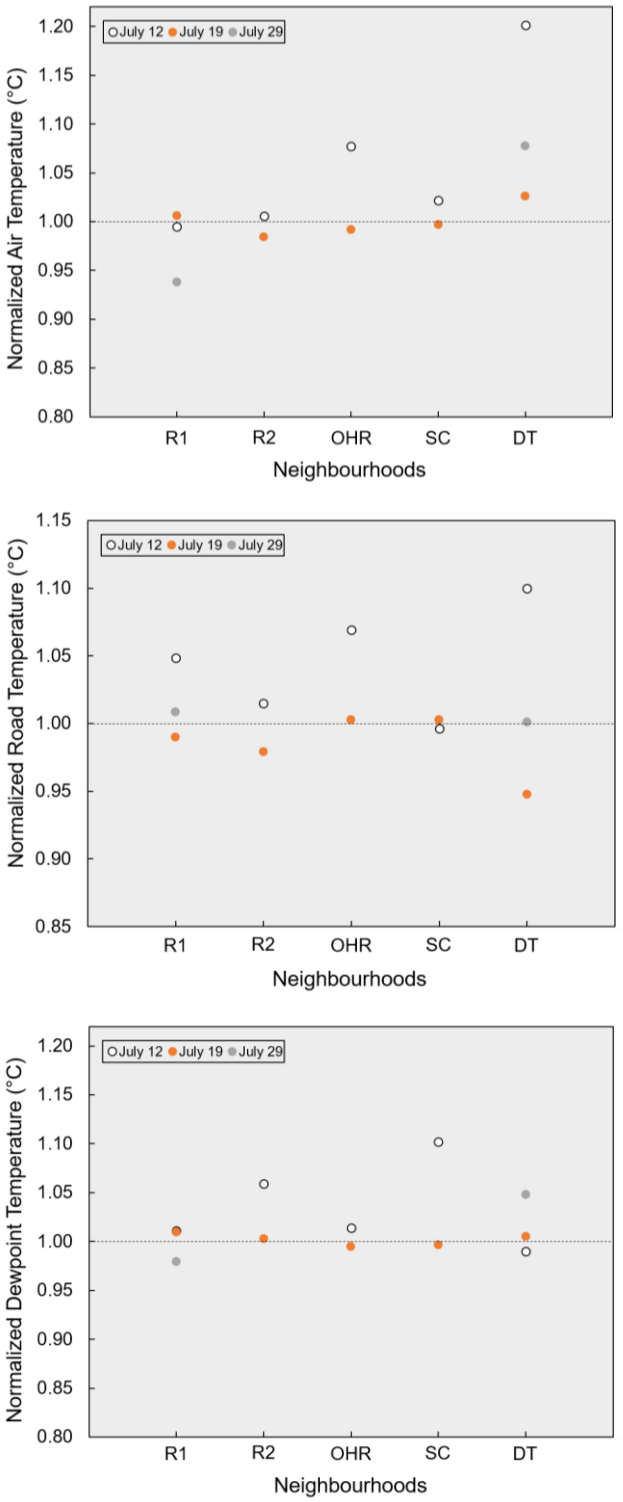

Figure 3-14. Normalized neighbourhood medians of air, road, and dewpoint temperature for all nighttime traverses. See Figure 3-11 for x-axis neighbourhood abbreviations.

3.4 Neighbourhood-Rural Differences

Neighbourhood-rural conditions presented in this section are defined as differences between the traversed urban neighbourhoods and the fixed 'rural' weather station in Claremont, ON, see Section 2.6.

Figure 3-15 shows the neighbourhood-rural differences in T_{air} for daytime and the average differences for nocturnal traverses. Daytime differences are significantly smaller relative to the nighttime, the maximum aUHI is defined with the Shopping Centre neighbourhood ($\overline{\Delta T}$ = 1.9 °C), and Downtown-rural, differences show a 'cool' island on 5 out of 9 traverse dates ($\overline{\Delta T}$ = -0.4 °C). This supports previous work conducted by Runnalls and Oke (2013) where they commonly observed a daytime "cool" island in downtown Vancouver, BC, CA. July 22nd and July 24th show slightly anomalous Downtown-rural differences, these are likely related to high winds speeds on July 22nd (23 km/h) and cloud cover on July 24th (broken, 5-7 oktas), as both are contributing factors in decreasing the T_{air} variability observed along a traverse (i.e. Downtown T_{air} is less differentiated relative to other sampled neighbourhoods). During the nighttime, the maximum aUHI is defined with the Downtown neighbourhood, where $\overline{\Delta T}$ = 9.5 °C. The reversal of the Downtown neighbourhood T_{air} – from coolest during the day to warmest at night – can be linked to differences in canyon geometry between the locations. The relatively small SVF_{DT} decreases the longwave radiation lost during the night, slowing the rate of cooling relative to the 'rural' fixed station with a larger SVF. An association between nocturnal aUHI and cloud cover and windspeed is also observed as magnitudes on July 12th, under 'clear sky' conditions with 11 km/h wind speeds are greater than those observed on July 19th, under 'broken sky' conditions with 14 km/h wind speeds. In general, observed nocturnal maximum aUHI are similar with previous studies in cities of similar size to Toronto (Oke, 1973).

Figure 3-16 shows the neighbourhood-rural differences in T_{dew} for daytime and the average differences for nocturnal traverses. Daytime differences indicate increased rural T_{dew} compared to all sampled neighbourhoods, with differences on average -2 °C. July 20th shows anomalous differences compared to other traverse dates, while meteorological

conditions are relatively similar to other dates, July 20th shows the highest wind speeds (27 km/h) of all traverses and thus increased on-shore winds that provides humid-air masses from Lake Ontario, may be attributed to the increased humid conditions observed Downtown. T_{dew} conditions are reversed at night, and all sampled neighbourhoods show more humid conditions relative to the rural site. These differences are fairly consistent in large cities, and supports previous findings conducted in Chicago, IL, USA (Ackerman, 1987).

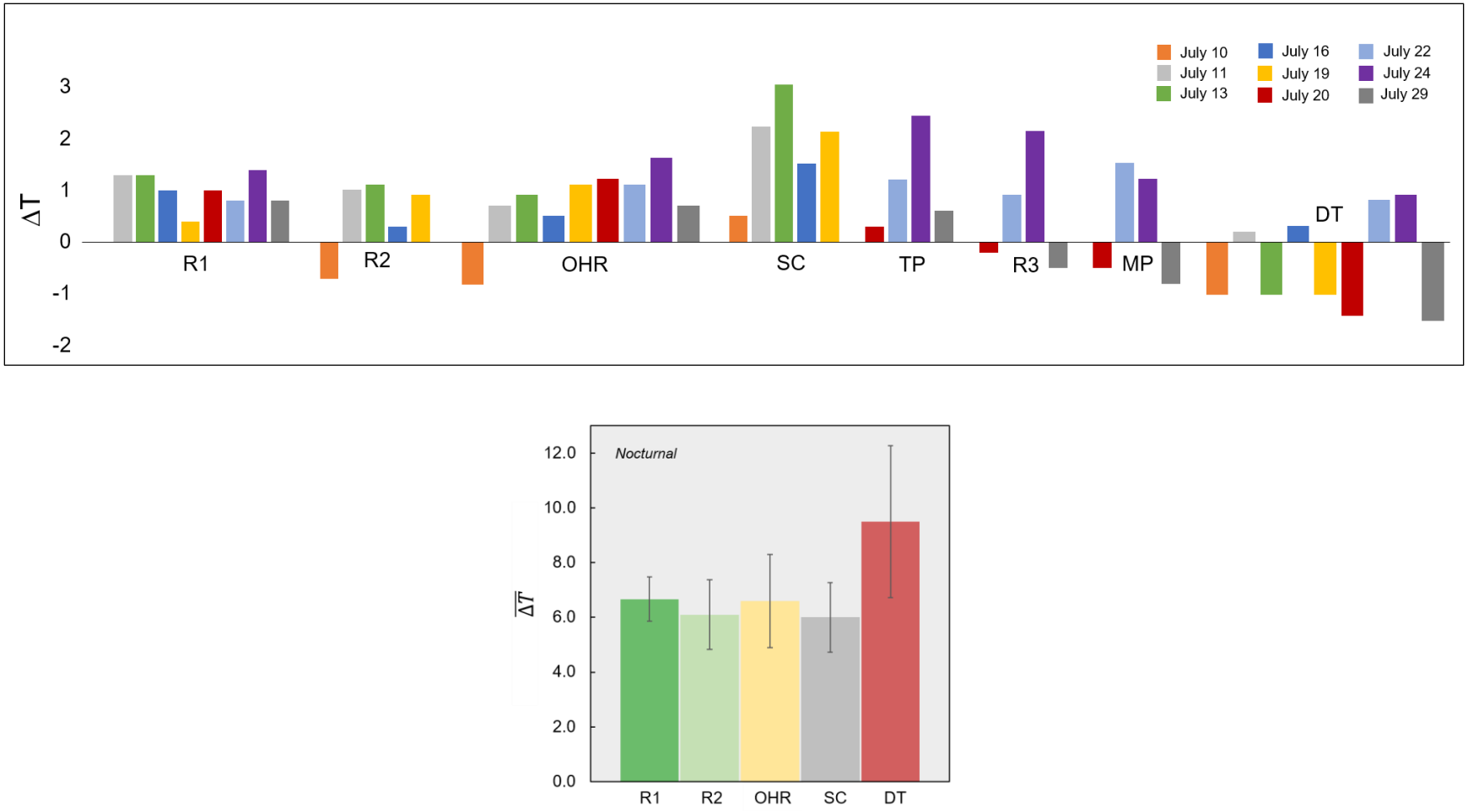

Figure 3-15. Neighbourhood-rural air temperature differences for all traverses (°C). Note: the nocturnal differences represent an average (N=3 for R1 and DT, N=2 for R2, OHR and SC) and differences in the y-axis. Error bars represent ± one standard deviation.

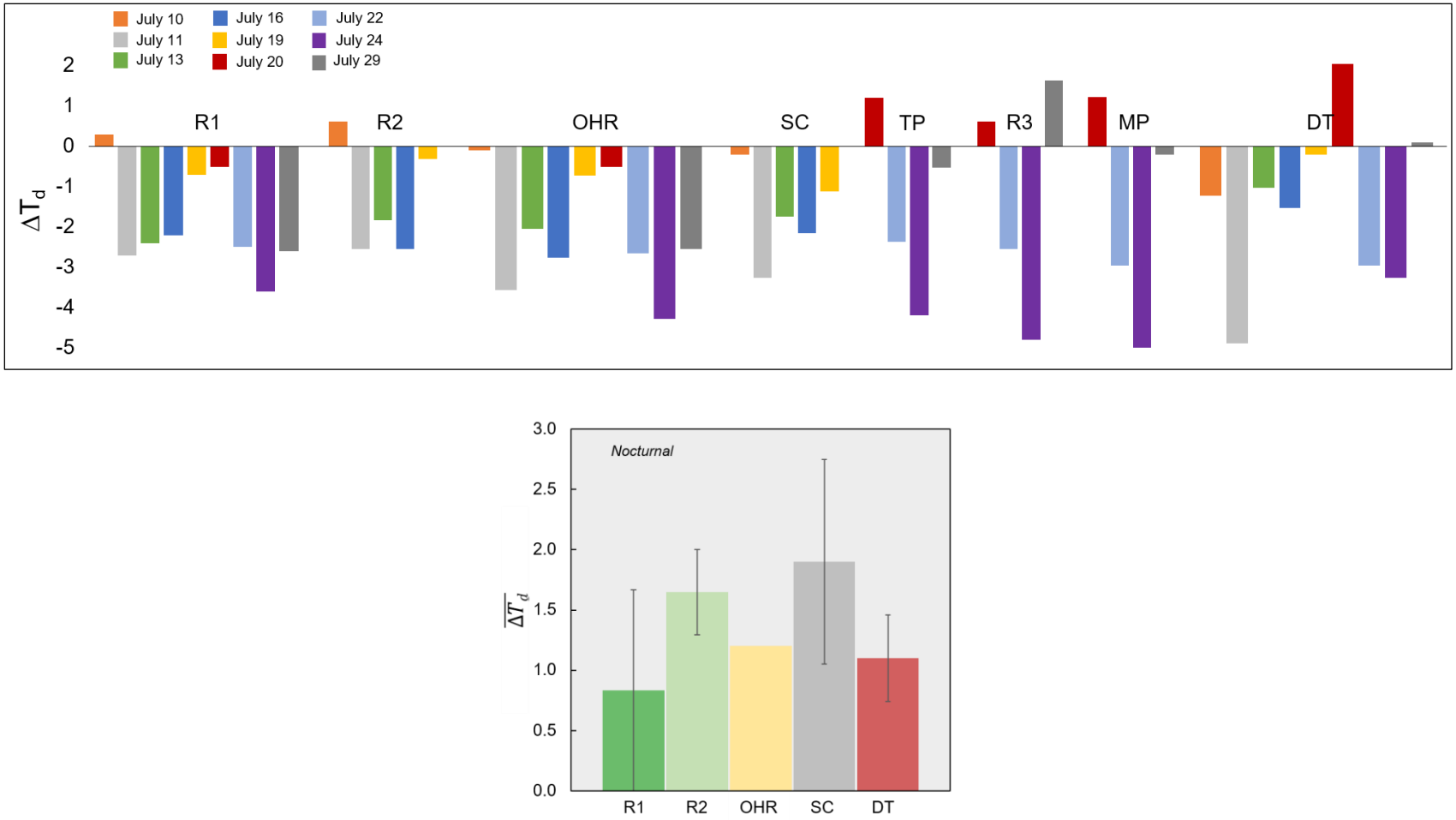

Figure 3-16. Neighbourhood-rural dewpoint temperature differences for all traverses (°C). Note: the nocturnal differences represent an average (N=3 for R1 and DT, N=2 for R2, OHR and SC) and differences in the y-axis. Error bars represent ± one standard deviation.

3.4.1 Fixed Weather Station Comparison

Observed traverse-scale medians of T_{air} exceed reported values from YYZ 10/12 times and 12/12 times from YTZ for all daytime traverses. For T_{dew}, large differences between YYZ and YTZ airports are observed during the daytime, where YTZ significantly over estimates daytime T_{dew}. At night, smaller differences in T_{dew} are observed between fixed stations and YYZ provides generally representative intra-urban conditions. For T_{air}, the differences between neighbourhood observed and reported temperatures from YYZ are generally less than 1°C. Relative to neighbourhood medians, YTZ significantly underestimates T_{air} and T_{dew} daytime and nighttime conditions. Differences experienced between airport locations are strongly linked to the geographical zone in which the weather station is located, as YTZ is located on Toronto Island and thus is fully under the influence of Lake Ontario while YYZ is located on-shore and located in an zone more representative of the traverse routes.

Appendix B provides a full list of neighbourhood medians and reported YYZ and YTZ conditions.

3.5 Chapter Summary

This chapter presents the findings from 12 eligible vehicle traverses that met the required meteorological criteria. Results indicate significant intra-urban differences in T_{air}, T_{road}, and T_{dew} along both daytime and nocturnal traverses. Observations of T_{road} showed the greatest variability, by far, along a traverse compared to T_{air} and T_{dew} observations. Two routes (A and B) sampled a total of 8 different intra-urban neighbourhoods, including the Thorncliffe Park and Moss Park 'high-risk' neighbourhoods. Of the sampled neighbourhoods, the Downtown and Shopping Center show the largest daytime T_{air} differences compared to other neighbourhoods, with Downtown showing the coolest T_{air}; this is reversed at night when observed T_{air} Downtown is the warmest. Furthermore, results from the vehicle traverse observations show that the Thorncliffe Park and Moss Park neighbourhoods do not show anomalous meteorological conditions relative to other sampled intra-urban neighbourhoods. T_{air} urban-rural differences, defined with the Claremont rural station, show a daytime 'cool island' with Downtown on 5 out of 9 traverse dates. All other sampled neighbourhoods show a daytime heat island on average less than

2 °C. A large heat island is observed during the nighttime, and the average maximum heat island = 9.5 °C, defined using Downtown. T_{dew} urban-rural differences, show moister rural conditions during the daytime relative to intra-urban conditions, and drier rural conditions during the nighttime.

Further results indicate that the YYZ fixed weather station provides more representative intra-urban conditions than the YTZ weather station, as the YTZ station significantly underestimates T_{air} and overestimates T_{dew} for both daytime and nighttime conditions. At the neighbourhood scale, daytime YYZ T_{air} and T_{dew} conditions most closely characterize the Residential and Open High-Rise neighbourhoods, while YTZ underestimates both T_{air} and T_{dew} daytime and nighttime conditions and more closely resembles conditions observed in the Downtown neighbourhood.

Chapter 4

4 GEM-LAM Model Evaluation

The GEM-LAM model was evaluated against 11 vehicle traverses – 9 daytime and 2 nighttime. All modeled output was provided by Environment Canada; see Section 2.8.1 for a complete description of how model outputs were obtained and analyzed. This chapter addresses research question 4. It follows a similar organization to Chapter 3, with traverse-scale results described first, followed by the neighbourhood scale. Day and night results are separated at each scale. The chapter concludes with a summary that highlights the key results.

Table 4-1 provides the modeled output times, modeled traverse-scale medians of T_{air} and $T_{dew,}$ and differences between the medians of modeled outputs and vehicle traverse observations. The table also provides modeled rural values defined as the pixel T_{air} and T_{dew} value at the Claremont station location used to assess daytime and nocturnal urban-rural differences. As reflected in the table, under both daytime and nighttime conditions, modeled median T_{air} generally underestimates observed median T_{air} from the vehicle traverses, with the largest difference of 3.1 ºC (July 19th) and smallest difference of 0.2 ºC (July 11th and July 24th). For T_{dew}, modeled outputs overestimated T_{dew} relative to the vehicle traverse observations 9 of 11 times.

Figure 4-1 compares modeled and observed T_{air} and T_{dew} for all evaluated vehicle traverses. Model performance statistics (Table 4-2) shows good agreement between GEM-LAM outputs and traverse observations.

Table 4-1. Traverse-scale summary results of the GEM-LAM modeled output for all daytime and nighttime (shaded) traverses. Note: traverse-scale medians from vehicle traverse observations are provided in Table 3-1.

Date (2015)	Output time (EDT)	Med mod T_{air} (ºC)	ΔT_{air} (mod-obs)	Med mod T_{dew} (ºC)	ΔT_{dew} (mod-obs)	Mod rural T_{air} (ºC)	Mod rural T_{dew} (ºC)
July 10	15:15	25.7	-0.7	13.2	1.7	23.2	16.5
July 11	13:30	27.5	-0.2	13.9	1.2	25.5	16.1
July 12	1:15	21.1	-0.3	17.4	2.0	18.4	16.7
July 13	13:15	26.6	-1.1	17.8	0.1	26.0	18.7
July 16	13:45	21.9	-0.8	9.7	1.0	19.9	11.3
July 19	13:15	27.9	-3.1	23.4	2.1	28.9	23.2
July 19	1:15	23.5	-1.6	20.6	-0.2	19.3	19.2
July 20	14:00	26.8	-1.8	16.1	-0.2	25.1	18.0
July 22	14:00	24.8	-0.7	9.4	0.5	21.4	10.9
July 24	14:00	27.8	-0.2	9.0	0.1	27.8	9.2
July 29	13:45	31.3	-1.0	18.4	2.1	31.0	14.3

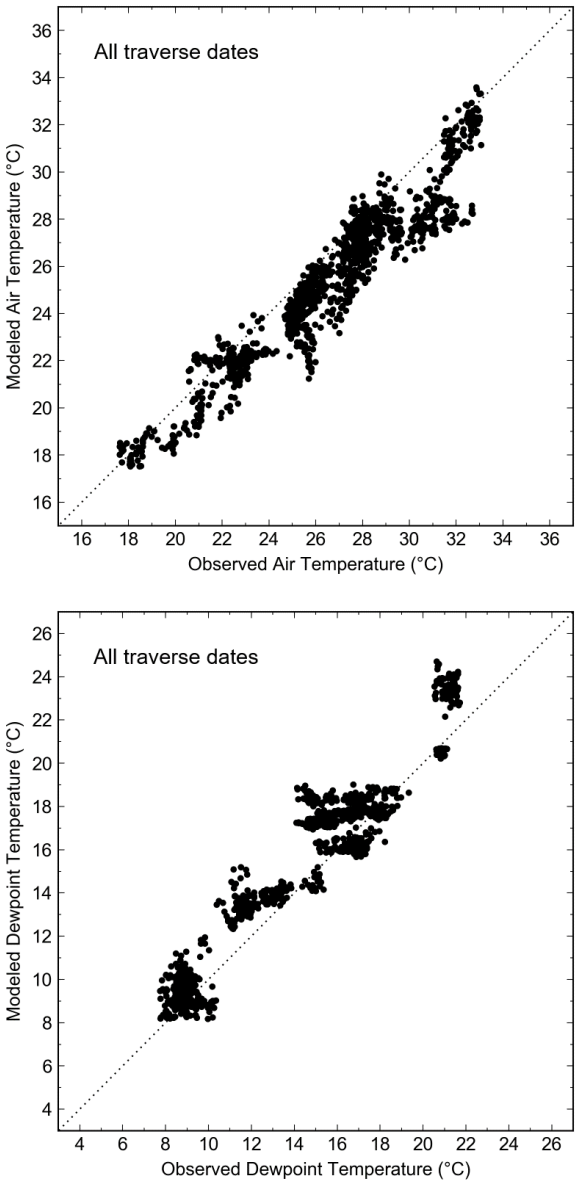

Figure 4-1. Modeled versus observed air and dewpoint temperature for all vehicle traverses. Dashed line represents the line of equality (1:1 line).

Table 4-2. Statistical performance summary of air temperature and dewpoint temperature for all 12 vehicle traverses. N = 1211.

Variable	**Slope**	**Intercept (ºC)**	**R^2**	**MAE (ºC)**	**RMSE (ºC)**	**$RMSE_s$ (ºC)**	**$RMSE_u$ (ºC)**	**d_r**
T_{air}	0.902	1.464	0.907	1.231	1.563	1.180	1.025	0.988
T_{dew}	0.989	1.138	0.928	1.210	1.517	0.975	1.163	0.985

4.1 Daytime Traverse-scale Model Evaluation

Two examples of modeled T_{air} and T_{dew} output from a daytime traverse (July 11) are shown in Figure 4-2 and Figure 4-3. Included in both figures is the vehicle traverse route overlaid in black. In general, for days with a lake-breeze present, it is common to observe T_{air} gradients of several degrees from the shore to the lake-breeze front. Whereas daytime modeled T_{dew} shows less consistent intra-urban spatial patterns, patterns are observed in highly vegetated areas around the study site and along the Don River.

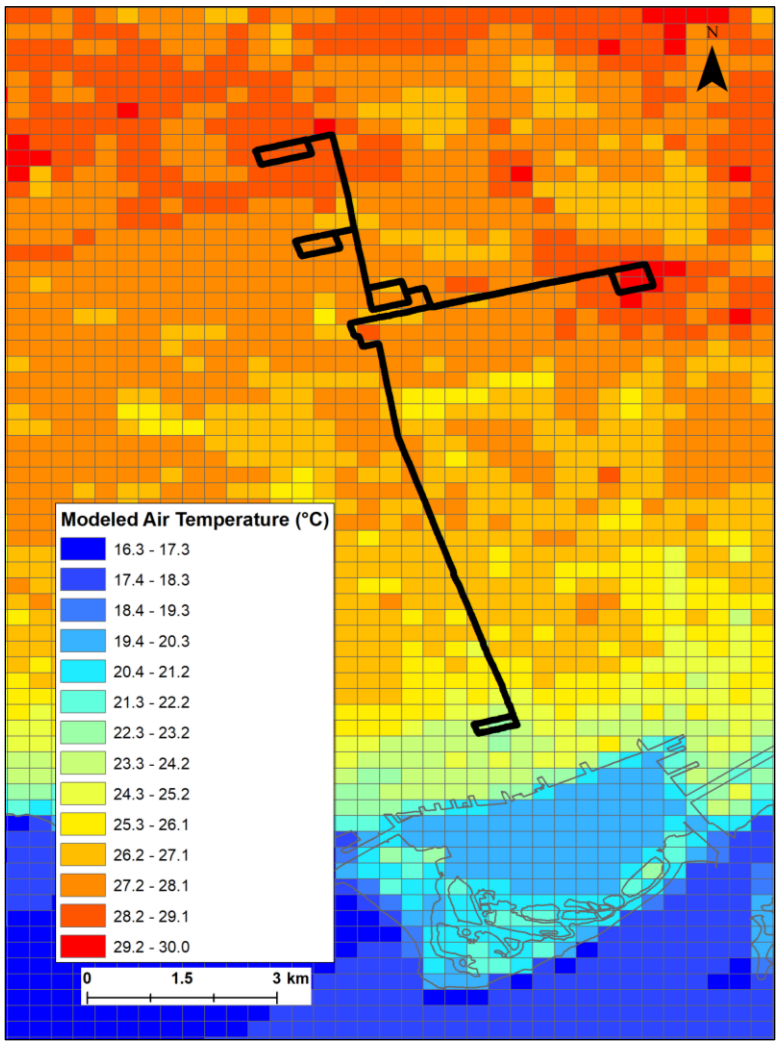

Figure 4-2. GEM-LAM modeled air temperature output on July 11, 13:30 EDT. Output represents 250 m resolution.

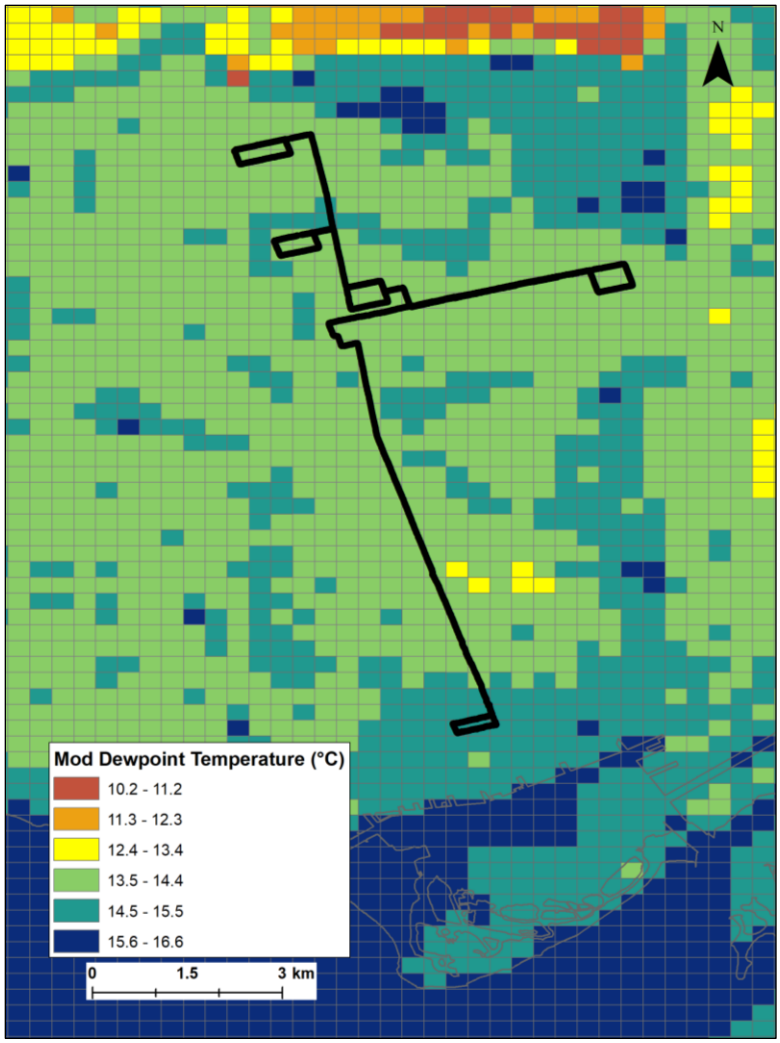

Figure 4-3. Modeled dewpoint temperature output on July 11, 13:30 EDT (250 m resolution).

Figure 4-4 to Figure 4-7 provide the results from the daytime traverse-scale scatterplots between observed and modeled T_{air} and T_{dew}. Each point represents a modeled output value for a pixel and a median observed value from the vehicle traverse observations within that pixel (N=5 threshold). Model performance statistics are given in Table 4-3 and Table 4-4.

A positive correlation in T_{air} is observed for all daytime traverses with a slope, in general, close to 1. The largest differences between modeled and observed occur in the Downtown neighbourhood. For other neighbourhoods, from both routes, the model shows good agreement with the vehicle traverse observations. Six of nine traverses show a negative intercept, highlighting the warm bias experienced by the vehicle traverse observations.

Examination of RMSE values associated with T_{air}, indicate that systematic error accounts for a larger percentage of error than unsystematic (or random) error. The underestimation in modeled T_{air} may be attributed to GEM-LAM's ability to represent Q_F (anthropogenic heat flux) relative to the vehicle traverse observations, as especially in the Downtown neighbourhood, Q_F may be a significant contributor to increased T_{air}.

For T_{dew}, a positive correlation is not consistently observed; on 5 daytime traverses a negative correlation was found and on traverse dates July 11th and July 24th, no correlation was observed. Furthermore, the agreement between model and observed neighbourhoods is shown to be very case dependent. For example, on July 19th and July 29th, the downtown neighbourhood shows the best agreement with the vehicle traverse observations, relative to the other neighbourhoods, however on July 11th and July 22nd, the downtown neighbourhood shows the worst agreement. Contrary to T_{air}, all intercepts from the T_{dew} comparison are positive, yet like T_{air}, the systematic error accounts for a larger percentage of error than unsystematic error when examining RMSE values.

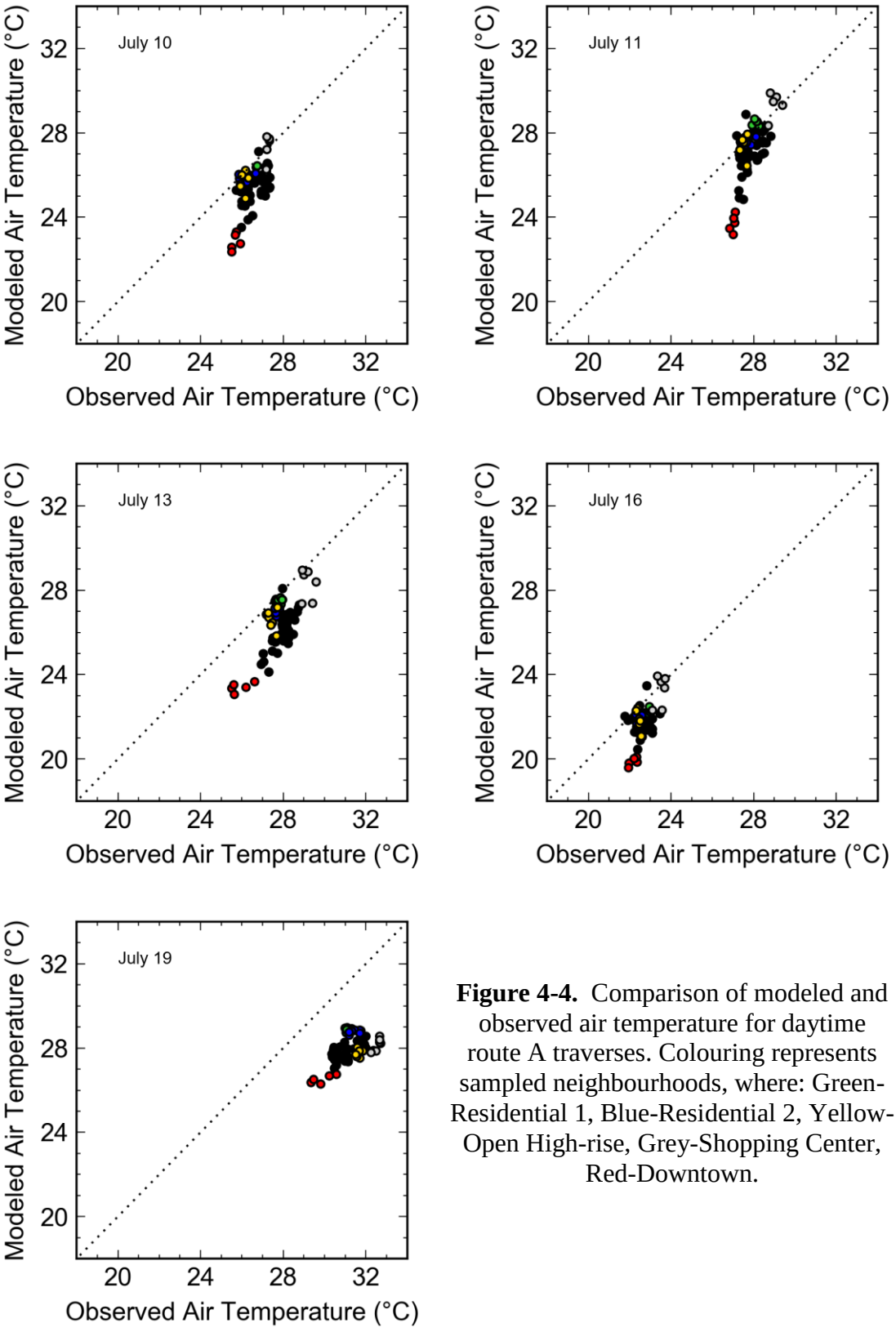

Figure 4-4. Comparison of modeled and observed air temperature for daytime route A traverses. Colouring represents sampled neighbourhoods, where: Green-Residential 1, Blue-Residential 2, Yellow-Open High-rise, Grey-Shopping Center, Red-Downtown.

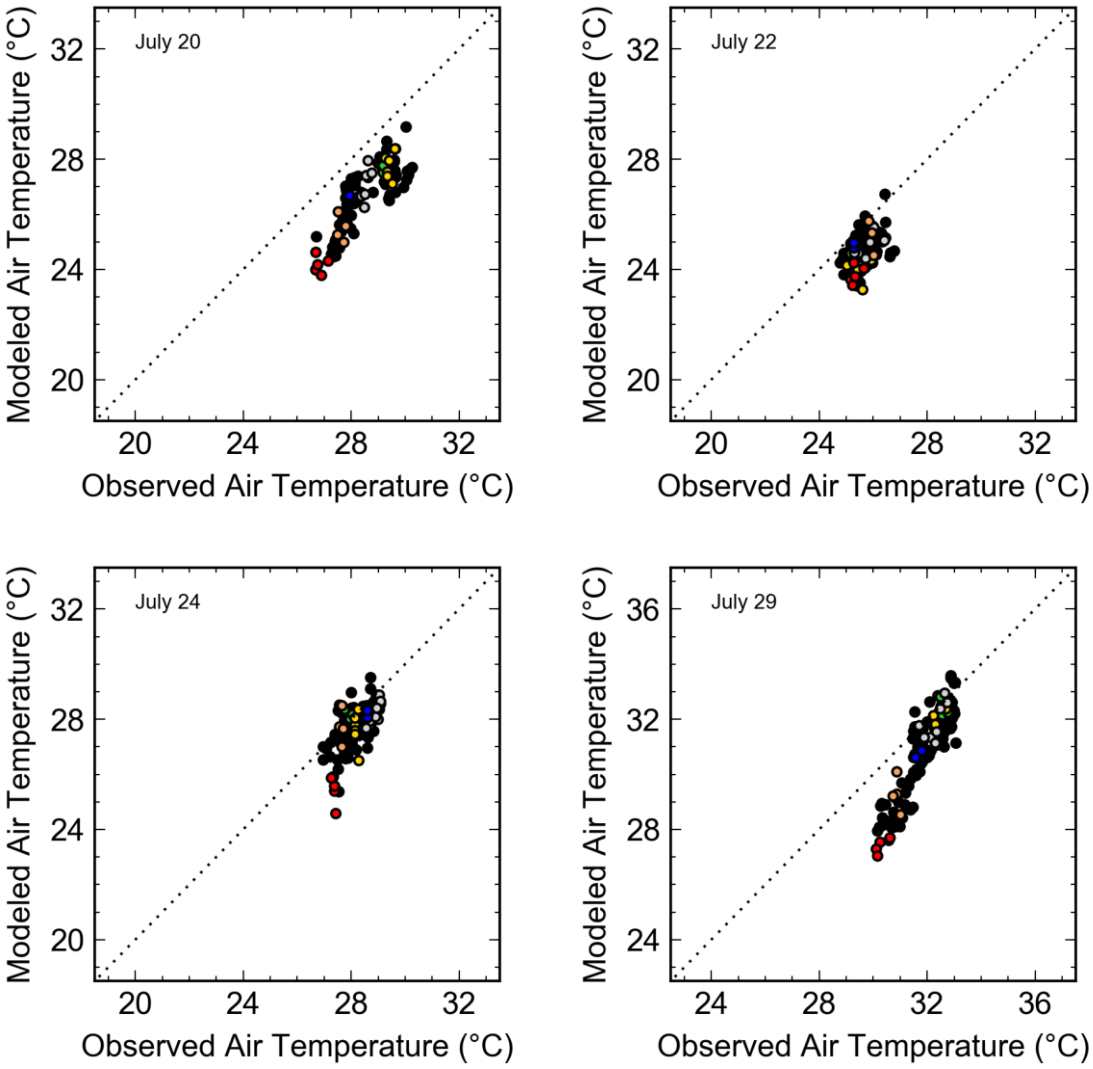

Figure 4-5. Comparison of modeled and observed air temperature for daytime route B traverse dates. Colouring represents sampled neighbourhoods, see Figure 4-4.

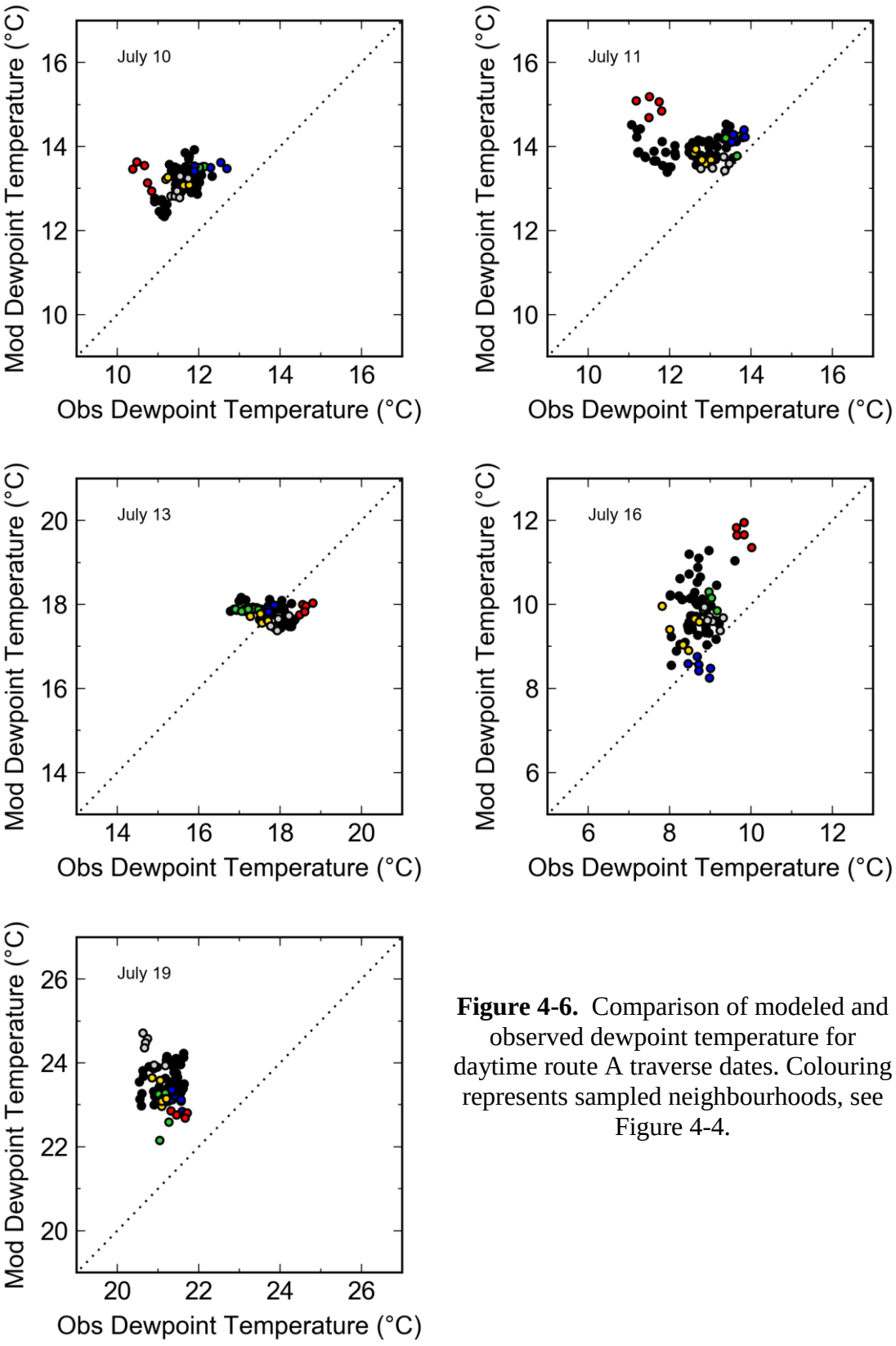

Figure 4-6. Comparison of modeled and observed dewpoint temperature for daytime route A traverse dates. Colouring represents sampled neighbourhoods, see Figure 4-4.

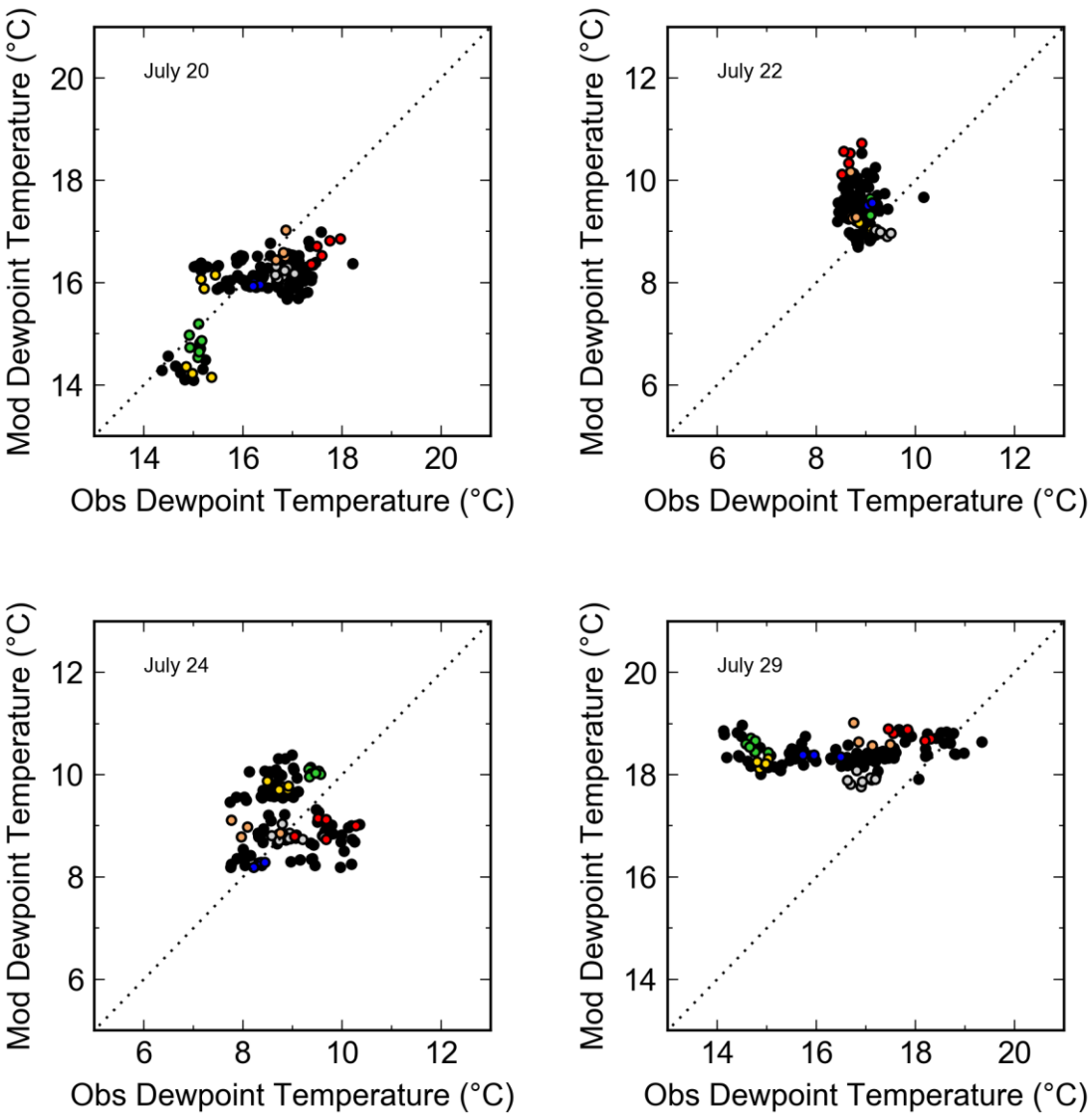

Figure 4-7. Comparison of modeled and observed dewpoint temperature for daytime route B traverse dates. Colouring represents sampled neighbourhoods, see Figure 4-4.

Table 4-3. Statistical performance summary of air temperature from all daytime traverses.

Date	Slope	Intercept (ºC)	R^2	MAE (ºC)	RMSE (ºC)	$RMSE_s$ (ºC)	$RMSE_u$ (ºC)	d_r
July 10 (n=76)	1.089	-3.318	0.322	1.014	1.284	0.964	0.848	0.474
July 11 (n=81)	1.674	-19.322	0.461	0.764	1.147	0.659	0.939	0.099
July 13 (n=82)	1.229	-7.787	0.545	1.416	1.630	1.421	0.798	-0.316
July 16 (n=82)	1.047	-1.841	0.295	0.822	1.008	0.775	0.645	-0.201
July 19 (n=81)	0.491	12.621	0.310	3.259	3.317	3.278	0.507	-0.660
July 20 (n=130)	1.011	-2.108	0.667	1.785	1.891	1.786	0.623	0.500
July 22 (n=125)	0.571	10.140	0.156	0.852	1.004	0.857	0.523	0.493
July 24 (n=127)	0.883	2.883	0.331	0.570	0.752	0.405	0.633	0.448
July 29 (n=129)	1.730	-24.138	0.825	1.056	1.326	1.151	0.654	0.526

Table 4-4. Statistical performance summary for dewpoint temperature from daytime traverses.

Date	Slope	Intercept (ºC)	R^2	MAE (ºC)	RMSE (ºC)	$RMSE_s$ (ºC)	$RMSE_u$ (ºC)	d_r
July 10 (n=76)	0.345	9.171	0.182	1.606	1.663	1.632	0.322	-0.575
July 11 (n=81)	-0.046	14.572	0.008	1.361	1.637	1.592	0.380	-0.027
July 13 (n=82)	-0.113	19.790	0.074	0.425	0.523	0.493	0.175	0.378
July 16 (n=82)	0.776	3.071	0.181	1.154	1.323	1.117	0.708	-0.431
July 19 (n=81)	-0.382	31.573	0.0618	2.269	2.354	2.309	0.461	-0.776
July 20 (n=130)	0.541	7.129	0.473	0.625	0.730	0.543	0.489	0.567
July 22 (n=125)	-0.294	12.067	0.0364	0.625	0.770	0.656	0.403	-0.311
July 24 (n=127)	-0.012	9.283	0.000	0.800	0.931	0.697	0.618	0.206
July 29 (n=129)	0.0299	17.914	0.022	1.955	2.302	2.880	0.256	0.090

4.2 Nocturnal Traverse-scale Model Evaluation

Examples of modeled T_{air} and T_{dew} outputs from the July 12th, extended night traverse, is shown in Figure 4-8 and Figure 4-9, with the vehicle traverse route overlaid in black. The maximum magnitude of $aUHI_{mod}$ (4.0 °C), defined as Downtown-Rural Transect, is about half that observed from the vehicle traverses. For nocturnal T_{dew}, less variability is captured by the model relative to T_{air}, the urban-rural difference in modeled T_{dew} is 0.2 °C. Similar to daytime $T_{dew,}$ large nocturnal spatial patterns are observed. Using Figure 4-8 as an example, a similar spatial pattern (as observed during the daytime) along the Don River and parks surrounding the Shopping Centre neighbourhood is present. Additionally, west of the traverse route, a similar spatial pattern is present along the Humber River and Lambton Golf and Country Club.

Figure 4-10 shows traverse-scale scatterplots between observed and modeled T_{air} and T_{dew} for two-night traverses in which model output was provided. Model performance statistics are provided in Table 4-5 and Table 4-6. Note the differences in routes between the two dates, July 12th sampled the extended UHI route, N = 217 and July 19th sampled route A, N = 81. Similar to daytime modeled T_{air}, there appears to be a warm bias in observed T_{air}, most evident during the night of July 19th. In addition, the largest differences between modeled and observed T_{air} occur in the Downtown neighbourhood, whereas other neighbourhoods (including the Rural Transect) show better agreement with the vehicle traverse observations. Unlike daytime modeled T_{air}, where a positive correlation was observed for all traverses, a negative correlation is observed on the night of July 19th. Furthermore, nocturnal RMSE values, are similar to daytime values.

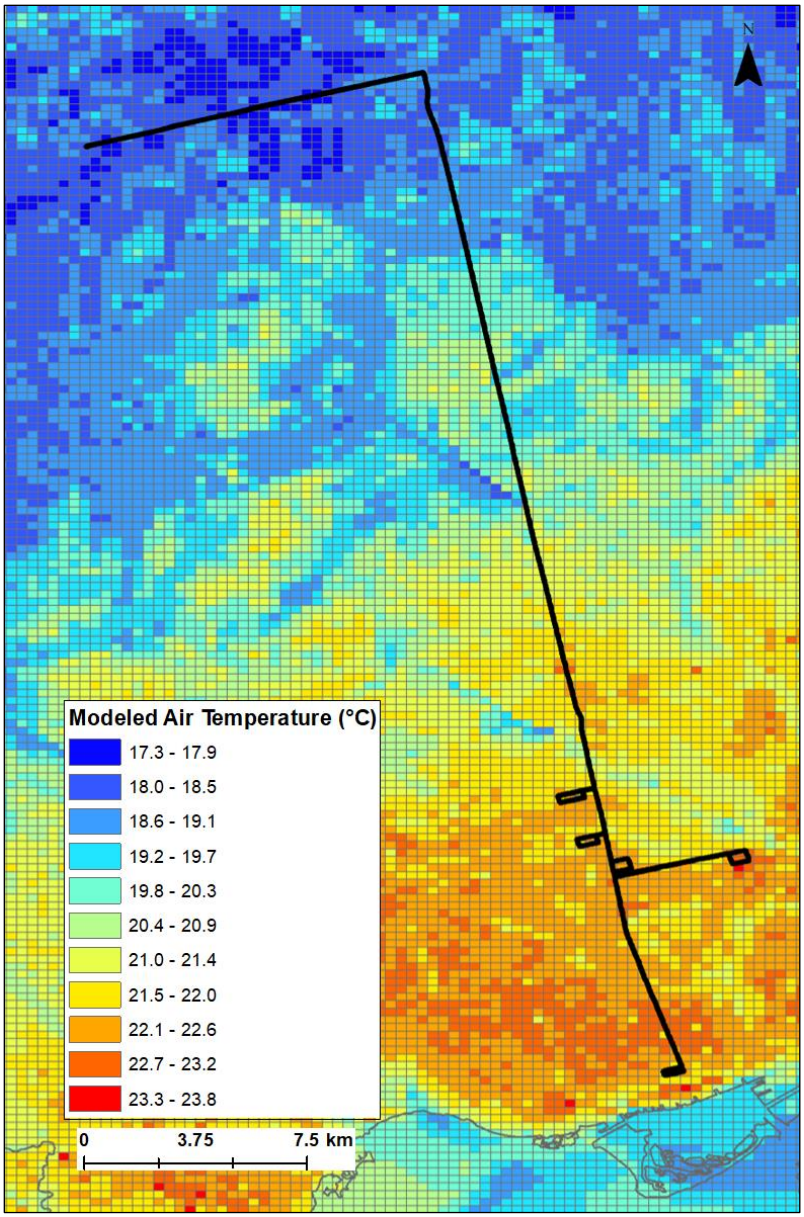

Figure 4-8. Modeled GEM-LAM air temperature output on July 12, 1:15 EDT.

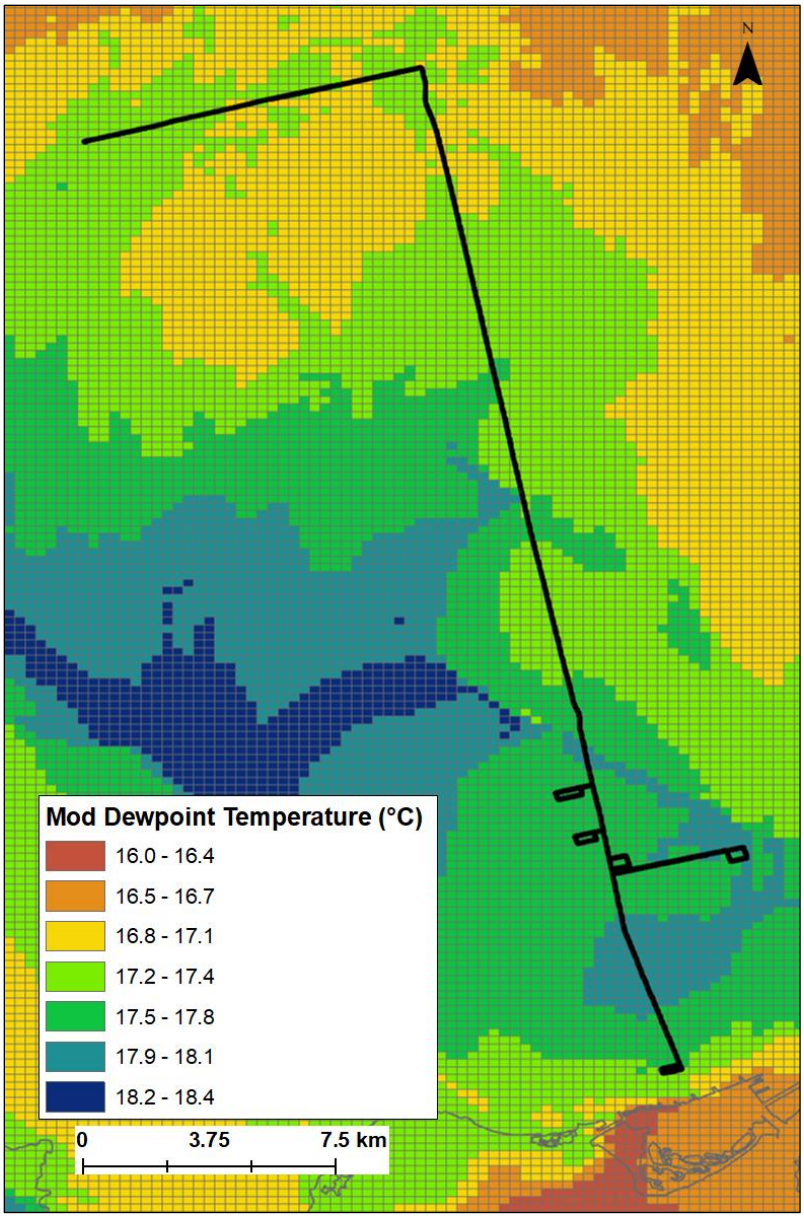

Figure 4-9. Modeled GEM-LAM dewpoint temperature output on July 12, 1:15 EDT.

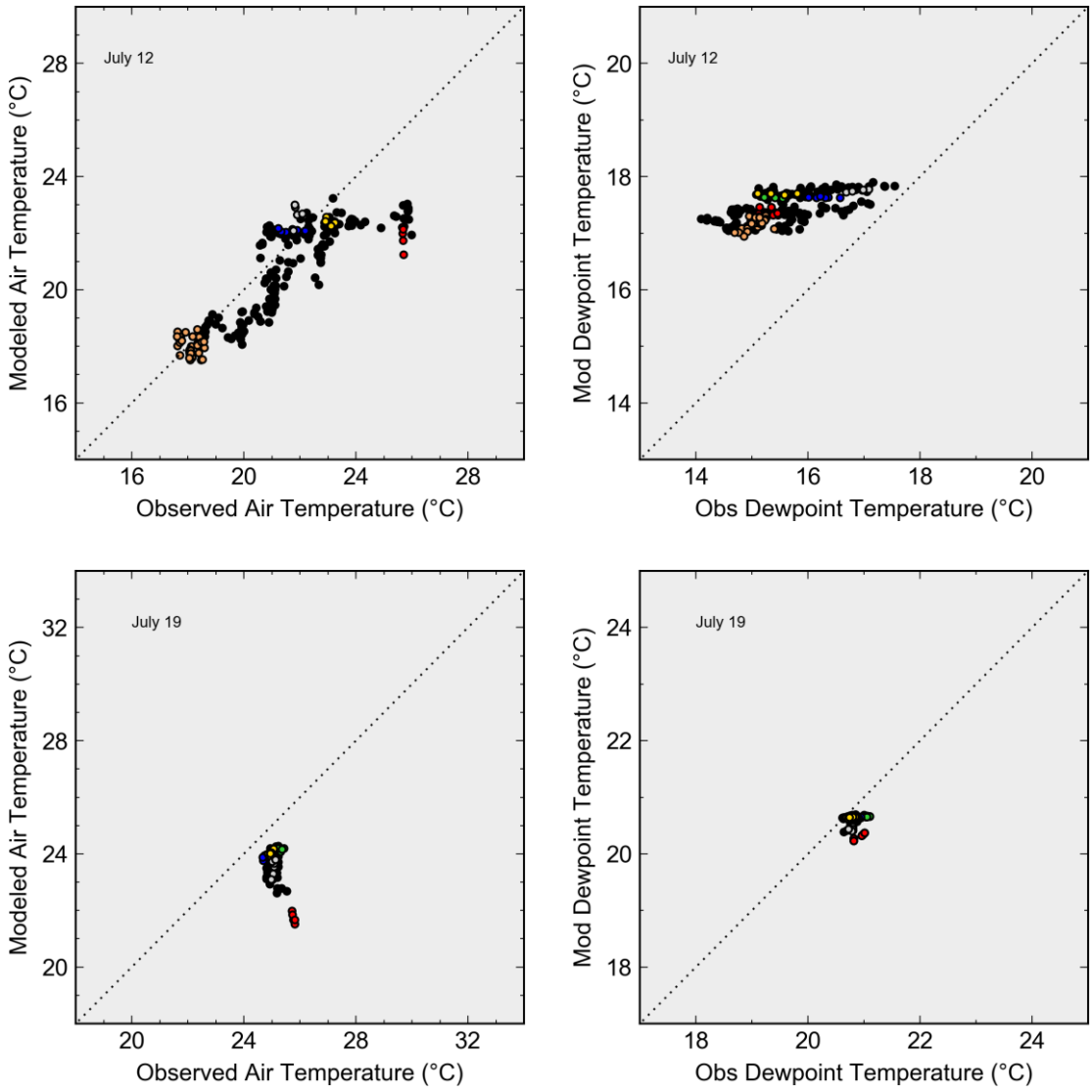

Figure 4-10. Comparison of modeled and observed air and dewpoint temperature for two nocturnal traverses. Colouring represents sampled neighbourhoods, where: *Green-Residential 1, Yellow-Open High-rise, Grey-Thorncliffe Park, Blue-Residential 3, Orange- Moss Park, Red-Downtown.* Note: rural transect points for July 12th are coloured in orange.

Table 4-5. Nocturnal traverse air temperature statistical performance summary.

Date	Slope	Intercept	R^2	MAE	RMSE	$RMSE_s$	$RMSE_u$	d_r
July 12 (n=217)	0.682	6.05	0.715	1.052	1.350	0.999	0.907	0.704
July 19 (n=81)	-1.287	55.77	0.284	1.573	1.746	1.671	0.504	0.500

Table 4-6. Nocturnal traverse dewpoint temperature statistical performance summary.

Date	Slope	Intercept	R^2	MAE	RMSE	$RMSE_s$	$RMSE_u$	d_r
July 12 (n=217)	0.219	14.02	0.404	1.897	1.990	1.980	0.194	0.500
July 19 (n=81)	-1.287	55.77	0.000	0.211	0.259	0.237	0.105	0.497

4.3 Nocturnal Neighbourhood-Scale Evaluation

This section compares observed neighbourhood rankings with modeled neighbourhood rankings. For daytime T_{air}, average modeled rankings show close agreement with observed rankings, where the Shopping Center is consistently ranked the highest neighbourhood and the Downtown is ranked the lowest. Furthermore, Residential 1 is also ranked second highest for both modeled and observed neighbourhood rankings of $T_{air.}$ The additional neighbourhoods along route B show less consistency between modeled and observed rankings (Table 4-7). A consistency in daytime rankings is not seen between modeled and observed neighbourhood T_{dew} medians, although results suggest the Downtown neighbourhood is on average the most humid neighbourhood (Table 4-8).

For nocturnal T_{air}, the largest difference between modeled and observed ranking is experienced in the Downtown neighbourhood, as the observed neighbourhood ranking is 1 (the warmest), however the modeled ranking is lowest. Table 4-9 lists modeled neighbourhood medians of T_{air} and their ranking for two nocturnal traverses. For nocturnal T_{dew}, average modeled ranking for neighbourhoods do not show a similar ranking compared to observed T_{dew}, as no neighbourhoods are ranked the same between modeled and observed neighbourhood ranking. Table 4-10 lists all modeled and observed nocturnal rankings of T_{dew}.

Table 4-7. Rankings of neighbourhood medians for observed and modeled air temperature for all evaluated daytime traverses. Note: a ranking of 1 indicates the highest median temperature and an asterisk indicates a ranking tie. N=5 (route A), N=6 (route B).

Date	R1		R2		OHR		SC		TP		R3		MP		DT	
	$Rank_o$	$Rank_m$	$Rank_o$	$Rank_m$	$Rank_o$	$Rank_m$	$Rank_o$	$Rank_m$	$Rank_o$	$Rank_m$	$Rank_o$	$Rank_m$	$Rank_o$	$Rank_m$	$Rank_o$	$Rank_m$
July 10	2	2	3	3	4	4	1	1	-	-	-	-	-	-	5	5
July 11	2	2	3	3	4	4	1	1	-	-	-	-	-	-	5	5
July 13	2	2	3	3	4	4	1	1	-	-	-	-	-	-	5	5
July 16	2	2	4	3*	3	3*	1	1	-	-	-	-	-	-	5	4
July 19	4	2	3	3	2	4	1	1	-	-	-	-	-	-	5	5
July 20	2	1	-	-	1	2	-	-	3	3	4	4	5	5	6	6
July 22	5	4	-	-	3	5	-	-	2	3	4	2	1	1	6	6
July 24	4	1*	-	-	3	3*	-	-	1	2	2	1*	5	3*	6	4
July 29	1	1	-	-	2	2	-	-	3	3	4	4	5	5	6	6

Table 4-8. Rankings of neighbourhood medians for observed and modeled dewpoint temperature for all evaluated daytime traverses

Date	R1		R2		OHR		SC		TP		R3		MP		DT	
	$Rank_o$	$Rank_m$	$Rank_o$	$Rank_m$	$Rank_o$	$Rank_m$	$Rank_o$	$Rank_m$	$Rank_o$	$Rank_m$	$Rank_o$	$Rank_m$	$Rank_o$	$Rank_m$	$Rank_o$	$Rank_m$
July 10	2	1*	1	1*	3	2	4	3	-	-	-	-	-	-	5	1*
July 11	2	2*	1	2*	4	3	3	4	-	-	-	-	-	-	5	1
July 13	5	2*	3	2*	4	3	2	4	-	-	-	-	-	-	1	1
July 16	3	2	4	5	5	4	2	3	-	-	-	-	-	-	1	1
July 19	3	3	2	2*	4	2*	5	1	-	-	-	-	-	-	1	4
July 20	6	6	-	-	5	5	-	-	3	3	4	4	2	2	1	1
July 22	2	3*	-	-	4	4*	-	-	1	4*	3	2	5	3*	6	1
July 24	2	1	-	-	4	2	-	-	3	5	5	6	6	4	1	3
July 29	6	1*	-	-	5	3*	-	-	3	4	4	2	2	1*	1	3*

Table 4-9. Rankings of neighbourhood medians for observed and modeled air temperature for all evaluated nocturnal traverses. Note: a ranking of 1 indicates the highest median temperature and an asterix indicates a ranking tie.

Date	R1		R2		OHR		SC		DT	
	$Rank_o$	$Rank_m$	$Rank_o$	$Rank_m$	$Rank_o$	$Rank_m$	$Rank_o$	$Rank_m$	$Rank_o$	$Rank_m$
July 12	5	4*	4	3	2	2	3	1	1	4*
July 19	2	1	5	3	4	2	3	4	1	5

Table 4-10. Rankings of neighbourhood medians for observed and modeled dewpoint temperature for all evaluated nocturnal traverses.

Date	R1		R2		OHR		SC		DT	
	$Rank_o$	$Rank_m$	$Rank_o$	$Rank_m$	$Rank_o$	$Rank_m$	$Rank_o$	$Rank_m$	$Rank_o$	$Rank_m$
July 12	4	2	2	2	3	1	1	1	5	3
July 19	1	1	3	2	5	2	4	4	2	5

4.4 Modeled Urban-Rural Differences

Modeled urban-rural differences presented in this section are defined as medians of modeled neighbourhood-modeled pixel values at the fixed weather station location. The results follow the same protocol as observed differences presented in section 3.4. Figure 4-11 shows modeled neighbourhood-rural differences in T_{air} for daytime traverse dates and the average differences for nocturnal traverses. Similar to observed, the maximium aUHI is defined with the Shopping Centre neighbourhood ($\overline{\Delta T}_{mod}$ = 2.3 °C). A 'cool' island between modeled Downtown-rural differences is also simulated on 7 out of 9 traverse dates ($\overline{\Delta T}_{mod}$ = -1.3 °C). An anomaly is experienced on the July 22nd traverse, in which $\Delta T_{dt\text{-}rural}$ = 2.4 °C, this coincides with a positive heat island also observed by the vehicle traverse observations. As discussed in section 3.4, the high wind speeds experienced on this date contributes to less variability observed between neighbourhoods, resulting in typical Downtown 'low T_{air}' to be reasonably close to other neighbourhoods. During the nighttime, the maximum modeled aUHI is defined with the Open-High Rise neighbourhood, where $\overline{\Delta T}$ = 4.4°C, contrary to observed maximum heat island defined with the Downtown neighbourhood.

Figure 4-12 shows modeled neighbourhood-rural differences in T_{dew} for daytime and the average differences for nocturnal traverses. Similar to observed results, the model indicates increased rural T_{dew} compared to the sampled neighbourhoods during the daytime, with July 29th showing anomalous conditions. Reasoning for this anomaly is not

directly apparent based on the meteorological conditions during the time of the evaluation, however, it is likely linked to the model underestimating rural T_{dew} on this specific date. On average, the modeled differences between the neighbourhoods-rural is -0.6 °C during the daytime and 1.1°C during the night. These findings, along with the observed results, highlight the importance of adequately defining ‘urban’ and ‘rural’ when quantifying urban-rural differences in the city Toronto.

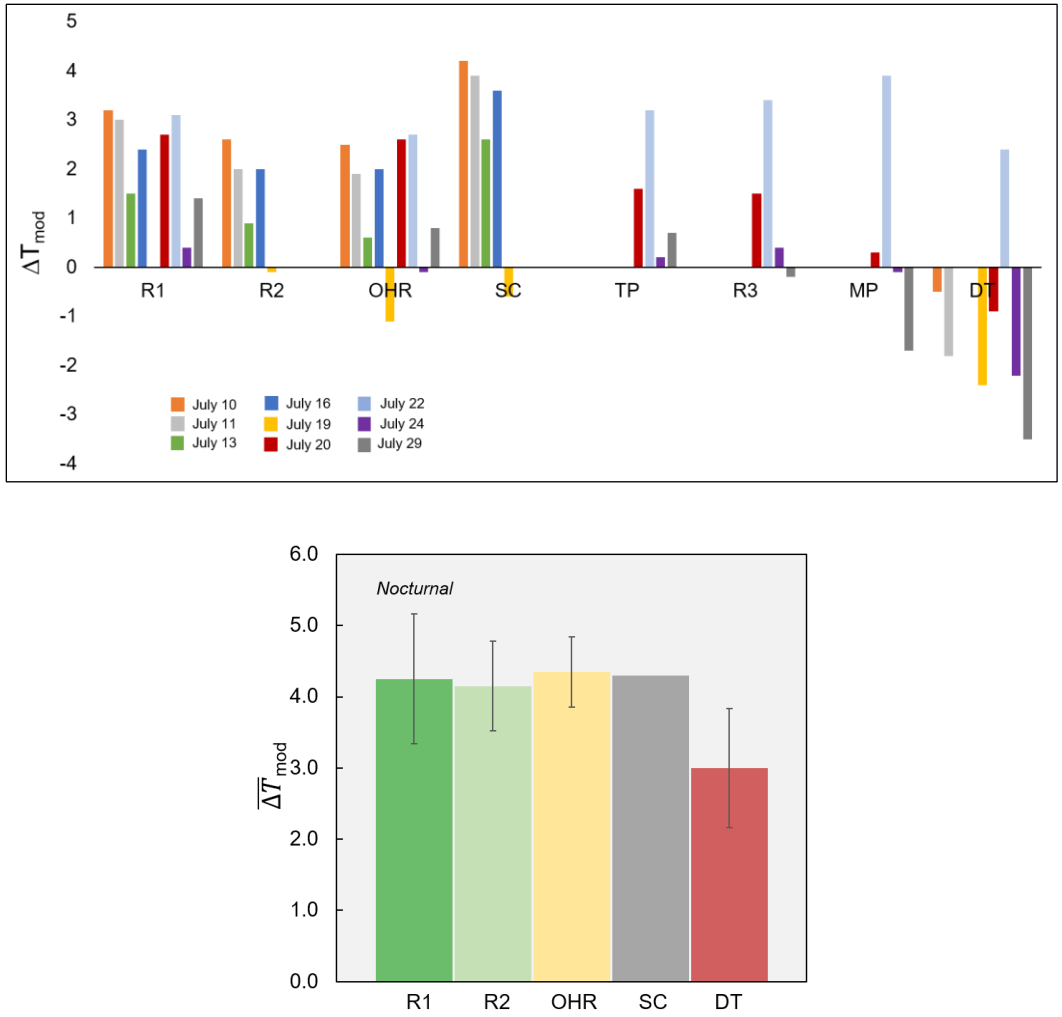

Figure 4-11. Modeled neighbourhood-rural air temperature differences for all traverses (°C). Note: the nocturnal differences represent an average (N=2) and differences in the y-axis. Error bars represent ± one standard deviation.

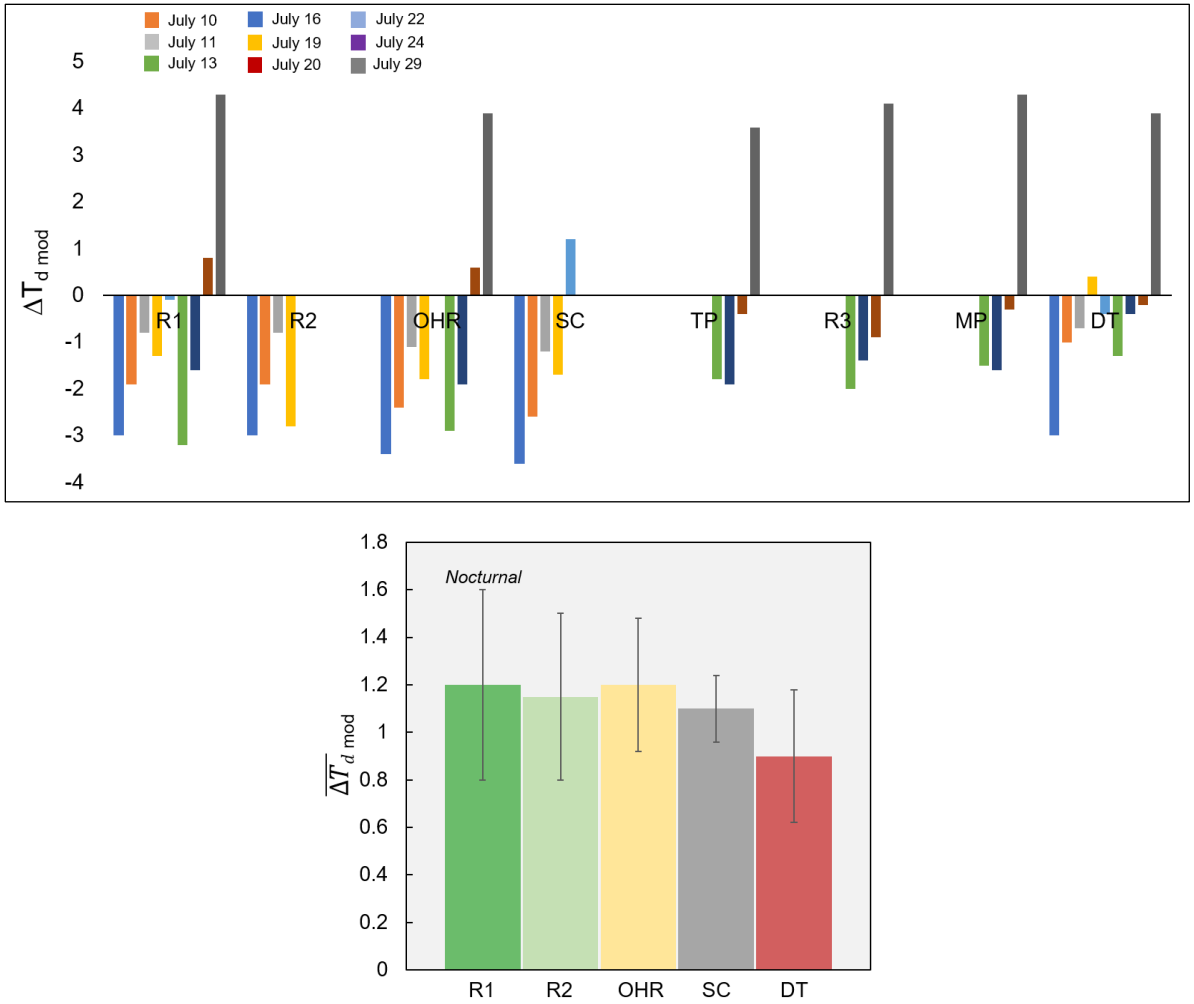

Figure 4-12. Modeled neighbourhood-rural dewpoint temperature differences for all traverses (°C). Note: the nocturnal differences represent an average (N=2) and differences in the y-axis. Error bars represent ± one standard deviation.

4.5 Chapter Summary

Results presented in this chapter evaluate GEM-LAM modeled outputs of T_{air} and T_{dew} with vehicle traverse observations. In total, 9 daytime and 2 nocturnal traverses were evaluated. This marks the first time GEM-LAM evaluations have been conducted using mobile traverse observations. Results between modeled and observed T_{air} for all combined traverse dates shows good results (R^2 = 0.907). However, results indicate that the model underestimates observed T_{air} from the vehicle traverses by an average of 1.0 ºC during both daytime and nighttime conditions. Median neighbourhood T_{air} (excluding Downtown) was modeled reasonably well, with differences between modeled and observed medians generally less than 1.0 ºC. Notable differences between modeled and observed values for the Downtown neighbourhood were experienced, during both daytime and nighttime conditions. During the daytime, GEM-LAM significantly underestimates T_{air} in the Downtown neighbourhood with median differences (i.e. modeled – observed) ranging from -3.3 ºC (July 11th) to -1.4 ºC (July 22nd). During the nighttime, these differences are even larger, with median differences ranging from -3.7 ºC (July 12th) and -4.1 ºC (July 19th). The underestimation in Downtown T_{air} is reflected in a modeled 'cool' island observed during 7 out of 9 evaluated days. In addition, the maximum modeled nocturnal aUHI is defined with the Open-High Rise neighbourhood, where $\overline{\Delta T}$ = 4.4°C.

Model outputs of T_{dew} show spatial patterns of increased T_{dew} around highly vegetated areas, such as parks, and along rivers, specifically the Don River and Humber River. Similar to T_{air}, evaluation results between modeled and observed T_{dew} show good results with all traverse dates combined (R^2 = 0.928) however, little consistency is shown over multiple dates. At the neighbourhood scale, modeled and observed neighbourhood medians of T_{dew} do not show a similar ranking, yet, differences between modeled and observed T_{dew} is generally less than 1.5 ºC. Modeled and observed urban-rural differences in T_{dew} show similar findings, with daytime rural conditions showing more humid conditions compared to all neighbourhoods and nighttime rural conditions showing drier conditions.

Chapter 5

5 Summary and Conclusions

This thesis assessed the intra-urban variability in T_{air}, T_{road}, and T_{dew} under hot, summertime conditions using vehicle traverse observations. In total, 23 vehicle traverses were conducted during the study period from July 7 – July 29, 2015 during the Pan and Parapan American Games held in Toronto, ON. Sampling occurred along two routes and incorporated sampling eight intra-urban neighbourhoods, including two identified by TPH as 'high-risk' in relation to human health – the Thorncliffe Park and Moss Park neighbourhoods. Using a satellite image to conduct a land cover classification, and hemispherical photographs to calculate SVF, surface properties were defined for each neighbourhood and a LCZ was assigned (Table 2-2). Urban-rural differences for daytime and nighttime traverses were assessed using a fixed weather station in Claremont, ON. 12 vehicle traverses – 9 daytime and 3 nighttime, met the required criteria to be included in the analysis presented in this thesis. Vehicle traverses were also used to evaluate model outputs of T_{air} and T_{dew} from an urban-scale model, GEM-LAM (250 m resolution).

Results from vehicle traverses indicate significant intra-urban T_{air}, T_{road}, and T_{dew} variability linked to surface properties and urban geometry within the sampled neighbourhoods. Most notable during the daytime are T_{air} differences between the Shopping Centre and Downtown neighbourhoods, with Downtown showing significantly cooler temperatures. During a traverse, T_{road} shows the largest intra-urban variability compared to T_{air} and T_{dew} (max range observed = 36.7 °C on July 11th) and similar to T_{air}, T_{road} Downtown shows the coolest daytime temperatures. A daytime influence of the lake-breeze is present as traverse-scale T_{dew} is on average higher when a lake-breeze front is identified, however, intra-urban variability in T_{dew} shows less consistent trends relative to the other variables. Daytime and nighttime neighbourhood-rural T_{air} differences illustrate the importance of defining 'urban' and 'rural' when assessing UHI magnitudes as a large range of magnitudes are observed.

GEM-LAM numerical model outputs show relatively good agreement with the observations at the traverse-scale, where $\Delta T_{air\ (mod\text{-}obs)} < -1.1$ ºC and $\Delta T_{dew\ (mod\text{-}obs)} < -1.7$ ºC

in 8 of 11 evaluated vehicle traverses. At the neighbourhood scale, median neighbourhood T_{air} was modeled reasonably well, excluding the Downtown neighbourhood. Evaluation between modeled and observed T_{dew} shows little consistency over multiple dates and is reflected in median neighbourhood ranking's. However, neighbourhood differences between modeled and observed T_{dew} is generally less than 1.5 ºC. Ultimately, while the GEM-LAM model shows encouraging results, especially for T_{air} outputs, continued evaluation with representative UCL observations is recommended, especially in deep urban canyons such as those experienced in downtown Toronto.

Additionally, results from vehicle traverse observations and GEM-LAM outputs indicate that the TPH "high-risk" neighbourhoods of Thorncliffe Park and Moss Park neighbourhoods do not show microclimates associated higher heat related health risks compared to other urban neighbourhoods. However, it should be noted that this is strictly from a microclimate perspective and thus other factors such as pre-existing health concerns, age, and socioeconomic factors were not considered. Lastly, as both observational and modeling results indicate high daytime temperatures within the Shopping Centre neighbourhood, this thesis suggests heat mitigation strategies should be focused in areas of the city with similar surface cover properties as the Shopping Centre neighbourhood.

5.1 Future Work

Vehicle traverse observations were aimed towards hot, summertime conditions and thus it is encouraged that future work examines how intra-urban microclimate conditions vary under different seasons. Furthermore, the results presented in this thesis are for a mid-latitude, North American city located along a Great Lake and thus the results are limited in their ability to represent other locations in which the extrinsic controls (i.e. latitude, altitude, proximity of water) on a city's climate vary.

Future work is also encouraged to expand on the findings presented in thesis by including additional meteorological variables to more fully characterize the microclimates of these neighbourhoods (e.g. in-situ observations of wind speed and direction, incoming radiation). The use of these metrological variables could be used to calculate human thermal comfort

indices (e.g. Universal Thermal Comfort Index) to objectively evaluate differences in thermal comfort levels within neighbourhoods of Toronto and to provide data for evaluation of these indices as calculated in the GEM-LAM system.

5.2 Final Remarks

With urban development and the number of people living in the GTA expected to increase (Ontario Ministry, 2005; United Nations, 2016), characterizing and understanding Toronto's UHI effect and impacts remains an important issue. The results presented in this thesis demonstrate significant microscale intra-urban variability not typically captured by routine meteorological observations. The application of these results can provide insight to where in Toronto public health is at highest risk and where heat mitigation strategies are most needed.

References

Ackerman, B. (1987). Climatology of Chicago Area Urban-Rural Differences in Humidity. *Journal of Applied Meteorology and Climatology*, *26*, 427–430.

Basara, J. B., & Rowell, M. D. (2012). Mesoscale observations of an extended heat burst and associated wind storm in Central Oklahoma, *Meteorological Applications*, *110*, 91–110.

Bélair, S., Crevier, L. P., Mailhot, J., Bilodeau, B., Delage, Y. (2003). Operational implementation of the ISBA land surface scheme in the Canadian Regional Weather Forecast Model. Part I: Warm season results. *Journal of Hydrometeorology*, *4*, 352-370.

Conrads, L. A., & Van Der Hage, J. C. H. (1971). A new method of air-temperature measurement in urban climatological studies. *Atmospheric Environment*, *5*(8), 629-635.

Delage, Y. (1997). Parameterising sub-grid scale vertical transport in atmospheric models under statically stable conditions. *Boundary Layer Meteorology*, *82*, 23-48.

Delage, Y., & Girard, C. (1992). Stability functions correct at the free convection limit and consistent for both the surface and Ekman layers. *Boundary Layer Meteorology*, *58*, 19-31.

Dutfield, S. (2015). *Personal communication*, July 16, 2015.

Environmental Systems Research Institute (ESRI). (2012). National Geographic [basemap]. *"National Geographic"*. February 19, 2012

Fillion, L., Tanguay, M., Lapalme, E., Denis, B., Desgagne, M., Lee, V., Ek, N., Liu, Z., Lajoie, M., Caron, J. F., Pagé, C. (2010). The Canadian Regional Data Assimilation and Forecasting System. *Weather Forecast*, *25*, 1645-1669.

Fung, W. Y., Lam, K. S., Hung, W. T., Pang, S. W., & Lee, Y. L. (2006). Impact of urban temperature on energy consumption of Hong Kong, *31*, 2623–2637.

Gough, W. A., & Rozanov, Y. (2002). Impacts of urbanization on the climate of Toronto, ONT, CA. *Journal of Chemical Information and Modeling*, *53*(9), 1689–1699.

Harlan, S. L., Brazel, A. J., Prashad, L., Stefanov, W. L., & Larsen, L. (2006). Neighborhood microclimates and vulnerability to heat stress. *Social Science and Medicine*, *63*(11), 2847–2863.

Heusinkveld, B. G., van Hove, L. W. A., Jacobs, C. M. J., Steeneveld, G. J., Elbers, J. A., Moors, E. J., & Holtslag, A. A. M. (2010). Use of a mobile platform for assessing urban heat stress in Rotterdam, 433–438.

Howard, L. (1833). The climate of London, volume 1 - 3. Harvey and Dorton, London.

Huizenga, C., Abbaszadeh, S., Zagreus, L., & Arens, E. (2006). Air quality and thermal comfort in office buildings: Results of a large indoor environmental quality survey. *Proceedings of Healthy Buildings*, *3*, 393-397.

James, W. (2002). Green Roads: Research into Permeable Pavers. *Stormwater*, *3*(2), 48-40.

Joe, P., Belair, S., Bernier, N.B., Brook, J.R., Brunet, D., Bouchet, V., Burrows, W., Charland, J.P., Dehghan, A., Driedger, N., Duhaime, C., Evans, G., Frenette, R., Gultepe, I., Henderson, D., Herdt, A., Hilker, N., Huang, L., Hung, E., Isaac, G., Johnston, D., Jeong, C-H., Klaassen, J., Leroyer, S., Lin, H., MacDonald, M., MacPhee, J., Mariani, Z., Reid, J., Robichaud, A., Rochon, Y., Sills, D., Shairsingh, K., Stroud, C., Su, Y., Taylor, N., Wang, J.M., Vanos, J., Voogt, J., Wiechers, T., Wren, S., Yang, H., & Yip, T. (2017). The Environment Canada Pan and ParaPan American Science Showcase Project. *Bulletin of the American Meteorological Society, 99,* 921-954.

Johansson, E., & Emmanuel, R. (2006). The influence of urban design on outdoor thermal comfort in the hot, humid city of Colombo, Sri Lanka. *International Journal of Biometeorology, 2*, 119–133.

Kolokotroni, M., Zhang, Y., & Watkins, R. (2007). The London Heat Island and building cooling design. *Solar Energy, 81*(1), 102–110.

Kottek, M., Grieser, J., Beck, C., Rudolf, B., & Rubel, F. (2006). World map of the Koppen-Geiger climate classifcation updated. *Meteorologische Zeitschrift, 15*(3), 259-263.

Lai, L., & Cheng, W. (2009). Air quality influenced by urban heat island coupled with synoptic weather patterns. *Science of the Total Environment, 407*(8), 2724–2733.

Leconte, F., Bouyer, J., Claverie, R., & Pétrissans, M. (2015). Using Local Climate Zone scheme for UHI assessment: Evaluation of the method using mobile measurements. *Building and Environment, 83*, 39–49.

Lemonsu, A., Belair, S., & Mailhot, J. (2009). The new canadian urban modelling system: Evaluation for two cases from the joint urban 2003 Oklahoma City experiment. *Boundary-Layer Meteorology, 133*(1), 47–70.

Leroyer, S., Bélair, S., Husain, S. Z., & Mailhot, J. (2014). Subkilometer numerical weather prediction in an urban coastal area: A case study over the Vancouver metropolitan area. *Journal of Applied Meteorology and Climatology, 53*(6), 1433–1453.

Leroyer, S., Bélair, S., Mailhot, J., & Strachan, I. B. (2011). Microscale numerical prediction over Montreal with the Canadian external urban modeling system. *Journal of Applied Meteorology and Climatology, 50*(12), 2410–2428.

Li, D., & Bou-Zeid, E. (2013). Synergistic interactions between urban heat islands and heat waves: The impact in cities is larger than the sum of its parts. *Journal of Applied Meteorology and Climatology, 52*(9), 2051–2064.

Lindberg, F., & Holmer, B. (2012). Sky View Factor Calculator, (November 2014).

Lowry, W. P. (1977). Empirical Estimation of Urban Effects on Climate: A Problem Analysis. *Journal of Applied Meteorology, 16*(2), 129-135.

Mann, H. B., & Whitney, D. R. (1947). On a test of whether one of two random variables is stochastically larger than the other. *The Annals of Mathematical Statistics*, *18*(1), 50-60.

Masson, V. (2000). A physically-based scheme for the urban energy budget in atmospheric models. *Boundary Layer Meteorology*, *94*(3), 357–397.

Masson, V., Grimmond, C. S. B., & Oke, T. R. (2002). Evaluation of the Town Energy Balance (TEB) scheme with direct measurements from dry districts in two cities. *Journal of Applied Meteorology*, *41*, 1011-1026.

Meehl, G. A. (2004). More Intense, More Frequent, and Longer Lasting Heat Waves in the 21st Century. *Science*, *305*(5686), 994–997.

Middleton, W. K., & Millar, F. G. (1936). Temperature Profiles in Toronto. *The Journal of the Royal Astronomical Society of Canada*, *30*(7), 265-272.

Mizuno, M., Nakamura, Y., Murakami, H., & Yamamoto, S. (1991). Effects of Land Use on Urban Horizontal Atmospheric Temperature Distributions. *Energy and Buildings*, *15*, 165–176

Mohsin, T., & Gough, W. A. (2010). Trend analysis of long-term temperature time series in the Greater Toronto Area (GTA). *Theoretical and Applied Climatology*, *101*(3), 311–327.

Mohsin, T., & Gough, W. A. (2012). Characterization and estimation of urban heat island at Toronto: Impact of the choice of rural sites. *Theoretical and Applied Climatology*, *108*(1–2), 105–117.

Munn, R. E., Hirt, M. S., & Findlay, B. F. (1969). A climatological study of the urban temperature anomaly in the lakeshore environment at Toronto. *Journal of Applied Meteorology*, 411-422.

Nakayoshi, M., Kanda, M., & Shi, R. (2015). Outdoor thermal physiology along human pathways : a study using a wearable measurement system. *International Journal of Biometeorolgy*, 503–515.

Ng, E., & Cheng, V. (2012). Urban human thermal comfort in hot and humid Hong Kong. *Energy & Buildings*, *55*, 51–65.

Noilhan, J., & Planton, S. (1989). A Simple Parameterization of Land Surface Processes for Meteorological Models.

Oke, T. R. (1973). City size and the urban heat island. *Atmospheric Environment*, *7*(8), 769–779.

Oke, T. R. (1982). The energetic basis of the urban heat island. *Quarterly Journal of the Royal Meteorological Society*, *108*, 1-24.

Oke, T. R. (1987). Boundary Layer Climates. *Routledge Books.*

Oke, T. R. (1995). The Heat Island of the Urban Boundary Layer. *Wind Climate in Cities*, 81–107.

Oke, T. R., Mills, G., Christen, A., & Voogt, J. A. (2017). Urban Climates. *Cambridge: Cambridge University Press.*

Ono, T., Kanai, K., Ishizuka, H., Thepvilojanapong, N., Iwai, M., & Tobe, Y. (2008). Analysis of Fine-grained Urban Temperature Collected with a Sensor Network. *Sesnors*, 712–715.

Pengelly, L. D., Campbell, M. E., Cheng, C. S., Fu, C., Gingrich, S. E., & Macfarlane, R. (2007). Anatomy of Heat Waves and Mortality in Toronto: Lessons for Public Health Protection. *Canadian Journal of Public Health, 98*(5), 364-368.

Penney, J. (2008). Climate Change Adaptation in the City of Toronto: Lessons for Great Lakes Communities. *Clean Air Partnership.* Toronto, Ontario.

Piringer, M., Grimmond, C. S. B., Joffre, S. M., Mestayer, P., Middleton, D. R., Rotach, M. W., Baklanov, A., De Ridder, K., Ferreira, J., Guilloteau, E., Karppinen, A., Martilli, A., Masson, V., & Tombrou, M. (2002). Investigating the surface energy balance in urban areas–Recent advances and future needs. *Water, Air and Soil Pollution: Focus*, 2 (5), 1-16.

Richards, K. (2005). Urban and rural dewfall, surface moisture, and associated canopy-level air temperature and humidity measurements for Vancouver, Canada. *Boundary-Layer Meteorology, 113*, 143–163.

Rinner, C., & Hussain, M. (2011). Toronto's urban heat island-exploring the relationship between land use and surface temperature. *Remote Sensing*, *3*(6), 1251–1265.

Runnalls, K. E., & Oke, T. R. (2013). Dynamics and controls of the near-surface heat island of Vancouver, British Columbia. *Physical Geography*, 234-304.

Shapiro, S. S., & Wilk, M. B. (1965). An analysis of variance test for normality (complete samples). *Biometrika*, *52*(3/4), 591-611.

Skelhorn, C. P., Levermore, G., & Lindley, S. J. (2016). Impacts on cooling energy consumption due to the UHI and vegetation changes in Manchester , UK. *Energy & Buildings*, *122*, 150-159.

Smoyer-Tomic, K., Kuhn, R., & Hudson, A. (2003). Heat wave hazards: an overview of heat wave impacts in Canada. *Natural Hazards*, *28*, 463-485.

Sofer, M., & Potchter, O. (2006). The urban heat island of a city in an arid zone: The case of Eilat, Israel. *Theoretical and Applied Climatology*, *85*(1–2), 81-88.

Statistics Canada. (2018). CANSIM, table 051-0056.

Stewart, I. D. (2011). A systematic review and scientific critique of methodology in modern urban heat island literature. *International Journal of Climatology*, *31*(2), 200–217.

Stewart, I. D., & Oke, T. R. (2012). Local climate zones for urban temperature studies. *Bulletin of the American Meteorological Society*, *93*(12), 1879–1900.

Toronto Public Health. (2017). The City of Toronto's Hot Weather Response Plan.

Tsin, P. K., Knudby, A., Krayenhoff, E. S., Ho, H. C., Brauer, M., & Henderson, S. B. (2016). Microscale mobile monitoring of urban air temperature. *Urban Climate*, *18*, 58–72.

United Nations (2014). World Urbanization Prospects: The 2014 Revision. *Technical Report.* Department of Economic and Social Affairs.

United Nations (2016). Urbanization and Development: Emerging Futures. *World Cities Report 2016.*

Vanos, J. K., Warland, J. S., Gillespie, T. J., Slater, G. A., Brown, R. D., & Kenny, N. A. (2012). Human energy budget modeling in urban parks in toronto and applications to emergency heat stress preparedness. *Journal of Applied Meteorology and Climatology*, *51*(9), 1639–1653.

Voogt, J. A., & Oke, T. R. (1998). Radiometric temperatures of urban canyon walls obtained from vehicle traverses. *Theoretical and Applied Climatology*, *60*(1–4), 199–217.

Voogt, J. A., & Oke, T. R. (2003). Thermal remote sensing of urban climates. *Remote Sensing of Environment*, *86*(3), 370–384.

Willmott, C. J., Ackleson, S. G., Davis, R. E., Feddema, J. J., Klink, K. M., Legates, D. R., O'Donnell, J., & Rowe, C. M. (1985). Statistics for the evaluation and comparison of models. *Journal of Geophysical Research*, *90*(5), 8995-9005.

Willmott, C. J., Robeson, S. M., & Matsuura, K. (2012). A refined index of model performance. *International Journal of Climatology*, *32*(13), 2088-2094.

World Meteorological Organization. (2008). Guide to meteorological instruments and methods of observations. WMO-No. 8.

Ye, C., Wang, M., & Li, J. (2017). Derivation of the characteristics of the Surface Urban Heat Island in the Greater Toronto area using thermal infrared remote sensing. *Remote Sensing Letters*, *8*(7), 637–646.

Zadra, A., Caya, D., Côté, J., Dugas, B., & Jones, C. (2008). The next Canadian regional climate model. *Physics in Canada*, *64*(2), 75–83.

Appendix A: Traverse-scale Observations

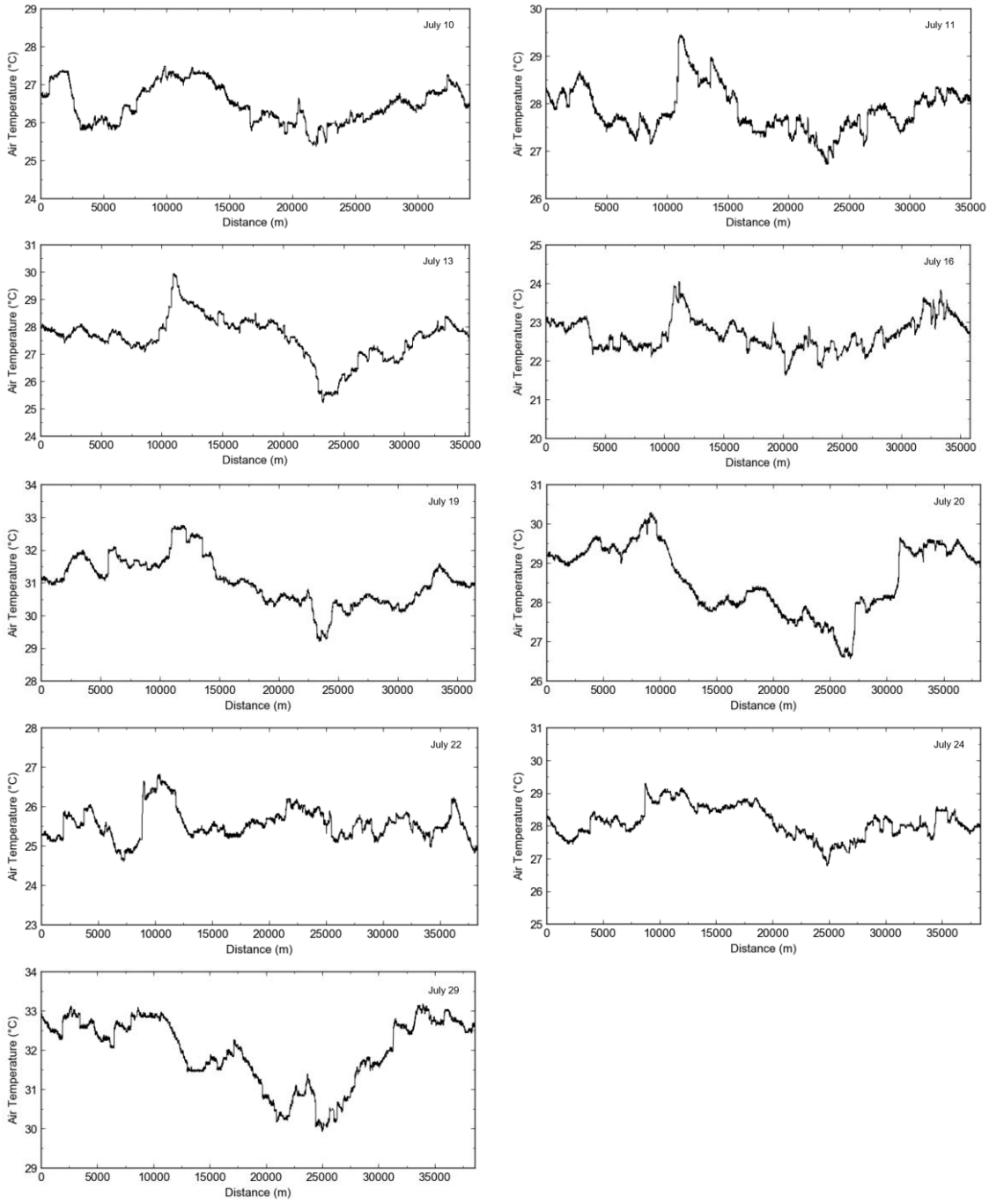

Appendix A-1: Traverse-scale air temperature plots from both intra-urban routes (A and B). Note: y-axis range may vary between dates.

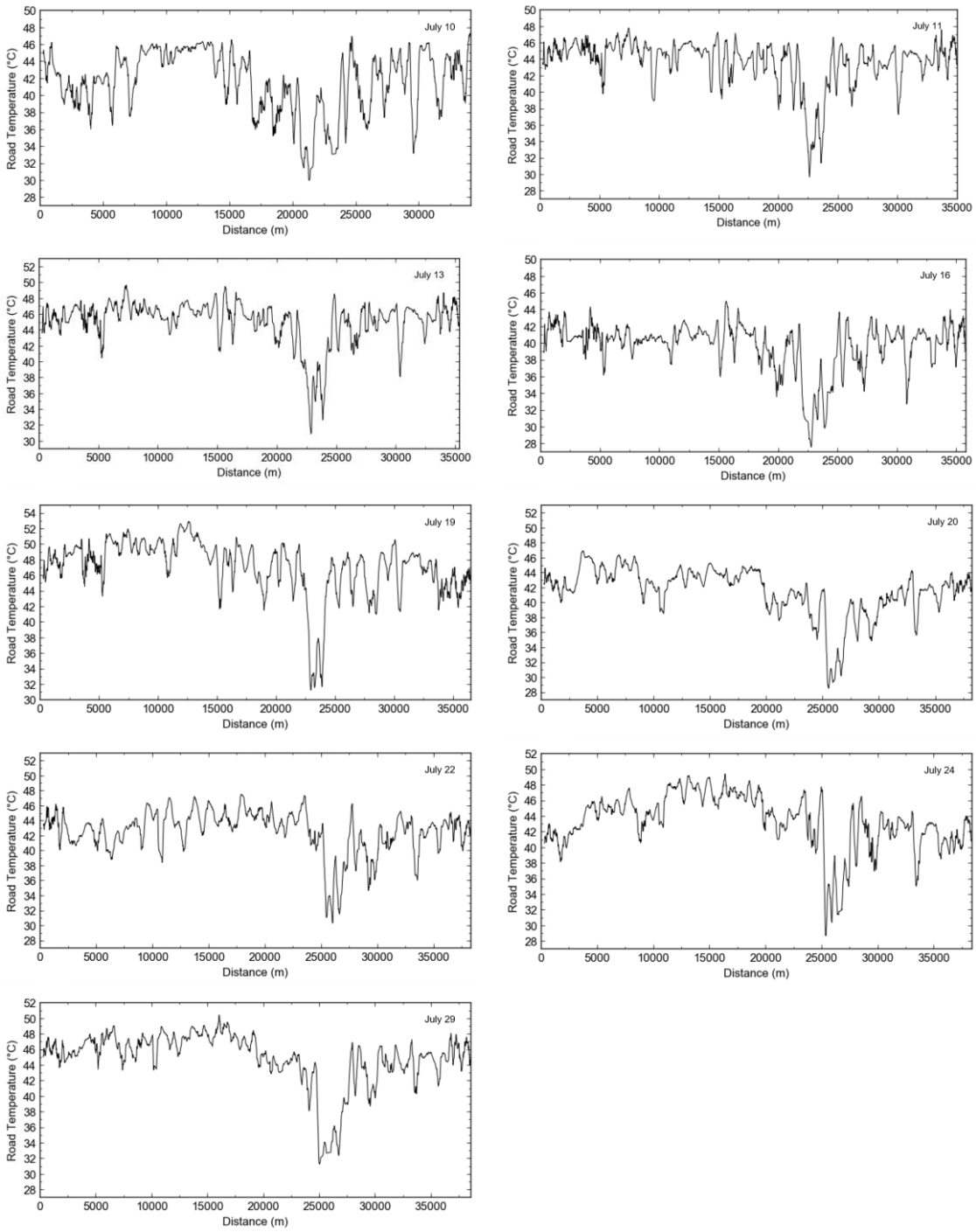

Appendix A-2: Traverse-scale road temperature plots from both intra-urban routes (A and B). Note: y-axis range may vary between dates.

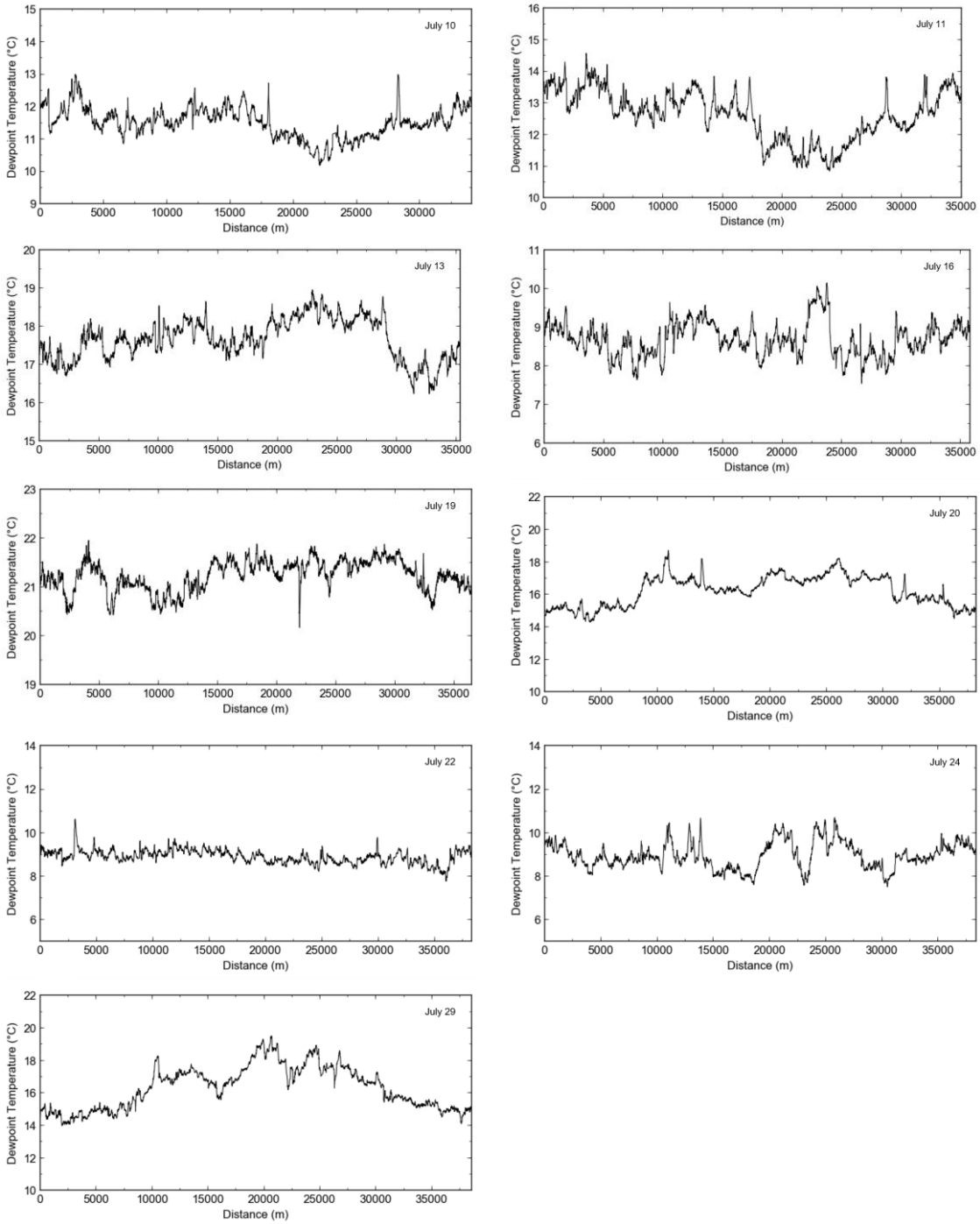

Appendix A-3: Traverse-scale dewpoint temperature plots from both intra-urban routes (A and B). Note: y-axis range may vary between dates.

.

Appendix B: Observed Neighbourhood Medians

Appendix B-1: Daytime neighbourhood medians of air, road, and dewpoint temperature for all sampled neighbourhoods. Also provided are reported air and dewpoint temperature conditions at Toronto International Airport (YYZ) and Billy Bishop Toronto City Airport (YTZ) (shaded).

Date	Variable	R1	R2	OHR	SC	TP	R3	MP	DT	YYZ	YTZ[1]
July 10	T_{air}	26.7	26.0	25.9	27.2	-	-	-	25.7	26.2	23.3
	T_{road}	45.9	41.2	43.3	45.6	-	-	-	39.2	-	-
	T_{dew}	12.0	12.3	11.6	11.5	-	-	-	10.5	12.5	13.6
July 11	T_{air}	28.1	27.8	27.5	29.0	-	-	-	27.0	26.4	25
	T_{road}	46.5	46.4	46.3	45.7	-	-	-	32.8	-	-
	T_{dew}	13.6	13.8	12.8	13.1	-	-	-	11.5	13.7	13.9
July 13	T_{air}	27.9	27.7	27.5	29.6	-	-	-	25.6	27.5	23.1
	T_{road}	47.9	47.6	47.5	46.9	-	-	-	34.3	-	-
	T_{dew}	17.2	17.8	17.6	17.9	-	-	-	18.6	18.1	19.1
July 16	T_{air}	23.0	22.3	22.5	23.5	-	-	-	22.3	22.1	20.6
	T_{road}	44.1	43.5	41.1	41.8	-	-	-	31.4	-	-
	T_{dew}	9.0	8.7	8.5	9.1	-	-	-	9.7	8.4	12.6
July 19	T_{air}	31.0	31.5	31.7	32.7	-	-	-	29.6	30.9	26.4
	T_{road}	49.4	49.6	50.4	51.8	-	-	-	33.8	-	-
	T_{dew}	21.1	21.5	21.1	20.7	-	-	-	21.6	21.9	21.5
July 20	T_{air}	29.2	-	29.4	-	28.5	28.0	27.7	26.8	28	23.9
	T_{road}	44.0	-	44.5	-	44.0	43.9	41.4	30.9	-	-
	T_{dew}	15.1	-	15.1	-	16.8	16.2	16.8	17.8	15.5	18.2
July 22	T_{air}	25.2	-	25.5	-	25.6	25.3	25.9	25.2	24.6	24.9
	T_{road}	45.9	-	42.6	-	43.9	44.9	44.9	33.6	-	-
	T_{dew}	9.1	-	9.0	-	9.3	9.1	8.7	8.7	9.6	11.1
July 24	T_{air}	27.9	-	28.1	-	28.9	28.6	27.7	27.4	28.3	25.4
	T_{road}	42.5	-	45.2	-	48.1	48.3	44.7	32.9	-	-
	T_{dew}	9.4	-	8.8	-	8.9	8.3	8.1	9.8	12.9	14.5
July 29	T_{air}	32.5	-	32.4	-	32.3	31.2	30.9	30.2	31.5	27.9
	T_{road}	47.9	-	48.0	-	47.5	49.9	45.0	33.3	-	-
	T_{dew}	14.8	-	14.9	-	16.9	19.0	17.2	17.5	17.7	21.9

Appendix B-2. Nocturnal neighbourhood medians of air, road, and dewpoint temperature for all sampled neighbourhoods. Also provided are reported air and dewpoint temperature conditions at Toronto Pearson International Airport (YYZ) and Billy Bishop Toronto City Airport (YTZ) (shaded).

Date	Variable	R1	R2	OHR	SC	DT	YYZ[1]	YTZ[1]
July 12	T_{air}	21.3	21.5	22.3	21.4	25.7	19.6	19.1
	T_{road}	25.5	24.7	26.0	24.3	26.7	-	-
	T_{dew}	15.5	16.3	15.6	16.9	15.2	15.5	17.8
July 19	T_{air}	25.3	24.7	24.9	24.6	25.8	24.0	22.2
	T_{road}	27.8	27.5	28.2	28.20	26.6	-	-
	T_{dew}	21.0	20.9	20.7	20.8	21.0	20.8	20.3
July 29	T_{air}	24.5	-	-	-	28.1	23.1	22.4
	T_{road}	29.1	-	-	-	28.9	-	-
	T_{dew}	16.1	-	-	-	17.2	17.7	17.7

[1] Open-access past climate data as reported every 1-hr by Environment Canada. Times of reported conditions correspond to closest hr. to traverse start time.

Appendix C: Mann-Whitney U Test Results

Appendix C-1. Results of the Mann-Whitney U tests for daytime air temperature. Values provided represent: Mann-Whitney U (p-value). * indicates non-significant differences (α=0.05).

	R2	OHR	SC	TP	R3	MP	DT
July 10	510 (.000)	0 (.000)	0 (.000)	-	-	-	45 (.000)
July 11	2822 (.000)	102 (.000)	288 (.000)	-	-	-	0 (.000)
July 13	3018 (.000)	1368 (.000)	0 (.000)	-	-	-	0 (.000)
July 16	0 (.000)	1 (.000)	810 (.000)	-	-	-	0 (.000)
July 19	275 (.000)	0 (.000)	0 (.000)	-	-	-	0 (.000)
July 20	-	52 (.000)	-	0 (.000)	0 (.000)	0 (.000)	0 (.000)
July 22	-	663 (.000)	-	2252 (.000)	4238 (.000)	0 (.000)	8389 (.000)
July 24	-	4607 (.000)	-	4 (.000)	0 (.000)	5459 (.000)	0 (.000)
July 29	-	5860 (.000)	-	6493 (.000)	0 (.000)	0 (.000)	0 (.000)

Appendix C-2. Results of the Mann-Whitney U tests for daytime road temperature. See table 4-2 for description of values.

	R2	OHR	SC	TP	R3	MP	DT
July 10	1509 (.000)	2305 (.000)	3228 (.486) *	-	-	-	573 (.000)
July 11	16053 (.424) *	17139 (.567) *	13566 (.017)	-	-	-	2289 (.000)
July 13	15924 (.526) *	15040 (.130) *	11688 (.043)	-	-	-	3425 (.000)
July 16	14432 (.291) *	10857 (.000)	9952 (.000)	-	-	-	3125 (.000)
July 19	12179 (.049)	10152 (.000)	4373 (.000)	-	-	-	1304 (.000)
July 20	-	12061 (.001)	-	15652 (.582) *	9961 (.211) *	6349 (.000)	282 (.000)
July 22	-	6363 (.000)	-	10409 (.000)	8632 (.026)	8797 (.101)	1951 (.000)
July 24	-	4422 (.000)	-	1065 (.000)	1144 (.000)	4243 (.000)	2956 (.000)
July 29	-	10335 (.955)	-	12490 (.099)	5523 (.000)	6675 (.000)	714(.000)

Appendix C-3. Results of the Mann-Whitney U tests for daytime dewpoint temperature. *See table 4-2 for description of values.*

	R2	OHR	SC	TP	R3	MP	DT
July 10	2546 .000)	5 (.000)	0 (.000)				0 (.000)
July 11	8885 (.000)	1160 (.000)	3349 (.000)				0 (.000)
July 13	554 (.000)	3283 (.000)	535 (.000)				0 (.000)
July 16	5391 (.000)	493 (.000)	9426 (.000)				50 (.000)
July 19	754 (.000)	10515 (.000)	3131 (.000)				701 (.000)
July 20		11144 (.000)		0 (.000)	0 (.000)	0 (.000)	0 (.000)
July 22		10876 (.054) *		6564 (.000)	9824 (.592) *	1937 (.000)	717 (.000)
July 24		1164 (.000)		6573(.000)	0 (.000)	0 (.000)	4316 (.000)
July 29		5769 (.000)		0 (.000)	0 (.000)	(.000)	0 (.000)

Appendix C-4. Results of the Mann-Whitney U tests for nighttime air temperature. See table 4-2 for description of values.

	R2	**OHR**	**SC**	**DT**
July 12	6738 (.000)	0 (.000)	0 (.000)	0 (.000)
July 19	0 (.000)	25 (.000)	185 (.000)	0 (.000)

Appendix C-5. Results of the Mann-Whitney U tests for nighttime road temperature. See table 4-2 for description of values.

	R2	**OHR**	**SC**	**DT**
July 12	10333 (.000)	11683 (.000)	5105 (.000)	4977 (.000)
July 19	15289 (.278)	10968 (.000)	11457 (.079)	7015 (.000)

Appendix C-6. Results of the Mann-Whitney U tests for nighttime dewpoint temperature. See table 4-2 for description of values.

	R2	**OHR**	**SC**	**DT**
July 12	136 (.000)	13400 (.013)	0 (.000)	3835 (.000)
July 19	257 (.000)	0 (.000)	0 (.000)	3319 (.000)

Appendix D: Modeled Neighbourhood Medians

Appendix D-1. Median values of air and dewpoint temperature for all modeled neighbourhoods for both daytime and nighttime (shaded) traverse times.

Date	Variable$_{mod}$	R1	R2	OHR	SC	TP	R3	MP	DT
July 10	T_{air}	26.4	25.8	25.7	27.4	-	-	-	22.7
	T_{dew}	13.5	13.5	13.1	12.9	-	-	-	13.5
July 11	T_{air}	28.5	27.5	27.4	29.4	-	-	-	23.7
	T_{dew}	14.2	14.2	13.7	13.5	-	-	-	15.1
July 12	T_{air}	22.0	22.1	22.4	22.7	-	-	-	22.0
	T_{dew}	17.6	17.6	17.7	17.7	-	-	-	17.4
July 13	T_{air}	27.5	26.9	26.6	28.6	-	-	-	23.4
	T_{dew}	17.9	17.9	17.6	17.5	-	-	-	18.0
July 16	T_{air}	22.3	21.9	21.9	23.5	-	-	-	19.9
	T_{dew}	10.0	8.5	9.5	9.6	-	-	-	11.7
July 19	T_{air}	28.9	28.8	27.8	28.3	-	-	-	26.5
	T_{dew}	23.1	23.2	23.2	24.4	-	-	-	22.8
July 19	T_{air}	24.2	23.9	24.0	23.6	-	-	-	21.7
	T_{dew}	20.7	20.6	20.6	20.4	-	-	-	20.3
July 20	T_{air}	27.8	-	27.7	-	26.7	26.6	25.4	24.2
	T_{dew}	14.8	-	15.1	-	16.2	16.0	16.5	16.7
July 22	T_{air}	24.5	-	24.1	-	24.6	24.8	25.3	23.8
	T_{dew}	9.3	-	9.0	-	9.0	9.5	9.3	10.5
July 24	T_{air}	28.2	-	27.7	-	28.0	28.2	27.7	25.6
	T_{dew}	10.0	-	9.8	-	8.8	8.3	8.9	9.0
July 29	T_{air}	32.4	-	31.8	-	31.7	30.8	29.3	27.5
	T_{dew}	18.6	-	18.2	-	17.9	18.4	18.6	18.2

Appendix E: The Vehicle Traverse Datalogger Program (CRBasic)

```
Public batt_volt

'Probe
Public Air_Temp, RH, Tcple, Tpanel

'GPS
Public NMEAStrings(3) As String * 80
Public GPSArray(18)
Public GPSchar(18) As String * 16
Public Latlon(2)

'pyranometer YES TSP-400 Ser No. 0005-2
  Public pyr
  Units pyr = W m-2

'Pyrgeometer Epply PIR Ser No. 32905FB... Inst = case
 Public Ld_thmp, Ld,
 Public Inst, Dome
 Public Rdome, Rinst
 Public Rinstln, Rdomeln
 Public Ld_Tinst, Ld_Tdome
 Const c1=0.0010295
 Const c2=0.0002391
 Const c3=1.568e-07
 Const sigma=5.67e-08
 Units Ld_thmp=mV
 Units Inst=mV/mV
 Units Dome=mV/mV
 Units Ld_Tdome=degC
 Units Ld_Tinst=degC

'IRRs
Public SBTempC(3), SBTempK(3), TargmV(3), m(3), b(3), TargTempK(3), TargTempC(3)
Public SBTempWallRiC, SBTempWallLeC,SBTempRoadC, TwallRC, TwallLC, TroadC,
Dim i
Dim mC0(3),mC1(3),mC2(3), bC0(3),bC1(3), bC2(3)

'Apogee IRR SI-131  SN 1167 - wall (RIGHT)
Const mC2_1 = 218628
Const mC1_1 = 22974400
Const mC0_1 = 4379500000
```

```
Const bC2_1 = 15951.1
Const bC1_1 = -70761.6
Const bC0_1 = -20837100

'Apogee IRR SI-131 SN 1168 - wall (LEFT)
Const mC2_2 =  263537
Const mC1_2 =  25206800
Const mC0_2 =  4931730000
Const bC2_2 =  8020.56
Const bC1_2 =  -69955.7
Const bC0_2 =  -20368000

'Apogee IRR SI-1H1  SN 1252 - road
Const mC2_3 = 89285.6
Const mC1_3 = 8576500
Const mC0_3 = 1713110000
Const bC2_3 = 2858.4
Const bC1_3 = 82019.3
Const bC0_3 = -4959750

'Thermistor
Public thermsi200
  Dim Rt
  Dim Tk

Units batt_volt = Volts
Units Air_Temp = mV
Units RH = mV

'Test Datatable
DataTable (Test,1,-1)
        DataInterval (0,1,Sec,10)
        Minimum (1,batt_volt,FP2,0,False)
  Sample (1,Air_Temp,FP2)
  Sample (1,RH,FP2)
  Sample (1,thermsi200,FP2)
  Sample (2,TargmV(),FP2)
  Sample (1,SBTempWallRiC,FP2)
  Sample (1,SBTempWallLeC,FP2)
  Sample (1,SBTempRoadC,FP2)
  Sample (1,TwallRC,FP2)
  Sample (1, TwallLC, FP2)
  Sample (1,TroadC,FP2)
  Sample (1,Tcple,FP2)

'Pyrgeometer
```

```
 Sample(1,Ld_thmp,FP2)
 Sample(1,Ld_Tinst,FP2)
 Sample(1,Ld_Tdome,FP2)
 Sample (1,Ld,FP2)

'Pyranometer Y.E.S. Ser No. 0005-2
 Sample(1,pyr,FP2)

'Output parsed GPS info:
'hhmmss (UTC) GPSchar(2)
'Latitude: degrees, minutes, thousandths of minutes GPSchar(3)
'N (North) or S (South) GPSchar(4)
'Longitude: degrees, minutes, thousandths of minutes GPSchar(5)
'E (East) or W (West)  GPSchar(6)
'GPS Quality Indicator: 0 = No GPS, 1 = GPS, 2 = DGPS GPSchar(7)
'Number of Satellites in use GPSchar(8)
'Horizontal Dilution of Precision GPSchar(9)
'Antenna altitude in meters GPSchar(10)
'Geoidal separation in meters GPSchar(12)

  Sample (1,GPSchar(2),String)
  Sample (1,GPSchar(3),String)
  Sample (1,GPSchar(4),String)
  Sample (1,GPSchar(5),String)
  Sample (1,GPSchar(6),String)
  Sample (1,GPSchar(7),String)
  Sample (1,GPSchar(8),String)
  Sample (1,GPSchar(9),String)
  Sample (1,GPSchar(10),String)
  Sample (1,GPSchar(12),String)
EndTable

'Main Program
BeginProg
Scan (1,Sec,3,0)
        Battery (batt_volt)
        VoltSe (Air_Temp,1,mV1000,4,1,0,_60Hz,0.1,-40)
        VoltSe (RH,1,mV1000,5,1,0,_60Hz,0.1,0)
        BrHalf (thermsi200,1,mV1000,2,Vx1,1,1000,True ,0,_60Hz,1.0,0)
        Rt = 24900*(1/thermsi200-1)
        Tk = (.001129241+.0002341077*LN(Rt)+.00000008775468*LN(Rt)^3)^1
        thermsi200 = Tk-273.15
        PanelTemp (Tpanel,_60Hz)
        TCDiff (Tcple,1,mV20c,4,TypeT,Tpanel,True ,0,_60Hz,1.0,0)
        SetStatus ("BaudrateCOM1",4800)
        GPS(GPSArray,Com1,0,100,NMEAStrings)
```

```
        SplitStr(GPSchar,NMEAStrings(2),",",18,5)

        SplitStr (Latlon(1),GPSchar(3),"String",1,0)
        SplitStr (Latlon(2),GPSchar(5),"String",1,0)

'IRR Wall (RIGHT)
    VoltDiff (TargmV,1,mV20,5,True ,0,_60Hz,1.0,0)
'Sensor body temperature
    Therm109 (SBTempC(1),1,16,Vx3,0,_60Hz,1.0,0)

'IRR Wall (LEFT)
    VoltDiff (TargmV(2),1,mV20,7,True ,0,_60Hz,1.0,0)
'Sensor body temperature
    Therm109 (SBTempC(2),1,18,Vx4,0,_60Hz,1.0,0)

'IRR Road
    VoltDiff (TargmV(3),1,mV20,6,True ,0,_60Hz,1.0,0)
'Sensor body temperature
    Therm109 (SBTempC(3),1,21,Vx4,0,_60Hz,1.0,0)

'Calculation of m (slope) and b (intercept) coefficients for target temperature calculation
 For i = 1 To 3
       'declare constants in array
       If i = 1 Then
         mC0(i)=mC0_1
         mC1(i)=mC1_1
         mC2(i)=mC2_1
         bC0(i)=bC0_1
         bC1(i)=bC1_1
         bC2(i)=bC2_1
       ElseIf i=2 Then
         mC0(i)=mC0_2
         mC1(i)=mC1_2
         mC2(i)=mC2_2
         bC0(i)=bC0_2
         bC1(i)=bC1_2
         bC2(i)=bC2_2
       ElseIf i=3 Then
         mC0(i)=mC0_3
         mC1(i)=mC1_3
         mC2(i)=mC2_3
         bC0(i)=bC0_3
         bC1(i)=bC1_3
         bC2(i)=bC2_3
       EndIf
```

```
    'get slope of curve for all IRRs
    m(i) = mC2(i) * SBTempC(i)^2 + mC1(i) * SBTempC(i) + mC0(i)
    b(i) = bC2(i) * SBTempC(i)^2 + bC1(i) * SBTempC(i) + bC0(i)

    'Calculation of sensor body temperature
    SBTempK(i) = SBTempC(i) + 273.15
    'Calculation of target temperature
    TargTempK(i) = ((SBTempK(i)^4) + m(i) * TargmV(i) + b(i))^0.25
    TargTempC(i) = TargTempK(i) - 273.15
Next
     SBTempWallRiC = SBTempC(1)
     SBTempWallLeC = SBTempC(2)
     SBTempRoadC = SBTempC(3)
     TwallRC = TargTempC(1)
     TwallLC = TargTempC(2)
     TroadC = TargTempC(3)

'Pyrgeometer Epply PIR Ser No. 32905FB
     VoltDiff(Ld_thmp,1,AutoRange,13,True,0,_60Hz,257.7,0)
     'Generic Half Bridge measurements Case
     BrHalf(Inst,1,AutoRange,23,Vx1,1,350,True,3000,_60Hz,1,0)
    'Generic Half Bridge measurements Dome
     BrHalf(Dome,1,AutoRange,24,Vx2,1,350,True,3000,_60Hz,1,0)
     Rinst = 10000*(Inst/(1-Inst))
     Rdome = 10000*(Dome/(1-Dome))
     Rinstln = LN(Rinst)
     Rdomeln = LN(Rdome)
     Ld_Tinst = 1/(c1 + c2*Rinstln +c3*(Rinstln)^3)
     Ld_Tdome = 1/(c1 + c2*Rdomeln +c3*(Rdomeln)^3)
     Ld= Ld_thmp + sigma*Ld_Tinst^4
     Ld_Tinst = Ld_Tinst-273.15
     Ld_Tdome = Ld_Tdome-273.15

'Pyranometer Y.E.S.- Ser No. 0005-2
 Dim CF
 CF=1/0.032
 VoltDiff (pyr,1,mV200,14,True ,0,_60Hz,CF,0)
          CallTable Test
          NextScan
```

Curriculum Vitae

Timothy David Wiechers

Education
M.Sc. Geography, 2018
University of Western Ontario, London, Ontario, Canada

B.Sc. (Honours) Environmental Science, 2015
University of Western Ontario, London, Ontario, Canada

Honours and Awards
The Brian Luckman Award – 2017
Department of Geography, University of Western Ontario

Related Work Experience
Research Assistant, Surface Climates Lab, University of Western Ontario, 2015 – 2018

Teaching Assistant, University of Western Ontario
Geography of Canada (Geo 2010) – 2017
Weather and Climate (Geo 2310) – 2015, 2016
Geography of Hazards (Geo 2152) – 2016

Work Study Student, University of Western Ontario, 2014

Publications
Joe, P., Belair, S., Bernier, N.B., Brook, J.R., Brunet, D., Bouchet, V., Burrows, W., Charland, J.P., Dehghan, A., Driedger, N., Duhaime, C., Evans, G., Frenette, R,. Gultepe, I., Henderson, D., Herdt, A., Hilker, N., Huang, L., Hung, E., Isaac, G., Johnston, D., Jeong, C-H., Klaassen, J., Leroyer, S., Lin, H., MacDonald, M., MacPhee, J., Mariani, Z., Reid, J., Robichaud, A., Rochon, Y., Sills, D., Shairsingh, K. Stroud, C., Su, Y., Taylor, N., Wang, J.M., Vano,s J., Voogt, J., Wiechers, T.,Wren, S., Yang, H., Yip, T. The Environment Canada Pan and ParaPan American Science Showcase Project. *Bulletin of the American Meteorological Society.* (2017).

Presentations
Wiechers, T.D., Liota, D., Sills, D., Voogt, J.A. 2015 Pan/ParaPan Am Games Mobile Measurements, *8th International Workshop on Air Quality Forecasting Research,* Toronto, ON, Canada. (2017). [Oral]

Wiechers, T.D., and Voogt, J.A. Microclimate Variability of Select Toronto Neighbourhoods, *8th International Workshop on Air Quality Forecasting Research,* Toronto, ON, Canada. (2017). [Poster]

Wiechers, T.D., and Voogt, J.A. UWO Mobile Measurements. *Pan and Parapan American Games Science Meeting*, Toronto, ON, Canada. (2016). [Oral]

Voogt, J.A., O'Carroll, D., Robinson, C., Lundholm, J., Sleep, B., Smart, C., Staniec, M., Kurukulaarachchi, D., Sims, A., Sia, M., Perelli, G., Wrona, E., Wiechers, T.D., Breach, P. Green Roofs in Canadian Cities. *University of Reading, Department of Meteorology*. (2015). [Oral]